NOTE TO USERS

This reproduction is the best copy available.

THE FOCAL SPREAD OF MACROMOLECULAR TRACERS IN VESSEL WALLS: FREQUENCY AND EFFECT OF INTIMA COMPACTION AND BLOOD PRESSURE

By

YU SUN

A dissertation submitted to the Graduate Faculty in Engineering
in partial fulfillment of the requirements for the degree of Doctor of Philosophy,
The City University of New York

2008

UMI Number: 3296979

UMI Microform 3296979

ProQuest Information and Learning Company
300 North Zeeb Road
P.O. Box 1346
Ann Arbor, MI 48106-1346

This manuscript has been read and accepted for the
Graduate Faculty in Engineering in satisfaction of the
dissertation requirement for the degree of Doctor of Philosophy.

Professor David S. Rumschitzki

January 29, 2008 — Chair of Examining Committee

Date

Professor Mumtaz Kassir

January 29, 2008 — Executive Officer

Date

Distinguished Professor Sheldon Weinbaum

Distinguished Professor John Tarbell

Associate Professor Bingmei Fu

Associate Professor Alexander Couzis

Associate Professor Kung-Ming Jan, M.D.

Supervisory Committee

THE CITY UNIVERSITY OF NEW YORK

Abstract

THE FOCAL SPREAD OF MACROMOLECULAR TRACERS IN VESSEL WALLS: FREQUENCY AND EFFECT OF INTIMA COMPACTION AND BLOOD PRESSURE

By

Yu Sun

Mentor: Professor David S. Rumschitzki
Co-mentor: Dr. Kung-ming Jan

Atherosclerosis appears to begin when a transmural pressure (ΔP)-driven water flow advects low-density lipoprotein cholesterol from the lumen into the subendothelial intima around rare, isolated endothelial cells with temporarily widened junctions. We compare frequencies of large-molecule leaks in the susceptible, large, high-pressure aorta, the rarely susceptible pulmonary artery and the immune inferior vena cava. The average horseradish peroxidase (HRP) leakage frequencies from 35 male Sprague Dawley rats are, respectively, 7.38±1.77, 3.34±0.87, 0.441±0.158 per 10^4 cells. Neither tracer circulation time nor acute blood pressure affects these numbers.

Our group's earlier theoretical work explained historic HRP localized spot growth vs circulation time data with a water and macromolecular transport theory. Our local theory based on the idea that the intima compresses under ΔP causing the endothelium to block IEL fenestrae, thereby lowering wall hydraulic conductivity Lp, clarified anomalous Lp data. Combining these theories, Chapter 3 predicts that only with initmal compaction do higher acute pressures mean smaller spots with shorter rise times. Our subsequent experiments verify these predictions.

Although Huang *et al*.'s axisymmetric convection-diffusion transport theory predicts HRP concentration near localized leaks vs r, z and t, experimental spot size tests correspond to integrating these predictions through the tissue. A more stringent test would be to compare predictions with 3D HRP concentration profiles. Chapter 4 uses confocal microscopy and an HRP substrate with fluorescent reaction products to observe such profiles. Our theory can mimic these experiments, including the washing period before fixation and we successfully compare experiment with theory. Such comparison involves using 3D interpolation to calculate an optimally (Bremerman's algorithm) locate the coordinate origin and tilt angles of the axes for each data set.

Aquaporins are ubiquitous water channel membrane protein. My labmates have found aquaporin1 in rat aortic endothelial cells and have shown their chemical blockage significantly lowers vessel wall hydraulic conductivity in a pressure-dependent manner. Our group believes blocking aquaporins shifts a larger fraction of the transmural ΔP to the endothelium, thereby compressing the endothelium at lower ΔP. We predict how, at low ΔP, aquaporin blockage-induced intimal compression would affect HRP spot growth and confirm these predictions with rat experiments.

Acknowledgements

I would like to express my deepest gratitude and appreciation to my mentor Professor David Rumschitzki for his patient and inspiring advisement and supervision. I would like to thank my co-mentor Dr. Kung-Ming Jan for his advisement and guidance on the experiment studies. I have gained so much inspiration from their physical insights and suggestions throughout this research work.

I would like to thank my parents and my fiancé Hui Huang for their support and love.

Also a special thank to Daniel Fimiarz and Dr. Tadmiri Venkatesh of Biology Department for constant help with the confocal microscopy.

I would like to thank the staffs: Zhenrong Xu and Andy Eng for their kindly help. I also thank other group members: Dr. Yi-Xin Shou, Dr. Zhongqing Zeng, Jinyong Bao, Chirag Braval, Tieuvi Nguyen, Jimmy Toussaint, Stewart Russell for their discussion and help. At last I thank all my friends: Dr. Fang Xu, Dr. Bo Jin, Jingqin Cui, Bin He and Lina Zhong for the share of my life.

This work is supported by NSF Grant CTS-0077520 and NIH Grant 5-R01-ML 067383.

Table of Contents

Lists of tables

Lists of Figures

Chapter 1 Introduction

Atherosclerosis is a well-known disease mainly of large arteries. It is the leading cause of death for individuals in the United States and in all western countries. Atherosclerosis appears to begin with the delivery of low density lipoprotein (LDL) cholesterol from the blood into the vessel wall, where it accumulates(68). Blood -borne monocytes enter the arterial intima in regions with high sub-endothelial lipid concentration, becoming macrophages that attempt to scavenge the extracellular cholesterol. When overwhelmed,

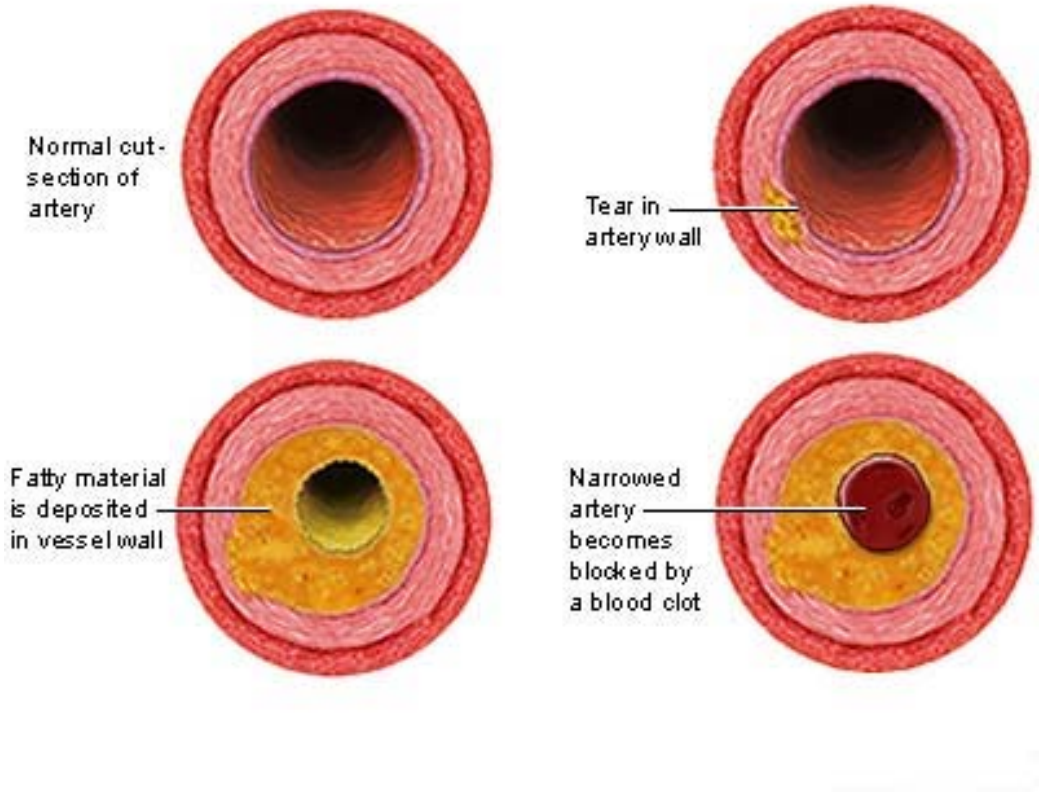

Figure 1.1 Developmental process of atherosclerosis

they progress to form foam cells, and this accumulation of lipid and necrotic cells appears to comprise the earliest lesions. Eventually, such lesions lead to stenoses that compromise the cross section for flow, causing the heart to be overworked and possibly leading to

heart attack. Figure 1.1 shows the developmental process of atherosclerosis. A crisis may occur when deposits of cholesterol and plaque accumulate at a tear in the inner lining of an artery, catastrophically releasing accumulated cholesterol into the blood which can form a plug. Alternatively, as the deposits harden and occlude the arterial lumen, blood flow to distant tissues decreases. A part of the lesion may break off and lodge as a clot in a downstream narrowing, completely blocking the artery.

As is well known, there is more than one type of lipoprotein cholesterol, and they are usually grouped by their corresponding fraction upon centrifugation. Low Density Lipoprotein (LDL) is termed the “bad” cholesterol because of its high concentration in atherosclerotic lesions. One LDL “molecule,” about 22 nm in diameter, is comprised of about 2000 cholesterol and cholesterol ester molecules, surrounded by a phospholipid coat (Fig. 1.2) to make it water/blood soluble, and an apoprotein to allow its recognition by specific cell surface receptors. Cholesterol in moderate concentrations is needed by cells to produce membranes. Nature has evolved two delivery methods to supply it to all cells. 1: The exogenous pathway, where cholesterol and other lipids absorbed from the intestines enter the blood stream and make their way to the adipose tissue and muscles for storage and use as an energy supply in liver; and 2: endogenous, in which the liver packages cholesterol and other lipids into lipoprotein packets that transport the cholesterol through the bloodstream to the body’s cells for use in cell membranes and in hormone production(9) .An overabundance of cholesterol due to a high blood LDL concentration can eventually lead to plaque formation and atherosclerosis.

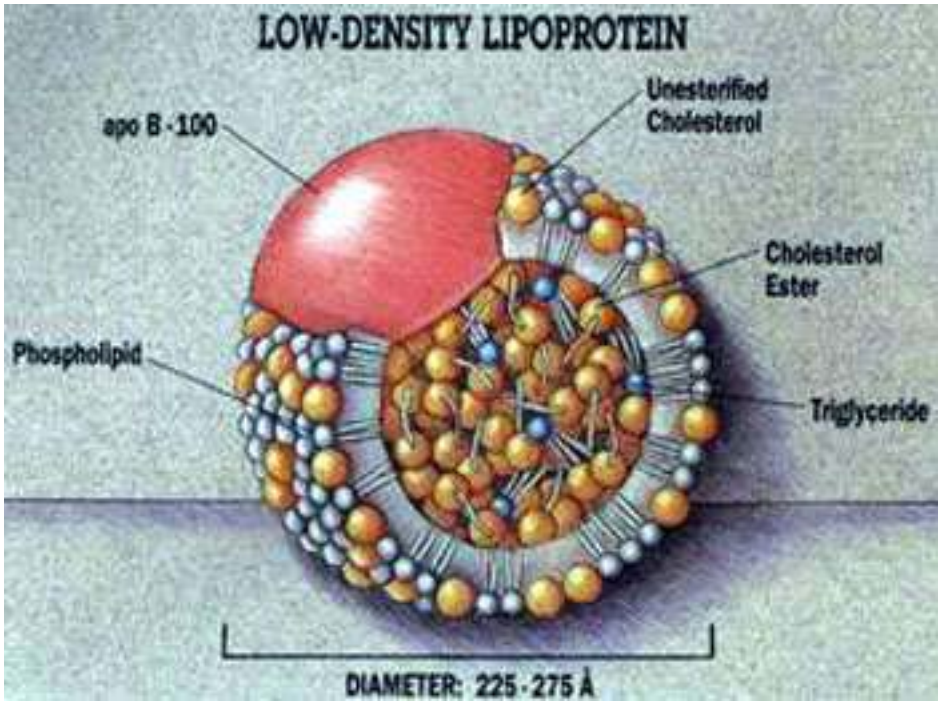

Figure 1.2 An LDL molecule

Let us briefly review the structure of the aorta (Fig. 1.3)(79). The aortic endothelium, which is a continuous, quiescent monolayer of endothelial cells, covers the lumen side of the arterial wall. The sub-endothelial intima, which in healthy animals is a thin (<1μm in rats and rabbits), cell-free region comprised of collagen and proteoglycans, separates the endothelium and internal elastic laminar (IEL). The IEL in the aorta and other large arteries is a continuous, cylindrical sheet of elastin having numerous fenestral holes . Adjacent to the IEL is the media, which contains smooth muscle cells (SMC), proteoglycans, and elastic fibers and sheets, and is much thicker than the other layers'

combined thickness.

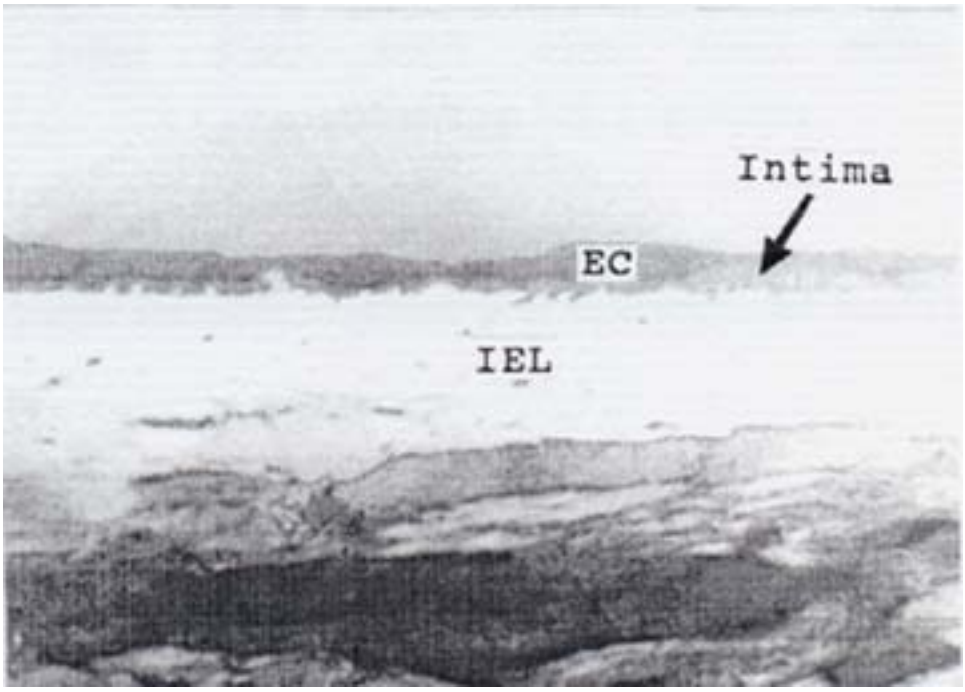

Figure 1.3 Electron micrograph of Aorta. Magnification x8,000 (Huang, *et al*. 1997).

Endothelial cells (10) have junctions that are tight enough to severely restrict the trans-endothelial migration of molecules with size as small as that of albumin (~ 8 nm diameter). This raises the question: how can a 22 nm LDL particle penetrate the endothelium's tight junction? Many groups proposed theories and performed experiments to explain the LDL's penetration of the endothelium. Frokjaer-Jensen's (19) thin serial sections belied the earlier proposed mechanism of free vesicles shuttling LDL and other large molecules across the endothelium by presenting a three-dimensional picture of these putative vesicles. The vesicles, which in isolated sections appeared to be free, tuned out in fact to be bound to one surface of the endothelium in another plane. Our group's collaborators (74, 75, 82) proposed and substantiated(33, 34) a hypothesis for an important pathway for large molecule to cross the aortic endothelium (in the rat). This

new pathway was via the junctions that surround rare isolated cells, many of which are dying or dividing, junctions that are temporarily not tight and therefore leak transiently. Experimental results showed that 99% of the cells in mitotic (M) phase were associated with EBA (Evans blue albumin conjugate) leakage(20) and 80% of cells in M phase were leaky to LY-LDL (Lucifer yellow-LDL)(67). Figure 1.4(34) shows a dual-staining experiment exhibiting the coincidence of tracer leakage and (via hematoxylin staining) a cell in M phase. The bright area indicates that the tracer is present under the endothelium. Chuang *et al.* (14) performed similar experiments using horseradish peroxidase (HRP) as a tracer and found complementary, consistent information. HRP was injected through the femoral vein of the rats, circulated for various amounts of time before animal sacrifice. These experiments showed the growth of HRP tracer spots in the aorta as function of time. Surprisingly, the HRP tracer spots in the rat's aorta grew extremely fast, reaching 200 μm diameter in only 2 min. These results were consistent with earlier similar experiments by Stemerman *et al.* on HRP(59). This rapid early time growth of the large spots represented a challenge to the theorists. This phenomenon suggested that a convective, rather than a diffusive, mechanism is controlling here. In addition, even for a convection-dominant view, if the sub-endothelial space were of uniform structure (i.e., with uniform transport parameters), the transport theories could not produce tracer spots

that were even close to the right size (82).

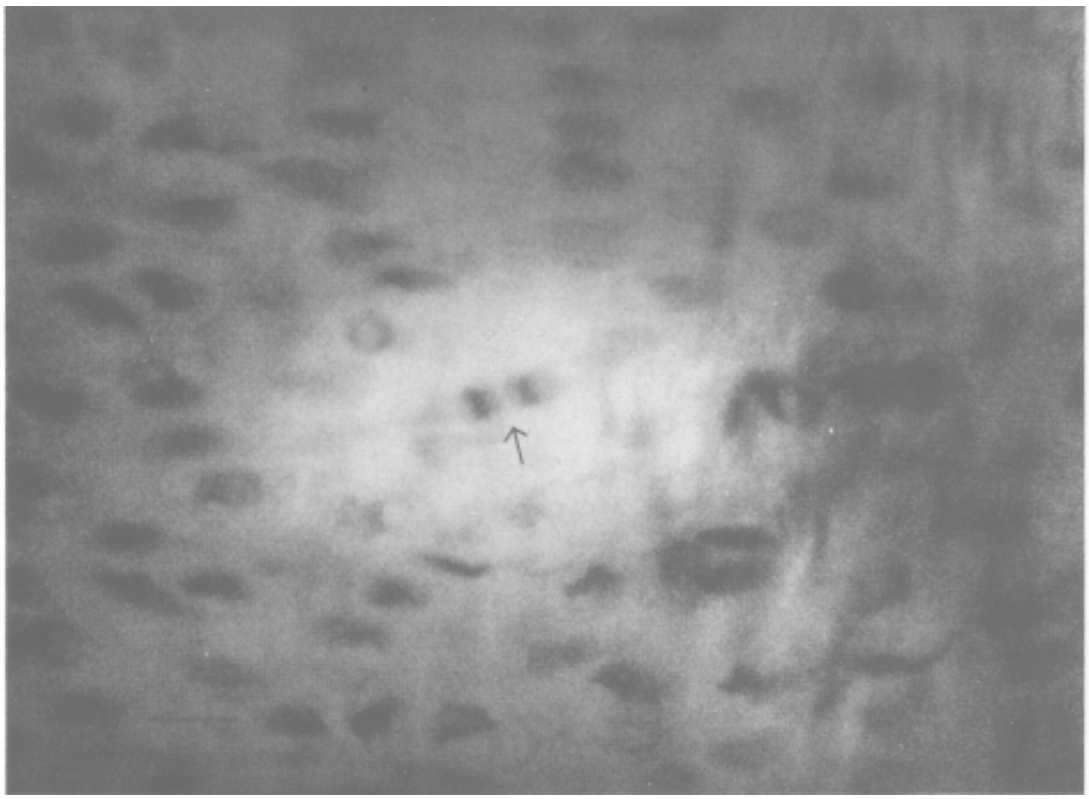

Figure 1.4 En face view of rat endothelium stained with hematoxilin to show mitotic cells (Lin, *et al*. 1990).

Recall that the wall of a large artery is comprised of an endothelium lying above the normally cell-free, thin, sub-endothelial intima. Frank and Fogelman's (18) ultra-rapid freezing technique revealed the detailed fiber matrix structure of the sub-endothelial intima comprised of collagen, elastin and proteoglycans. The thin intima layer usually makes up less than 1% of the artery wall in a healthy individual. From their freeze etchings, one could see and quantitatively estimate that the intima was practically all void with over 90% space for albumin and 50% for LDL(25). In contrast, the media that had only about 8% void for albumin and less than 1% for LDL.

Our group and others have developed a number of theoretical models to describe the transport processes for water and macromolecules in the aortic wall. The earlier one dimensional (20, 21, 65) or two dimensional (67, 73-75) models consider either diffusion or diffusion coupled with convection in the direction normal to the endothelium, or just 2D diffusion. These models are not capable of describing the spots' early ultra-rapid growth unless one postulates diffusivities in the intima that are orders at magnitude too high to be realistic. Yuan *et al.*, (82) was the first to consider the sub-endothelial intima separately from the media, separated by the IEL barrier, in a two-dimensional model, but assigned both regions the same transport parameters. Huang *et al.* (25) used Frank and Fogelman's freeze etchings that showed the enormous intimal void space to construct an *ab initio* theory for the intimal transport parameters and found values 1-2 orders of magnitude higher than the corresponding media parameters. Using these results in a two-dimensional, convection-diffusion multi-region wall model, Huang *et al.*(25) found a highly non-uniform pressure field in the sub-endothelial layer. This non-uniform pressure field controls the flow of water through the normal and leaky clefts and subsequently in the intima. Huang *et al.*,(25) found the pressure drop across the intima to be very small, so that the normal velocity is almost uniform and most of the flow and transport is *parallel* to the endothelium away from the leaky junction in the intima at the leading order. This is the key factor accounting for the very fast-growing, large tracer spots. Therefore the time-dependent numerical solution of this model for the concentration distribution in response to a step change in the lumen's tracer concentration agrees well with the experimental spot size growth results. The LDL concentration as a function of distance from the center of a leaky cell profile solution ten minutes after LDL injection

also agrees well with data culled from Truskey's (66) autoradiographic pictures of the radioactive LDL distribution about a leak at 10 min.

As the above discussion demonstrates, pressure is the driving force for the advective tracer transport into the artery wall, and therefore it is natural to consider the effect of pressure on this transport. Tedgui and Lever (63, 64) and Baldwin and Wilson (2, 3) each showed that the overall hydraulic conductivity (the ratio of the water flux to the transmural pressure) Lp of the wall exhibitted anomalous behavior with increasing transmural pressure. The measured low pressure Lp value decreased by over 40% as the transmural pressure increased from 50 to 90 mm Hg and then remained constant thereafter up to the edge (180 mm Hg) of the physiological range. In order to explain this behavior, our group's insight into the structure of the aorta and, in particular, the intima, was crucial. Huang *et al.* (79) postulated that, under high transmural pressures, the intima would compress. Once compressed to a certain extent, the strong collagen fibers in the intima would resist further compression. This compression would decrease the intima's inter-fiber spacing, thereby decreasing the intima's transport parameters and, more critically, cause the endothelium to partially block some of the IEL's fenestra and thereby lower the hydraulic conductivity drastically. To check this theory, our group developed a model for the local flow into an IEL fenestra as a function of the degree of compression of the intima(26). Comparison of the theoretical results with the Lp Tedgui and Lever and Baldwin and Wilson's Lp measurements yielded a prediction that the intima compresses to 1/6 of its unstressed value under physiological pressure. Huang *et al.*'s subsequent measurements of intimal thickness under different transmural pressures (79) found

compression to 1/5 the unstressed intima value, which was surprisingly close to the value that the theory, built upon many simplifying assumptions, predicted.

With these insights into the situation in the early, disease-free large artery, it seems that mechanical transport processes play an important, potentially triggering role in atherogenesis there. Can this framework then explain why other vessels are disease-resistant? The aorta and heart valve leaflets (44, 47) (100 mmHg) are both atherosclerosis-prone, but the lower pressure pulmonary (16 mmHg) artery (PA) is vulnerable only when under pulmonary hypertension. Veins (5 mmHg) do not develop atherosclerosis except when exposed to arterial condition, i.e., high pressure, as in a coronary bypass, where atherosclerosis often develops rapidly as the vessel remodels(30). To shed light on the differing disease susceptibilities of different vessels, we compare the frequencies of such large-molecule leaks in the susceptible large, high-pressure aorta with those of the rarely susceptible pulmonary artery and the immune inferior vena cava in chapter 2. The average horseradish peroxidase leakage frequencies from 35 male Sprague Dawley rats are $7.36\pm1.76/10^4$cells (aorta; $7.60\pm1.64/10^4$cells for 51 rat aortas), $3.40\pm1.16/10^4$cells (pulmonary artery) and $3.71\pm1.15/10^5$cells (inferior vena cava). These data are necessary inputs that one must combine with mathematical convection-diffusion models for transport around an isolated endothelial leak in these other vessels(85, 86). and the kinetics of LDL binding to its wall tissue (80, 87) in order to see if transport and kinetic modeling alone can distinguish disease susceptible from resistant vessels.

Huang *et al.* (26) used their theory to predict the HRP spot size as a function of time in the arterial intima for several different transmural pressures. Due to a paucity of data available at the time, they needed to mix parameters from both rat and rabbit data.

Their plots made predictions that both took into account and ignored the effect of intimal compaction; see Fig. 1.5. For an incompressible intima in which permeability properties are independent of luminal pressure, the long-time asymptotic spot size is independent of pressure; the higher pressure serves only to shorten the time needed to reach its asymptotic size. This is because the porous media flow is a Darcy, i.e. potential flow, whose stream lines are independent of the driving force. In contrast, with intimal compaction, the geometry and associated parameters change with pressure. As a result the model predicts that asymptotic size of the HRP spot at 4min decreases when transmural pressure increases. It also predicts that the time needed for the spot to reach its asymptotic size decreases rapidly as the pressure increases as well.

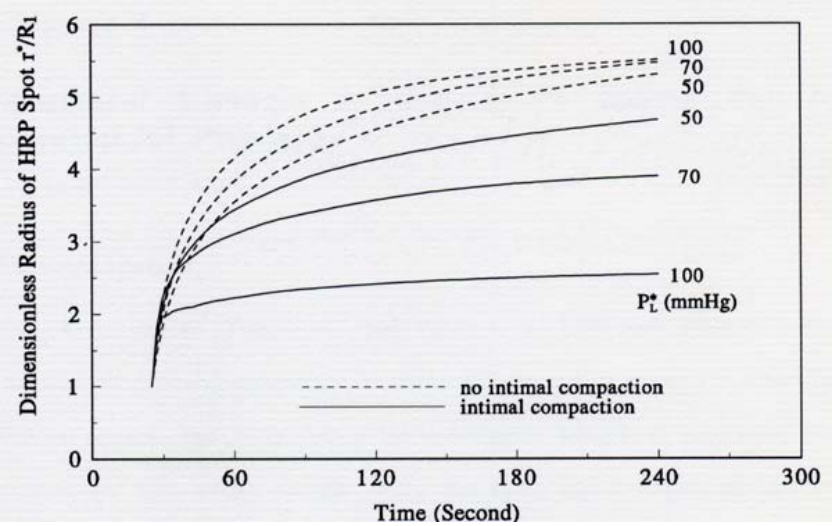

Figure 1.5 Predicted time-dependent HRP spot sizes for several different transmural pressures in arterial intima. (Huang *et al.* 1997)

Since that time, Shou *et al.* (53)measured the remaining data for the rat and Zeng *et al.* (87-89) corrected Huang *et al.*'s basic two-dimensional convection-diffusion theory(26) using now the complete set of rat parameters. In the chapter 3, we begin by

using these parameters and this corrected theory to see if the predictions noted in the last paragraph still result; they do. We then test these predictions experimentally by measuring the growth of HRP spots with HRP circulation time for normal, acute hypertensive and acute hypotensive rats. Our results for normotensive rats are consistent with earlier measurements(14) and those from our lab(53). Before we use pharmaceuticals to adjust blood pressure in the rat, we must make sure that these chemicals have no effect on Lp of the aorta, since the theory assumes identical vessels and only differing transmural pressures. We measure Lp of the aorta as a function of the transmural pressure, first without, then with one of these agents on the same vessel to verify that the chemical does not affect tissue properties. With norepinephrine, which elevates the rat's blood pressure, Lp is well within the error bars of the drug-free measurements. But, administration of nitroprusside or labetalol, drugs that depress the rat's blood pressure, change Lp substantially. To induce acute hypotension without such a change, we instead opened the rat's chest and held the exposed heart with a hook. This restricted the motion of the heart and lungs and resulted in a lowering of the mean blood pressure to 45 mmHg. Using these techniques to control blood pressure, our HRP spot growth measurements show a clear decrease in asymptotic spot size with increasing Δp and, for the two higher pressures, a rise time decrease as well. We compare these results with the above-mentioned theory and extend the theory to include the effects (that we measure) of nitroprusside and labetalol on the intrinsic Lp of the endothelium and media.

The convection-diffusion transport theories of Huang *et al*.(26) predict the tracer concentration as a function of the cylindrical coordinates r and z (the theories assume axisymmetry about an axis perpendicular to the endothelium through the center of the

leaky cell) and time. However, the experimental spots thus far have only been characterized in terms of the effective radius of their projection into a plan parallel to the endothelium. This is because the experimental procedure thus far shines light and observes its absorbance through the vessel wall, *i.e.*, it is a projection. Clearly, a more refined, non-projective experimental technique would be a more stringent test for the theory. As such, we have employed a Zeiss LSM 510 confocal microscope and the tracer HRP together with a substrate that yields a fluorescent reaction product to measure the three-dimensional structure of tracer leakage spots. The confocal microscope does this by scanning many thin sections through the sample and assembling them into a clean, three-dimensional images of the tracer spots in blood vessel walls. We take these images as a function of time between tracer injection and animal sacrifice. Since neither the orientation of the sample in the confocal microscope nor the position of the center of the leak is known exactly, we allow these quantities to be parameters to be optimized in the comparison of theory with experiment. By using 3-D interpolation to adjust the location of the origin and the tilt of the endothelial plane for the experimental 3-D images, we have written an optimization program based on Bremerman's method (7) to find the most unbiased values of these parameters that give the best comparison of theory with experiment. Chapter 4 shows this procedure yields a very good comparison.

Recent well-publicized work has shown that there is a family of transmembrane proteins – the aquaporins (AQP) - that transport water molecules at very little or not ATP cost and reject everything or nearly everything else(37, 60). AQP exist in plants (29), red blood cells (13), epithelium and endothelium (39), and many other cell types. Shou (51) did pilot studies on their role in transendothelial water transport in rat aorta. She, and

later, in a more refined set of experiments, Nguyen *et al*.(38) measured the Lp of the aorta as a function of transmural pressure, first without, then with, mercuric chloride ($HgCl_2$), a well-established aquaporin water channel blocker, on the same vessel. Nguyen found that the aorta's hydraulic conductivity Lp decreases, on average, by 32% and its endothelial+intima Lp by 56% at 60 mmHg. This effect is not straightforward, since these reductions are transmrual pressure-dependent, being order 11-21% for total Lp at 100 and 140 mmHg. In order to explain this dependence, we guess that blocking endothelial AQPs lowers its Lp. This results in a larger fraction of the overall transmural pressure to act across the endothelium. Thus, the transendothelial pressure required to compress the intima should be reached at a lower transmural pressure when AQPs are blocked than when they are open. This line of reasoning predicts that at a transmural pressure, e.g., 45 mmHg, where the intima is uncompressed, the blocking of AQPs by, say the administration of $HgCl_2$, might result in intimal compression without change in overall transmural pressure. Chapter 3 confirmed that intimal compaction corresponds to smaller HRP spots. In Chapter 5, we investigate if $HgCl_2$ infusion into a rat can induce aquaporin blockage and intima compaction in vivo by examining the HRP spot size as a function of HRP circulation time. As we shall see, the experimental results agree with the prediction based on this line of reasoning.

Each of the following 4 chapters is intended to be self-contained. It contains its own abstract, introduction, literature review, methods, results and discussion sections. As such, at the cost of some repetition, one can read Chapters 2-5 in any order. We conclude this thesis with a summary and outlook in Chapter 6.

Chapter 2. HRP Leakage Spot Frequency in Various Rat Vessels

2.1 Introduction

Why do certain vessels get atherosclerosis and others do not? The aorta and heart valve leaflets (44, 47) (100 mmHg) are atherosclerosis-prone, but the lower pressure pulmonary (16 mmHg) artery (PA) is vulnerable only with pulmonary hypertension. Veins (5 mmHg) do not develop atherosclerosis except when exposed to arterial condition, i.e., high pressure, as in a coronary bypass, where atherosclerosis often develops rapidly as the vessel remodels(30).

Atherosclerosis appears to begin with low-density lipoprotein (LDL) cholesterol delivery from the blood into the vessel's intima, where it can bind to extracellular matrix and accumulate (68). An LDL particle has a diameter of ~22nm(9). Endothelium cell (10) junctions are tight enough to severely restrict the trans-endothelial migration of molecules as small as albumin (~ 8 nm diameter). Early theoretical and experimental studies tried to explain how LDL could penetrate these tight junctions. Frokjaer-Jensen's (19) thin serial sections belied the earlier proposed mechanism of free vesicles shuttling LDL and other large molecules across the endothelium. The vesicles, which in isolated sections appeared to be free, turned out in their three-dimensional reconstruction to be bound to a surface of the endothelium in another plane. Weinbaum *et al* (73) hypothesized that an important pathway by which large molecules cross the aortic endothelium is through widened junctions that surround certain rare, isolated cells. Stemerman *et al*(59) found that labeled LDL crossed the rabbit aortic endothelium in local hot spots, rather than uniformly. Chien's group showed that junctions around many dividing (~1/3 of all leaks) (33, 34) and dying (32) cells leaked macromolecules. 80% of

the cells in mitotic M phase (marked with hematoxylin) leaked LY-LDL (Lucifer yellow-LDL) (34); 99 % leaked the smaller molecules EBA (Evans blue albumin conjugate)(33) and horseradish peroxidase (HRP – diameter ~6nm), which in short-time experiments showed pronounced focal brown spots coexisting with and superimposed on diffuse staining (14). Mitotic cells accounted for 23% of EBA leaks and 42% of LDL leaks in rat thoracic aorta. Interestingly, Hermann *et al* (23) found that although 71-78% of mitotic cells in rabbit aorta leaked ^{125}I-LDL, they only accounted for 13% of LDL leaks. Spontaneously hypertensive rat aortas have 2-3 times the frequency of leaks of normotensives (78).

Chuang *et al*. (14) performed similar tracer (HRP) experiments and tracked the spot size as a function of time between HRP injection and rat sacrifice. One dimensional (20, 21, 65) or subsequent two dimensional (2D) diffusion-only models(67, 73-75) could not describe Chuang *et al*'s observed rapid spot growth (to >100 μ radius in 2-4 min) unless one postulated lateral, i.e., parallel to the endothelium, tracer diffusivities in the vessel intima that are orders of magnitude too high to be realistic. Yuan *et al*. (82) and Huang *et al*.'s (25) 2D convection-diffusion models solved for the pressure drop and the water flow that it drives across the normal and leaky endothelial junctions and used this to calculate the tracer that this leaky junction flow advects into the intima. Huang *et al* (25) found a highly non-uniform pressure field in the subendothelial intma that spreads advected tracer parallel to the endothelium away from the leak. Due to the enormous intimal void space, they constructed an *ab initio* fiber matrix theory to predict intima transport coefficients 10-100 times media values and used them in their 2D, convective-diffusive transport model. Its predicted time-dependent tracer concentration distributions

that result from a step change in the lumen's tracer concentration agree well with Chuang *et al*'s rapid experimental spot size growth results. This model also explains the LDL concentration as a function of distance from the center of a leaky cell 10 min after LDL injection culled from Truskey's (66) autoradiographic ^{125}I-LDL images about a leak.

The time-average physiological pressure (in mmHg) for the aorta (100), the PA (16) and the IVC (5) differ. It is natural to suspect that lower transmural pressure (ΔP) implies less convection and therefore less tracer entry. Shou (53) measured the water flux, $Lp\Delta P$ (Lp is the hydraulic conductivity), through the vessel wall and found the lower pressure vessels had higher conductivities. In fact, surprisingly, $Lp\Delta P$ was the same for all three vessels. Shou (52) also measured focal HRP spot growth as a function of tracer circulation time in these three vessels and found that, whereas spot growth in the PA and the aorta are very similar in initial size and in rapid growth, the IVC began with much larger spots that hardly grew with HRP circulation time. Thus it is conceivable that each IVC leak may deliver more tracer to the tissue than each arterial leak (although differences in drainage from the tissue might lead to different tissue concentrations). In order to compare the total rate per unit vessel area of macromolecular (LDL) entry via localized leaks into these vessels' walls, which may correlate with disease susceptibility, what is missing – and what we measure here - is each vessel's macromolecular leakage site frequency. Lin *et al*.(33, 34) report ~5 rat aorta cells in 10^4 leaked EBA, while, in rabbit aorta, Hermann *et al* (23) find 2.7 cells in 10^4 leaked ^{125}I-LDL and Barakat *et al*(4) find 1.9 cells in 10^4 leaked HRP. No data is available for the other vessels. Therefore the present study measures the HRP leakage frequency in the PA and IVC and compares with the aorta. We also check if different tracer circulation times affect the measured spot

frequency (does one miss spots at shorter circulation times?) and, given the known increase in leakage frequency with chronic hypertension, we check if altering the animal's acute blood pressure can influence observed spot frequencies (do higher ΔPs spot holes?). We also examine the integrated HRP staining of individual spots in each vessel to compare total HRP per spot. These data will be valuable inputs into mathematical models that will include LDL transport within and the kinetics of lipid binding to extracellular matrix in the walls of these vessels. These models may help explain these vessels' very different vulnerability to atherogenesis.

2.2 Materials and methods

We report experiments on 51 male Sprague Dawley rats weighing 250g-350g. To prepare the tracer, we dissolve 0.58g NaCl in 100 ml distilled water; then add 0.024 g HRP (for a 300 g rat) in 1mL normal saline. All procedures are IACUC approved.

30 mg Pentobarbital Sodium/kg body weight rat in a 1% solution (100 mg Pentobarbital Sodium in 10 ml of distilled water, shaken gently) by intraperitoneal injection anesthetizes the rat. We shave the rat's left leg, dissect it and cannulate the left femoral vein and artery. We attach a pressure transducer hooked to an AD Instruments Powerlab 4SP unit to the femoral artery to monitor the rat's arterial blood pressure (for PA and IVC pressures, see below) and attach the venous cannula to a KD Scientific-100 micropump (26 rats) and an injection port. Four rats received nitroprusside (4μg/hr per 300g rat), six labetalol (0.6mg/hr per 300g rat) and sixteen norepinephrine (10μg/hr per 300g rat) through the venous cannula pump, which, after ~10 min results in changing the mean rat blood pressure to ~45 mmHg (nitroprusside and labetalol) or 180mmHg (norepinephrine). In 15 of the 51 rats, after anaesthesia, we intubate the rat by attaching

its trachea to a rodent respirator, split the sternum longitudinally to expose the heart and lungs and use a smooth hook to pull the heart to one side, thereby reducing the rat's blood pressure to 45 mmHg without pharmacology.

After maintaining this pressure (45mmHg or 180mmHg) for 15 min in these 41 rats, or immediately in the 10 rats with normal pressure, we inject 1ml HRP and 0.5 - 1ml Heparin (5000 units/1 ml, Elkins-Sinn Inc. NJ). At 0.5, 1, 2, or 4 min blood circulation, an overdose of Pentobarbital Sodium sacrifices the rat. After flushing with 10ml PBS (Phosphate Buffered Saline; Sigma) and then perfusion-fixing the vessels *in situ* at room temperature with 1% Glutaraldehyde (Sigma) (1 ml 50% Glutaraldehyde in 50 ml PBS) introduced into the carotid vein and artery and draining from the femoral arteries, we excise the thoracic aorta, PA and IVC from the rat with blood pressure of 45mmHg or 100mmHg. We excised the aorta in all 16 (4 at each circulation time) norepinephrine-induced acutely hypertensive rats (180mmHg), and excised the other vessels in some of the others (2 PA (1 at 30s; 1 at 1min) and 5 IVC (2 at 30s;; 2 at 1min; 1 at 2min). We prepare the excised vessels for examination by peeling away the connective tissues and the adventitia, further fix them in 1% Glutaraldehyde for 1 hour, rinse with PBS three time to wash out the fixative and run the HRP-DAB reaction to develop the tracer spot. We dissolve 0.045 g DAB in a solution of 5 ml 0.3M Tris (0.182 g Tris (MW=121.1) in 5 ml H_2O) in 25 g distilled water, add 20 μl of 30% H_2O_2, followed by 1M HCl to adjust the pH to 7.0~7.4 and then place the tissue in it. The DAB solution is changed after 30 min and allowed to continue for another 30 min. The tissue is washed with PBS solution and prepared on slides for *en face* examination with an Olympus BX51 light microscope. The reaction product is brown, and so the leak is a brown spot. Since HRP can slowly

penetrate normal junctions, focal spots coexist with diffuse staining as in (14). We count the number of HRP spots by eye and measure the area of each piece of tissue. We then calculate the leakage frequency or the average number of HRP spots per 10^5 ECs by using Shou's average EC radius characteristic of that vessel measured on the same rat species in our lab: aorta 15μm, PA 12μm and IVC 11μm.

Control Experiment

We carried out control experiments on 2 rats using exactly the same procedure as for the normotensive rats above but without HRP. We still ran the DAB reaction, checked the aorta, PA and IVC for brown staining and compare with the vessels that received HRP.

Measurement of PA, IVC pressures

We measure the PA and IVC pressures in two rats at the three arterial pressures used. We monitor the aorta pressure through the femoral artery as noted, the IVC pressure through the femoral vein and the PA pressure by inserting a PE10 tubing through the right ventricle into the PA. We first measure the pressures at 100mmHg aortic pressure, raise it to 180mmHg with norepinephrine and remeasure. Shortly after we stop introducing norepinephrine, the aorta pressure returns to 100mmHg. We then decrease the aortic pressure to 45mmHg with nitroprusside.

Integrated intensities

We digitally photograph (through the microscope) HRP spots of representative sizes from the three vessels four times, once at each of four light intensities. For each spot at each exposure, we convert to a gray-scale (original scale 0-255, normalized to 0-1)

image, integrate the intensity within the spot and of background (scaled to the spot's size) and take the difference.

Estimation of branch area

The thoracic aorta has small branches. We use NIH ImageJ to calculate the average diameter of small branches from pictures of the branch holes. By assuming the branch area is ~5 times the area of the holes (46), we estimate the total branch area from the average diameter and number of small branches. In contrast, the PA has a Y-shape with the pulmonary trunk as its base and no other branches. We measure the diameter of branches and trunk with a digital caliper.

Statistics Analysis

We divide the range of leakage frequency evenly, count the number of vessels in each small bin and plot histograms to verify the normality of the HRP spot frequencies in each vessel. We then calculate means and standard deviations. Student' t-tests (P=0.05 cutoff) compare average tracer spot frequencies for one vessel type at different times or between vessel types.

2.3 Results

We conducted our experiments on rats at three different time-averaged large artery blood pressures, 45, 100 (normal) and 180 mmHg. Our measurements show that, when the aorta is at these pressures, the PA pressures are 14, 19 and 28mmHg and the IVC pressures are 3, 5 and 8mmHg. The percentage change in time-averaged blood pressure in these vessels is ~-25% in the PA, ~-40% in the IVC when lowering the aortic pressure by ~55% and ~47% in the PA, ~60% in the IVC when raising it by ~80%. In all discussion below, we characterize the pressure state of the rat by its aortic blood pressure.

Figures 2.1-3 show en face views of a portion of the thoracic aorta, PA and IVC after 1 min HRP circulation, with Fig. 1b the aortic control; the PA and IVC controls were nearly identical. The isolated brown spots outlined (by eye) in the figures are HRP leakage spots. (Not identical) illumination of Figs. 2.1-3 chosen for clarity. The precise outline defining the spot size vary very slightly between experimenters, but analysis of such spot data by more than one lab member resulted in no significant changes in spot number or size. As in (14), these spots coexist/ are superimposed upon diffuse HRP staining since HRP slowly passes through normal junctions. As in Shou(52), HRP spots in the aorta and PA are similar in size for the same circulation times but IVC spots (Fig. 2.3, one of the smaller IVC spots, ~ 2x the size of Figs. 2.1&2's spots) are larger.

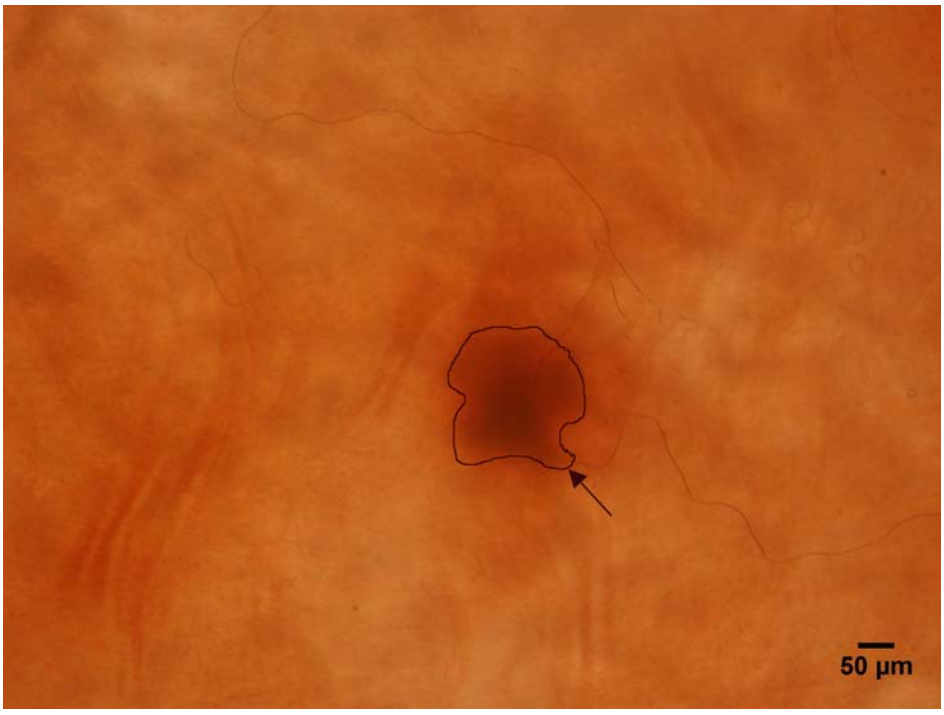

(1A)

(1B)

Figure 2.1. *en face* view of the aorta endothelia with 60s HRP circulation(1A) and the control(1B). The dark brown spot indicates the focal HRP leakage. Bar=50 μm (We marked the edge of the HRP spot here. The arrow pointed at the edge line.)

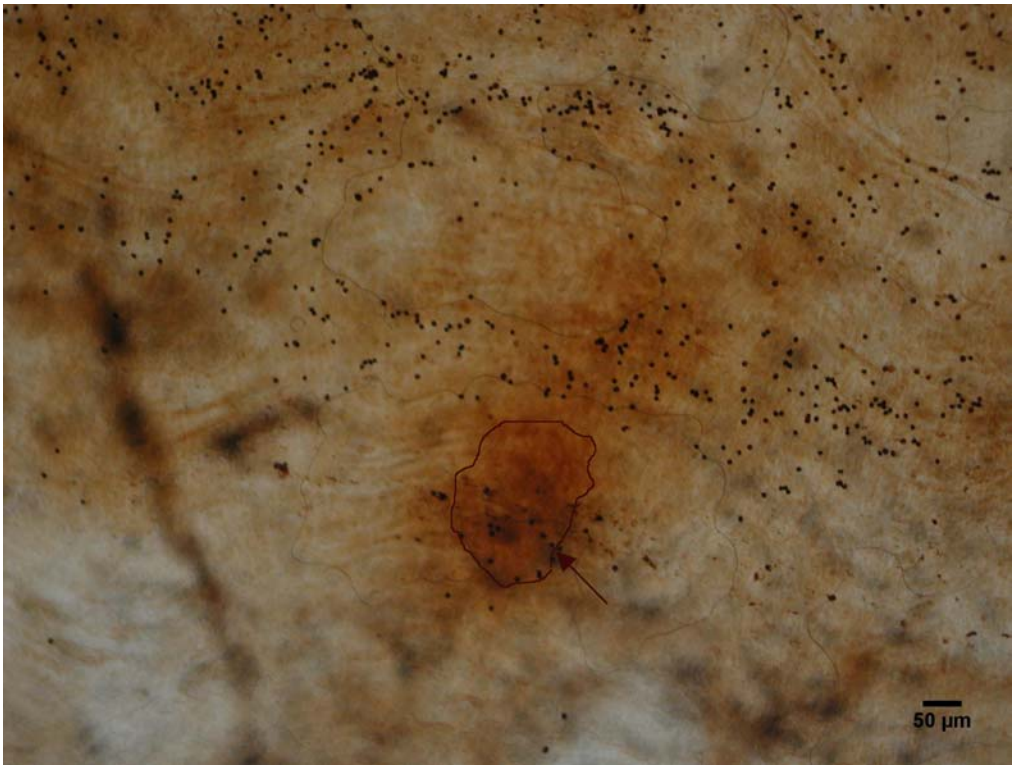

Figure 2.2. *en face* view of the pulmonary artery endothelia with 60s HRP circulation. The dark brown spot indicates the focal HRP leakage. Bar=50 µm (We marked the edge of the HRP spot here. The arrow pointed at the edge line.)

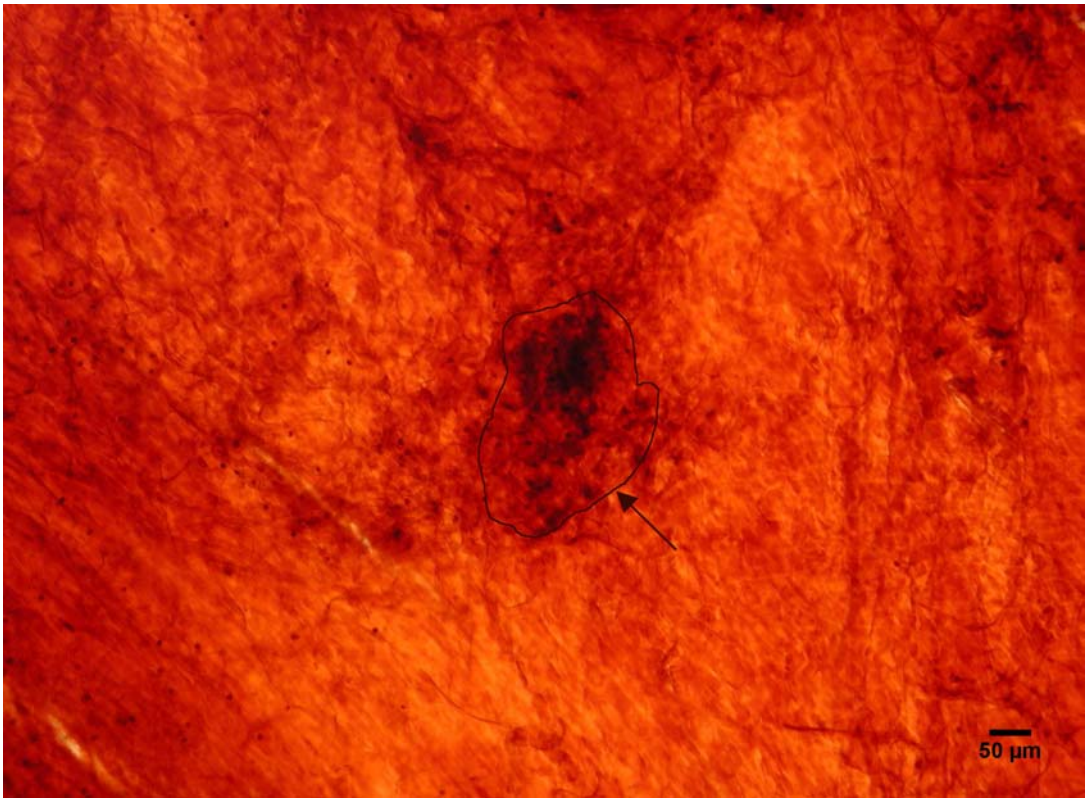

Figure 2.3. *En face* view of the inferior vena cava endothelia with 60s HRP circulation. The dark brown spot indicates the focal HRP leakage. Bar=50 µm (We marked the edge of the HRP spot here. The arrow pointed at the edge line.)

Table 2.1 lists the pooled average leakage frequencies of each of the three vessels, as well as the frequencies for the vessels segregated either by acute blood pressure (and method of pressure adjustment) or by circulation time. Frequency histograms appeared Gaussian for all three vessels. Table 2.3 in the appendix gives the complete raw HRP spot frequency data. The pooled data from vessels from 35 animals yield average HRP spots per unit vessel surface area : ~1.04 spots/mm^2 in the aorta, ~0.74 in the PA and ~0.12 in the IVC. Using the average EC area for each vessel, these numbers translate to the HRP leakage frequencies of $7.38\pm1.77/10^4$cells (aorta), $3.34\pm0.87/10^4$cells (PA) and $0.441\pm0.158/10^4$cells (IVC). The HRP leakage frequency is $7.60\pm1.64/10^4$cells for all 51

rat aortas, including the 16 acute hypertensive rats. These data indicate the aorta's HRP leakage frequency (per 10^4 ECs) is about double the PA's, which is almost 10 times that of the IVC.

P/mm Hg	Circulation Time	Aorta	Pulmonary Artery	Inferior Vena Cava
		Leakage Frequency (/10^4cells)	Leakage Frequency (/10^4cells)	Leakage Frequency (/10^4cells)
45	**30s**	8.59	3.34	0.469
	1min	6.67	3.69	0.565
	2min	7.53	4.12	0.457
	4min	8.51	3.29	0.533
	Average HRP leakage frequency (15rats)	7.84±1.34/10^4cells	3.58±1.00/10^4cells	0.510±0.162/10^4cells
45/LA	**30s**	4.72	3.25	0.331
	1min	3.92	3.11	0.339
	4min	8.78	3.34	0.354
45/NP	**30s**	6.53	4.41	0.289
	1min	6.18	2.48	0.280
	2min	6.43	3.10	0.274
	4min	5.94	3.98	0.613
	Average HRP leakage frequency (10rats)	5.99±1.80/10^4cells	3.33±0.84/10^4cells	0.350±0.158/10^4cells
100	**30s**	9.54	2.56	0.372
	1min	8.87	2.64	0.319
	2min	6.20	2.85	0.444
	4min	8.48	3.62	0.528
	Average HRP leakage frequency (10rats)	9.32±1.67/10^4cells	3.68±0.59/10^4cells	0.518±0.134/10^4cells
Average HRP spots/ unit vessel surface area (35rats)		1.04 spots/mm^2	0.74spots/mm^2	0.12 spots/mm^2
Average HRP leakage frequency		7.38±1.77/10^4cells	3.34±0.87/10^4cells	0.441±0.158/10^4cells

(35rats)				
180	**30s**	7.95	2.43	0.431
	1min	7.39	2.92	0.334
	2min	8.07		0.395
	4min	8.48		
	Average HRP leakage frequency (16rats)	$7.97\pm1.28/10^4$ cells	$2.68\pm0.35/10^4$ cells	$0.385\pm0.051/10^4$cells
Average Leakage Frequency (51rats)		$7.60/10^4$cells	$3.30/10^4$cells	$0.434/10^4$cells
Standard Deviation		$1.64/10^4$cells	$0.86/10^4$cells	$0.149/10^4$cells

Table 2.1. The pooled average leakage frequencies of the aorta, the PA and the IVC.

Table 2.1 compares the spot frequencies calculated from different subgroups of rats. Ten of the 35 rats received Nitroprusside or Labetalol to acutely adjust their arterial blood pressure from ~100 to 45mmHg before introducing HRP. For these animals, the average HRP leakage frequency is slightly, but insignificantly, lower than average only in the aorta. We lowered the arterial blood pressures of 15 of the 35 rats from 100 to 45mmHg by mechanical means. Their average HRP leakage frequency is slightly, but insignificantly higher than average only in the IVC. The other 10 rats had normal blood pressure of 100mmHg. Their average HRP leakage frequency is, again close to average. The same is true for the HRP leakage frequency at 180mmHg. Pooling the data according to HRP circulation time does not show a significant circulation-time dependence ($P>0.05$). We use circulation times only up to 4 min because at much longer times, too much of the relatively small HRP penetrates the normal junctions to clearly distinguish localized spots (84). In summary, neither the pharmaceuticals used, the rat's acute blood pressure, the method used to adjust it, nor the HRP circulation time appears to

significantly (P>0.05) affect the observed HRP leakage frequency in any of these three vessel types studied.

A single leak in each vessel need not result in a similar amount of HRP in each vessel's tissue. Table 2.2 compares the integrated HRP (integrated brown intensity) of 4 spots at 60 sec circulation in each vessel, each photographed at four different light intensities. Intensity 1 appeared too dim for the IVC and intensity 4 too bright for the aorta. Using either of the other two intensities, we find that the average integrated intensity per spot minus the vessel's background is similar in all three vessels, with the PA slightly higher than the other two. Note that small adjustments in spot outlines are immaterial, since these occur at the boundary where the intensity is nearly identical to background.

Table 2.2. Average integrated intensities for four spots in each vessel (reported as average spot intensity:-average background intensity = their difference), each photographed at four different light intensities, increasing from 1 to 4. Units are arbitrary. All spots examined were from vessels exposed to 1 min. HRP circulation before sacrifice and fixation.

Vessel	**Light 1**	Light 2	**Light 3**	**Light 4**
Aorta	246.5-236=10.5	183.5-138.5=45	123.25-61.5=61.75	80-40.5=39.5
PA	251.25-242.75=8.5	190.75-133.25=57.5	137.75-68.5=69.25	111.75-51=60.75
IVC	253.5-253.5=0.0	217.5-165.5=52	157-110.5=46.5	124-80=44

2.4 Discussion

Although the absolute changes in time-averaged blood pressure in the PA and IVC are much lower than those we induce in the aorta, their percentage changes are still quite significant. It is therefore worth examining if these changes affect macromolecular leakage frequency.

It is our goal to measure and compare the macromolecular leakage frequency in the aorta, PA and IVC, and LDL is clearly the most important tracer. Smaller tracers should get through more junctions, and should therefore have a higher leakage frequency than LDL. However, as long as the tracer is larger than the average width of a tight junction, but small compared with a wide-open junction, one would expect the *ratio* of tracer leaks between vessels to be fairly independent of the choice of tracer. As such, even though there should be fewer LDL than HRP leaks in a given vessel, we follow previous investigators (4, 14, 59, 83, 84) and use the far easier and more available tracer, HRP. Our results appear to be the first leakage frequency data for the PA and IVC. It is natural to wonder whether the measured leakage frequency depends on the animal's acute blood pressure (will higher pressures pop open more leaks?), on any pharmaceuticals used and on the tracer circulation time (will shorter circulation times tend to miss a portion of the leaks?). We use both pharmaceutical and mechanical methods to acutely lower the rats' mean blood pressure to 45 mmHg and compare with normotensive rats. We also investigate the HRP leakage frequency in rat aorta with a pharmaceutically acutely elevated mean arterial blood pressure of 180mmHg. Comparing spot frequency as a function of acute blood pressure and of blood pressure regulation method, irrespective of HRP circulation time, shows no significant effect of acute blood pressure or of the method of controlling it on measured HRP spot frequency. It has been documented that spontaneously (chronically) hypertensive rats exhibit 2-3 times the leakage frequency of normals and their vessels exhibit significant remodeling. We did not consider chronic blood pressure changes. Comparing spot frequencies for different HRP circulation times irrespective of blood pressure shows that circulation time does not affect the spot number

counted, just the spot size. As noted, intense spots coexisting with the regions of diffuse staining as in Figs. 2.1-3 is consistent with previous HRP leakage spot studies.

Our HRP leakage frequency of $7.60\pm1.64/10^4$ cells in the aorta of SD rats is similar to, but slightly higher than, the average $\sim4.71\pm2.86/10^4$ cells reported by Lin *et al (33)* for Evans blue albumin (EBA) leakage frequency in 12 male normotensive Wistar Kyoto rats weighing approximately 500g. Aside from the different species and weight of rats that they used, another reason for our slightly higher values may be that EBA (~8 nm) and HRP (~6 nm) have slightly different diameters, both of which are far smaller than LDL (22nm). As noted, our smaller molecule HRP data should, and indeed seems to, show a slightly higher leakage frequency. Another source for this difference may be that, in determining the number of cells scanned, Lin divided the total endothelial surface area of each aortic segment by an average surface area $520\mu m^2$ (12.9μm radius) for a single endothelial cell. The single EC area measured in our lab on our rat species is $706\mu m^2$ (15μm radius). If we instead use $520\mu m^2$ in our calculation of the HRP leakage frequency, our result reduces to $5.7\pm1.23/10^4$ cells, much closer to Lin's EBA frequency of $4.71\pm2.86/10^4$ cells. The rabbit frequencies quoted above for LDL ($2.7/10^4$) and HRP ($1.9/10^4$) are slightly smaller, but both of these investigations used a rabbit aorta EC area of $300\mu m^2$(23).

The PA leakage frequency is roughly half that of the aorta. In rat aorta, the leakage frequency at the sites surrounding the intercostals branches of the aorta is approximately twice that of the non-branch areas(14). The rat aorta has more than 10 small branches, each having a far smaller diameters (~0.3mm) than the aorta (~3mm) and diverging from it at a sharp angle, over its ~5cm length. Assuming the branch area is

about 5 times the area of the branch vessel's cross section (46), we estimate the aorta's branch area fraction to be about 0.04. The PA has a simple Y-shape with the pulmonary trunk as its base and no other branches. The two pulmonary branches (left and right pulmonary arteries) are of nearly equal diameters (~1mm), much less of a mismatch with the trunk (~2 mm) than in the aorta, and the angle they make with the trunk is much closer to 180 degrees than in aortic branches. Thus there is far less change in the direction of flow and likely in the hydrodynamic shear during branching in the PA than in the aorta. This smaller disturbance may account for the PA's lower leakage frequency. The section of the IVC that we have examined has no branches, and thus has far less flow-and consequent shear-disturbance than the arteries. This is consistent with its having ~1/10 the leaks of the PA.

Shou(52) found very similar spot sizes in the PA and the aorta for comparable HRP circulation times despite their very different transmural pressures. Because of the equality of $Lp\Delta P$ in the PA and the aorta, one would expect a leak in each vessel to carry similar amounts of HRP into its wall. Differences in HRP drainage might nevertheless lead to different wall HRP concentrations. Our simple measurements of the integrated HRP intensity per unit spot area at 60 sec HRP circulation show that all three vessels appear to have similar integrated spots minus background HRP reaction product intensities. This seems to indicate that HRP also exits the PA as easily as the aortic wall, at least at 1 min circulation. Since the PA has only half the leaks of the aorta, the large difference in their susceptibility to atherosclerosis cannot only be due to its fewer leaks, but likely also depends on the details of the LDL transport once in the wall. It will be interesting to develop a detailed, structure-based transport theory to sort out how tracer entering the PA

wall distributes between the intima, where LDL binds to extracellular matrix, and media. Our group has already published such an aortic theory and is completing a similar PA theory.

The IVC is the largest vein in the body with a physiological pressure of 5mmHg. It has a much looser structure, much higher void space and hydraulic conductivity (Lp=5.8×10^{-7}cm/s/ mmHg(53)) than the arteries (Lp(aorta)=2.8×10^{-8}cm/s/mmHg). It lacks an internal elastic lamina to provide a clear intima-media boundary and has only rare fragments of elastin. Chuang(14) noticed that, unlike in the arteries, venous leaks are more often associated with dead/dying rather than mitotic cells. The junctions amongst the cluster of cells around a dying cell tend to leak, which accounts for the IVC's very large short-time HRP spots. The IVC's large leaks and LpΔP nearly identical to the arteries suggest a large lipid advection per leak into the venous wall. This begs the question, why is the IVC nearly immune to atherosclerosis? We find an IVC HRP leakage frequency ~$1/10^{th}$ that in the arteries and an integrated HRP reaction product spot-minus-background intensity similar to an arterial leak, despite the IVC spot's larger size. Thus, even though more HRP may be entering the IVC wall per spot, it likely also leaves faster, another symptom, like its far lower wall resistance, of its far looser wall structure. The balance apparently results in similar instantaneous HRP amounts per spot. Our integrated intensity measures, which depend on light intensity, are rough and only qualitative. Of interest, of course, is the rate of binding of LDL to intima extracellular matrix, which appears to lead to lesion formation. LDL or HRP entering the wall partitions between the intima and media and this partitioning may differ in different vessels depending on its relative intima and media structures. Measurements such as

reported here are projections through the tissue and cannot distinguish in which wall layer the tracer resides. We are currently doing confocal microscopy with a fluorescent HRP reaction product to resolve these distributions in three dimensions. Our group is also developing mathematical transport models to clarify tracer entry into and exit from the IVC wall and its intima/ media distribution there. The HRP spot leakage frequency coupled to theories for lipid transport and the kinetics of its binding to intimal extracellular matrix (18, 81) will allow us to compare the predicted rates of LDL entrainment in all three vessels. We can then see if/how they correlate with the aorta, the PA and the IVC's different disease susceptibilities to atherogenesis.

Atherosclerosis typically occurs in large, high-pressure arteries, not in low-pressure arteries or in veins. The vessels differ from each other in wall thickness, wall composition, transmural pressure, etc., and it is not obvious which of these differences is responsible for the different disease susceptibilities. A better understanding of what accounts for vessel immunity might lead to strategies/targets to lessen the disease risk in a patient's susceptible vessels. We have measured the macromolecular leakage frequencies in the susceptible aorta, the rarely susceptible PA and the immune IVC and found relative HRP leakage frequencies ~20:10:1 for these vessels. Despite the IVC's larger leakage spots, it lower leakage frequency and similar total HRP per spot appear to indicate its having far less tracer in its wall per unit vessel area than the arteries. This may be an important factor in the IVC's resistance to atherosclerosis.

Appendix

No. of Rat	P (mmHg)	Circulation Time /min	Aorta			Pulmonary Artery			Inferior Vena Cava		
			No. of leaks	No. of cells ($\times 10^6$)	Leakage Frequency ($/10^4$cells)	No. of leaks	No. of cells ($\times 10^6$)	Leakage Frequency ($/10^4$cells)	No. of leaks	No. of cells ($\times 10^6$)	Leakage Frequency ($/10^5$cells)
1			163	0.15505	10.51273	21	0.057219	3.67013	5	0.139737	3.578162
2			166	0.211542	7.847127	30	0.106336	2.821257	5	0.100774	4.961594
3			147	0.179601	8.184804	31	0.099871	3.104016	8	0.16907	4.731779
4		0.5	107	0.136875	7.817334	32	0.084637	3.780859	10	0.181749	5.502087
5			123	0.16111	7.634557	31	0.079206	3.913821	7	0.198261	3.530694
6			89	0.143467	6.203513	33	0.114554	2.880734	10	0.166595	6.002591
7	45		127	0.167501	7.582041	54	0.115589	4.671727	9	0.129096	6.971532
8		1	116	0.220715	5.255638	25	0.075769	3.299513	11	0.180134	6.106575
9			115	0.150806	7.625694	23	0.036382	6.321725	7	0.145433	4.813214
10			124	0.175182	7.078352	29	0.101003	2.871197	10	0.184419	5.422424
11		2	153	0.193848	7.892777	34	0.107396	3.165865	5	0.143739	3.478533
12			135	0.198892	6.787608	25	0.13218	1.891367	8	0.157252	5.087361
13			146	0.181707	8.034901	33	0.09036	3.652056	12	0.128691	9.324634
14			147	0.160145	9.179169	27	0.078513	3.438915	7	0.185286	3.777947
15		4	187	0.186564	10.02339	23	0.055302	4.158974	4	0.12712	3.146631
16			97	0.210529	4.607446	24	0.067392	3.56125	5	0.193	2.590667
17		0.5	123	0.254652	4.830122	21	0.071666	2.930269	9	0.223472	4.027348
18	45/		96	0.230938	4.156967	33	0.081872	4.030665	10	0.206722	4.837412
19	LA	1	92	0.2504	3.674128	25	0.116858	2.139353	4	0.205487	1.946596
20			211	0.220875	9.55292	22	0.092618	2.375354	8	0.157694	5.073104
21		4	200	0.24952	8.015389	35	0.081288	4.305653	5	0.250296	1.997632
22		0.5	206	0.315278	6.533916	30	0.067996	4.412006	6	0.207618	2.889922
23	45/	1	173	0.279787	6.183272	16	0.06459	2.477165	7	0.2503	2.796649
24	NP	2	197	0.306395	6.429611	29	0.09359	3.098618	6	0.21905	2.739096
25		4	185	0.311558	5.937895	31	0.077943	3.977244	13	0.211984	6.132538
26			210	0.23357	8.990865	24	0.097111	2.471405	11	0.219359	5.01462
27		0.5	317	0.314275	10.08671	22	0.08277	2.657967	5	0.206225	2.42454
28			243	0.297615	8.164903	27	0.103586	2.606538	9	0.249224	3.611204
29		1	280	0.292615	9.568901	24	0.089615	2.678132	5	0.18069	2.767177
30	100		218	0.288006	7.569288	23	0.098736	2.329453	7	0.184577	3.792449
31			185	0.287067	6.44448	21	0.067565	3.108137	10	0.178627	5.598253
32		2	142	0.309557	4.587195	23	0.073724	3.119748	7	0.177688	3.939488
33			265	0.314577	8.423997	36	0.086227	4.175005	10	0.159042	6.287628
34			248	0.261509	9.483437	27	0.073646	3.666162	9	0.215129	4.183532
35		4	210	0.279118	7.523702	23	0.076493	3.006818	10	0.186607	5.358861
36	180		172	0.193905	8.870315						
37			165	0.224775	7.34068						
38			212	0.255808	8.287463	30	0.123526	2.428648	5	0.121636	4.110624
39		0.5	180	0.246556	7.300573				4	0.088852	4.501872
40			170	0.250645	6.782493						
41			192	0.238577	8.047714	27	0.092316	2.924751	6	0.180574	3.322742
42			211	0.268291	7.864586				5	0.148959	3.356621
43		1	176	0.255877	6.878293						
44		2	249	0.234372	10.62414						
45			198	0.315353	6.278684						
46			219	0.241266	9.07713				7	0.177325	3.947557

47			167	0.264723	6.308488		
48			235	0.253276	9.278415		
49			205	0.259224	7.908216		
50			266	0.270794	9.822978		
51		**4**	177	0.255628	6.924112		
Average Leakage Frequency				$7.60/10^4$cells		$3.30/10^4$cells	$4.34/10^5$cells
Standard Deviation				$1.64/10^4$cells		$0.86/10^4$cells	$1.49/10^5$cells

Table 2.3. The complete raw HRP spot frequency data.

Chapter 3. The Effect of Acute Transmural Pressure on Water and Macromolecular Transport Processes in Rat Aorta

3.1 Introduction

Atherosclerosis is a well-known disease mainly of large arteries. It appears to begin with the delivery of low-density lipoprotein (LDL) cholesterol from the blood into the vessel wall, where it accumulates. Blood-borne monocytes enter lipid-laden subendothelial arterial intima regions and transform into macrophages as they and media-derived smooth muscle cells scavenge extracellular cholesterol (44, 47)When overwhelmed, they form foam cells, which appear to start the formation of the earliest lesions. These eventually thicken the arterial wall, narrowing the cross section for blood flow, making arterial wall less complaint and increasing the risk of a lesion rupture or of blockages.

A monolayer of the endothelial cells (10) separates the lumen from the thin, sparse subendothelial intima(26). Endothelial cells have junctions that are tight enough to severely restrict the trans-endothelial migration of molecules with sizes as small as that of albumin (~7 nm diameter). This raises the question: how can a 22 nm LDL particle penetrate the endothelium's tight junction? Many groups have proposed theories and performed experiments to explain the LDL's penetration of the endothelium. Frokjaer-Jensen's(19) thin serial sections belied the earlier proposed mechanism of free vesicles shuttling LDL and other large molecules across the endothelium by presenting a three-dimensional picture of these putative vesicles. The vesicles, which in isolated sections appeared to be free, tuned out in fact to be bound to one surface of the endothelium in another plane. Our group's collaborator proposed (74, 75, 82) and experimentally

substantiated (33, 34) the hypothesis that an important pathway for large molecule to cross the aortic endothelium (in the rat) was via the junctions that surround rare isolated cells, many of which are dying or dividing, whose junctions are temporarily not tight and therefore leak transiently. The result showed that 99% of the cells in mitotic (M) phase were associated with EBA (Evans blue albumin conjugate) leakage(20) and 80% of cells in M phase leaked the larger LY-LDL (Lucifer yellow-LDL)(67). Truskey et al.(66) used ^{125}I-LDL autoradiography to show that only 25% of leaks were associated with mitosis. Chuang *et al*.(14) performed similar experiments using horseradish peroxidase (HRP) as a tracer and mined their complementary, consistent data for more information. HRP was injected into rats through their femoral vein and circulated for various amounts of time before animal sacrifice. These experiments showed the growth of the tracer spot in the subendothelial space as function of time. Surprisingly, the HRP tracer spots in the rat's aorta grew extremely fast, reaching 200 μm diameter in only 2 min. These results were consistent with earlier similar experiments by Stemerman *et al*.(59). The rapid growth of these HRP spots at early times represented a challenge to the theorists. This phenomenon suggested that a convective, rather than a diffusive, mechanism is controlling here. In addition, even for a convection-dominant view, if the sub-endothelial tissue were of uniform structure (i.e., with uniform transport parameters), the transport theories could not produce tracer spots that were even close to the right size(82).

Our group and others have developed a number of theoretical models to describe the transport process in the aorta. The earlier one dimensional (20, 21, 65) models consider either diffusion or diffusion coupled with convection in direction normal to the endothelium and the early two dimensional models (67, 73-75) just 2D diffusion. One-

dimensional models cannot describe individual spots and the two dimensional models cannot describe the observed rapid spot growth unless one postulates diffusivities in the intima that are orders of magnitude too high to be realistic. Yuan *et al*.(82) first introduced a two-dimensional convection-diffusion model that separated the subendothelial tissue into an intima and a media, separated by an IEL barrier. Despite these added sophistications, by assuming that similar transport parameters characterized the intima and media their model still found spot growths an order of magnitude too slow. Frank and Fogelman's(18) ultra-rapid freezing technique revealed that the intima was practically void with over 90% space for albumin and 50% for LDL. In contrast, the media that had only about 8% void for albumin and less than 1% for LDL. Motivated by this enormous intimal void space, Huang et al.(25) constructed an *ab initio* fiber matrix theory to predict transport coefficients for the intima and found values that are one to two orders of magnitude larger than the corresponding media values. Huang et al.(25) used these parameters in a two dimensional, convective-diffusive transport model for the intima and media and found a very non-uniform pressure field in the sub-endothelial layer. The non-uniformity of the pressure field controls the distribution of water flux through the normal and leaky clefts and drives an appreciable transport parallel to the endothelium away from the leak. It is this flow that generates the observed very large tracer spots. Since the pressure drop across the intima is very small, the intima's normal velocity is nearly uniform and much smaller than the flow parallel to the endothelium at the leading order in the ·small) ratio of intima thickness to characteristic distance between neighboring leaks (25). The model's time-dependent numerical solutions for the concentration distribution in response to a step change in the lumen's tracer concentration

agrees well with the experimental spot growth. Its results for the concentration profiles as a function of distance from the center of a leaky cell after 10 min LDL circulation also agree well with data that one can cull from Truskey's (66) autoradiographic pictures of the radioactive LDL distribution about a leak for such an experiment. Atherosclerosis is a well-known disease mainly of large arteries. It appears to begin with the delivery of low-density lipoprotein (LDL) cholesterol from the blood into the vessel wall, where it accumulates. Blood-borne monocytes enter lipid-laden subendothelial arterial intima regions and transform into macrophages as they and media-derived smooth muscle cells scavenge extracellular cholesterol(44, 47). When overwhelmed, they form foam cells, which appear to start the formation of the earliest lesions. These eventually thicken the arterial wall, narrowing the cross section for blood flow, making arterial wall less complaint and increasing the risk of a lesion rupture or of blockages.

As we have seen, pressure is the driving force for the transport and therefore it is natural to consider the effect of pressure on this transport. Tedgui and Lever (63, 64) and Baldwin and Wilson (2, 3) each showed that the overall hydraulic conductivity (the ratio of the water flux through the wall to the pressure across it) Lp of the wall exhibited anomalous behavior with increasing transmural pressure ΔP. The intact wall's low pressure Lp value decreased by over 40% as the transmural pressure increased from 50 to 90 mm Hg and then remained constant thereafter up to the edge (180 mm Hg) of the physiological range. Shou et al. (52, 53)repeated these measurements of $Lp(\Delta P)$ on rat vessels and the aorta's nearly superimposed on Tedgui and Lever's Lp vs ΔP from rabbit aortas.

Our group's insight into the aortic intima's structure was crucial in explaining this behavior. Huang(26) postulated that under high transmural pressures, the intima would compress substantially from its unstressed value. Once the intima compressed to maximally, the intima's strong collagen fibers would resist further compression. Such compression would decrease the inter-fiber spacing, thereby decreasing its transport parameters and, more importantly, cause the endothelium to partially or totally block some of the IEL's fenestra, thereby drastically lowering the wall's hydraulic conductivity. To check this theory, our group developed a mathematical filtration model for the local flow into an IEL fenestra as a function of the degree of compression of the intima (26). Due to the paucity of data available at the time, this calculation used parameters taken from both rat and rabbit data. The result of this theory confirmed the strong alteration of the flow field due to fenestral plugging and, by comparison with Tedgui and Lever and Baldwin and Wilson's data, predicted that the intima's maximal compression was to 1/6 its unstressed value. The theory also provided, as an output, values of Lp_I as a function of pressure to be used in the model. By fixing rat aortas under pressure *in situ* and then viewing LM and EM sections, Huang et al then measured intimal layer thickness vs transmural pressure (27) and found surprisingly good agreement, given the simplifying assumptions in the model, with these predictions – a factor of five compression of intima with transmural pressure. (They find average intimal thicknesses of 0.62±0.26, 0.27±0.14, 0.15±0.10, and 0.12±0.07μm for 0, 50, 100, and 150mmHg lumen pressure, respectively, but the average diameter of a fenestral pore increases only 10 percent from 0 to 150mmHg.) Since then, the parameters that Huang et

al. had either taken from rabbit or guessed have been measured(53). Zeng (85) has corrected and modified this original theory using these newly available parameters.

As a sidenote, in this reference, we combined the intimal compaction theory with the overall convection-diffusion model of transport in the artery wall(26) to predict the time-dependent growth of HRP spots size in the arterial intima for several different transmural pressures with and without the effect of intimal compaction; see Fig 3.1. For an incompressible intima in which permeability properties are independent of luminal pressure, the long-time asymptotic spot size is independent of pressure; the higher pressure serves only to shorten the time needed to reach its asymptotic size. This is because the porous media flow is a Darcy, i.e. potential flow, whose stream lines are independent of the driving force. In contrast, with intimal compaction, the geometry and associated parameters change with pressure. As a result the model predicts that both the asymptotic size of the HRP spot at 4min and the time needed to reach its asymptotic size decrease when transmural pressure increases.

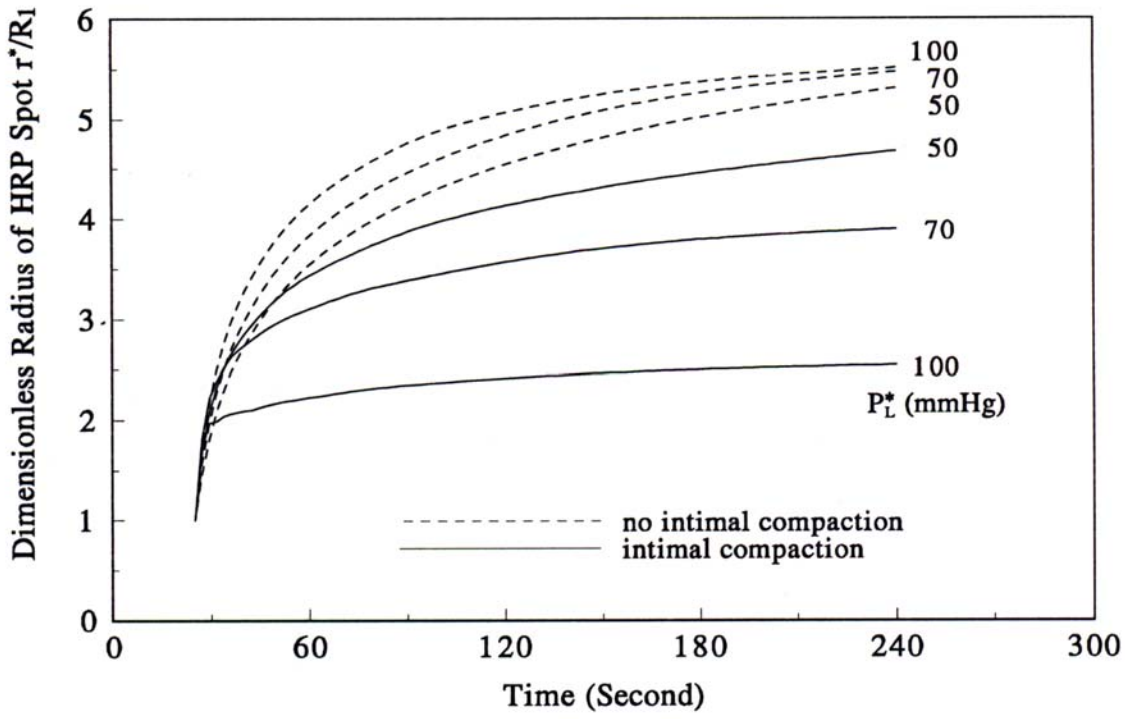

Figure 3.1 Predicted time-dependent HRP spot sizes for several different transmural pressures in arterial intima. (Huang et al. 1997)

We have now combined Zeng's corrected theory with the appropriate rat parameters with Huang et al.'s intimal compaction theory to recalculate the predicted spot growth as a function of transmural pressure both with and without compaction. The qualitative conclusions do not change. Below we present these quantitative theoretical predictions and test them experimentally.

Pharmaceuticals are common agents for inducing acute hypertension(49, 50, 71) and acute hypotension(49). Norepinephrine, as a naturally occurring catecholamine, increases blood pressure by acting on a type of adrenoceptor known as an alpha receptor in smooth muscle cells, causing blood vessels to contract. Nitroprusside(8) and labetalol(61) decrease blood pressure. Sodium nitroprusside breaks down in the blood

and releases nitric oxide (NO) which enters the muscle cells in the walls of the blood vessels and causes them to relax. Labetalol is an alpha-1 and non-selective beta blocker. Labetalol relaxes blood vessels by preventing the combination of catecholamine with the adrenoceptors. When the muscles relax, the blood vessels become wider and the blood pressure decreases.

The theory assumes that the only difference between vessels used is its ΔP, and not in its intrinsic vessel transport properties. Therefore, before using these pharmaceuticals to adjust the rat's acute blood pressure as a prelude to the HRP spot size growth experiments we examine the effect of the chemical on the aorta's Lp. We measure the Lp without and then with the proposed pharmaceutical on the same vessel ex vivo. If the chemical does not affect the vessel's Lp, as the theory presupposes, we can use it to adjust blood pressure in the HRP spot growth experiment. Otherwise we will adjust the blood pressure by non-drug induced methods. For example, both hypoxia and mechanically holding the exposed heart and lung to restrict their motion can induce acute hypotension. We then measure spot growth results in normotensive and acute hypertensive and hypotensive rats and compare with the theory.

3.2 Methods:

3.2.1Theoretical:

Water Filtration and its Boundary Conditions

The aorta has a continuous, quiescent endothelial layer covering the lumen side of the wall. A very thin layer of extracellular matrix, called the sub-endothelial intima, separates the endothelium and the IEL. The media, which is beneath the IEL, consists mostly of proteoglycans, elastic fibers and sheets and smooth muscle cells.

Following Huang(26) and Zeng(85), for a slab of the aorta wall we define a cylindrical coordinate system whose origin is at the center of a leaky cell and whose z-axis is perpendicular to the endothelium. The r coordinate is, in the context of the whole artery wall, a radial position in the "plane" "parallel" to the endothelium and we assume the problem is axisymmetric. Note, the wall's radius of curvature is negligible with respect to its thickness and thus we take the endothelial "plane" to be flat. By abuse of geometry (since circles do not tile the plane) we take a cylindrical slab of radius ξ (defined below) to be periodic. Let us begin with the fluid filtration problem. The lumen pressure is higher than the extravascular pressure and this transmural pressure drives a transmural flow. We assume that water (by which we mean the cell-free portion of the blood) enters the artery wall through all of the inter-endothelial junctions, but fluid that bears large solute molecules can only enter through rare, isolated leaky junctions. Since both the intima and the media are porous media, the transport through them is a Darcy (potential) flow, rather than a Navier-Stokes flow, i.e., for each of the intima and the media, one has

$$0 = \nabla^2 p_k^*,$$

$$u_k^* = -\frac{Kp_k}{\mu}\frac{\partial p_k^*}{\partial r}, \text{ and } w_k^* = -\frac{Kp_k}{\mu}\frac{\partial p_k^*}{\partial z}, \text{ k= i(intima), m(media), (1a-c)}$$

where u^* and w^* are the horizontal (r direction) and vertical (z direction) velocities, respectively. K_p (different for the intima and for the media) is the Darcy's permeability, μ is the fluid viscosity and p^* is the pressure. The asterisk represents a dimensional variable. The continuity equation, which expresses conservation of mass, for each of the intima and the media, is:

$$\frac{1}{r^*}\frac{\partial}{\partial r^*}\left(r^* u_k^*\right)+\frac{\partial w_k^*}{\partial z}=0,\ \text{k= i(intima), m(media). (2)}$$

The non-dimensionalizations are the following:

$$r=\frac{r^*}{L_m},\ z=\frac{z^*}{L_m},\ P=\frac{p^*-p_o^*}{p_L^*-p_o^*},\ Kp=\frac{Kp^*}{Kp_m},\ U=\frac{u^*}{Lp_m(P_L^*-P_o^*)},\ \text{and}\ W=\frac{w^*}{Lp_m(P_L^*-P_o^*)},$$

where L_m is the thickness of the media. P_L^* is the lumen pressure and, P_o^* is the pressure outside of the aorta. Kp_m and Lp_m are the Darcy permeability and hydraulic conductivity of the media, respectively. So, the nondimensional forms of the governing equations, after normalization, become:

$$U_k=-\frac{\partial P_k}{\partial r},\ W_k=-\frac{\partial P_k}{\partial z},\ \text{(3a, b)}$$

$$\frac{1}{r}\frac{\partial}{\partial r}\left(rU_k\right)+\frac{\partial W_k}{\partial z}=0,\ \text{k=i(intima),m(media).}\qquad (4)$$

Boundary conditions are needed at the three z-surfaces, the endothelium, the IEL (both assumed here to be infinitely thin) and the media-adventitial boundary, as well as at the centerline r=0 and at the edge r=ξ of the periodic unit. At r=0 and ξ, symmetry and the periodicity conditions lead to no flow in the r-direction:

$$U=0 \text{ at } r=0,\ \xi. \qquad (5)$$

At the media-adventitia boundary, the pressure is the fixed adventital pressure:

$$P_m(z=0)=0. \qquad (6)$$

At the IEL, W is continuous and the IEL is a barrier characterized by a hydraulic conductivity Lp i.e., the W is linearly related to the pressure difference. Thus

$$W_I(z=1)=W_m(z=1-L_I/L_m)=Lp_I(P_i(z=1)-P_m(z=1-L_I/L_m)) \qquad (7)$$

Where L_I is the thickness of IEL. Huang et al.(25), by using a simplified periodic unit model for the fenestral pore interaction, found the hydraulic conductivity of the IEL to be

$$L_{p_I} = \frac{W_f \phi_I}{1 - W_f \phi_I} \tag{7a}$$

where $\phi_I = a_f^2 / \xi_I^2$ is the fractional area of the fenestra in the IEL, a_f the mean radius of the fenestra, and $2\xi_I$ the mean distance between the fenestrae. The water velocity, W_f, through the fenestra is

$$W_f = \frac{(L_m / L_I)(K_{p_1} / K_{p_2})}{1 + G_0 (L_m / L_I)(K_{p_1} / K_{p_2})}, \tag{7b}$$

$$G_0 = \Phi_I + \sum_{n=2}^{\infty} \frac{2 a_f J_1(\mu_n a_f)}{\mu_n^2 \coth(\mu_n) \xi_I^2 J_0^2(\mu_n \xi_I)}$$

where $J_0(x)$ and $J_1(x)$ are the zeroth and the first order Bessel functions, and μ_n (n = 1, 2, 3, …) are the roots of the eigenvalue equation $J_1(\mu_n \xi_I) = 0$.

At the endothelium's normal junctions (the nondimensional lumen pressure is 1),

$W_i = Lp_{nj}(1-P_i)$ at $R_2 < r < \xi$ and $z = 1 + L_i/L_m$; (8)

Where L_i is the thickness of the intima.

At the endothelium's leaky junctions,

$W_i = Lp_j(1-P_i)$, at $R_1 < r < R_2$ and $z = 1 + L_i/L_m$; (9)

$W_i = 0$ at $0 < r < R_1$ and $z = 1 + L_i/L_m$ (10)

where the subscripts I, nj, j correspond to the IEL, the normal endothelial junctions and the leaky junctions, respectively. Yuan et al.(82) modeled the hydraulic conductivity of the leaky junction, normalized by L_{pm}^*, as

$$L_{p_j} = \frac{(\Delta R)^2}{12 \mu L_l L_{p_m}^*} \tag{9a}$$

where L_l is the length of the leaky junction and μ the fluid viscosity, $\Delta R = R_2 - R_1$, is the average width of the leaky junction.

The Macromolecular Transport Problem and its Boundary Conditions

In a similar manner, one can define the convection-diffusion problem in this geometry, using as an input the velocity distribution from the above solution. Due to the complexity of the velocity field, this problem, subject to an initial condition of zero tracer (i.e., HRP) concentration in the wall and a lumen boundary condition of a fixed, non-zero lumen concentration corresponding to the above-mentioned experiment, requires a numerical solution. The solutions give tracer concentrations in the artery wall as a function of position (r,z) and time t. The nondimensional convection-diffusion equation for the tracer transport is:

$$\frac{\partial C_k}{\partial \tau} = \underline{\nabla} \bullet \underline{q_k}\ , \text{ k= i(intima), m(media).} \tag{11}$$

where $\underline{q_k} = (q_{kr}, q_{kz})$ is the nondimensional vector of solute flux in the r and z directions.

$$q_{kr} = -D_k \frac{\partial C_k}{\partial r} + Pe_{kr} C_k\ ,\ q_{kz} = -D_k \frac{\partial C_k}{\partial z} + Pe_{kz} C_k\ , \tag{12}$$

$$C_k = \frac{C_k^*}{C_L^*}, \tau = \frac{D_m^* t}{L_m^{*\,2}},\ D_k = \frac{D_k^*}{D_m^*} \tag{12a}$$

$$Pe_{kr} := \frac{f_k L_m^* U_k^*}{\gamma_k D_m^*},\ Pe_{kz} := \frac{f_k L_m^* W_k^*}{\gamma_k D_m^*},\ q_{kr} = \frac{q_{kr}^*}{D_m^* C_L^* / L_m^*},\ q_{kz} = \frac{q_{kz}^*}{D_m^* C_L^* / L_m^*}. \tag{12b}$$

C_k^* is the dimensional macromolecular concentration locally averaged over all phases present in the tissue in each of the intima or media. C_k for the region k is normalized by the lumen concentration C_L^*. Pe_{kr} and Pe_{kz} are the local Peclet numbers in the r and z directions that include the retardation coefficients f_k in their definitions. τ is the dimensionless time and D_k is the dimensionless diffusivity. f_k and γ_k are the retardation

coefficient, representing the ratio of the solute velocity to water velocity, and volume fraction for macromolecules, representing the fractional volume available for macromolecules per unit total tissue volume.

We begin with the initial condition that the wall is tracer-free, i.e..,

$$C_k(t=0)=0. \tag{13}$$

At the intima-media interface, the solute concentration in the fluid is continuous,

$$\frac{C_i}{\gamma_i} = \frac{C_m}{\gamma_m} \ \ at\ z = 1 \tag{14}$$

The boundary conditions in r are simple. At r=0, ξ, symmetry and periodicity for both the intima and IEL require no flux:

$$\left.\frac{\partial C_k}{\partial r}\right|_{r=0,\xi} = 0\,. \tag{15}$$

Before moving to the z-boundary conditions, we note that both the endothelium and the IEL have significant transport through holes of far smaller dimension than the other scales of that surface and the holes that occupy a small fraction of that surface's area. The nondimensional tracer flux q_l through such a hole requires a local model on that scale. Ref (67) posits such a local, one-dimensional quasi-steady, convection-diffusion junctional model:

$$q_l = -\frac{\partial C_l}{\partial x} + Pe_l C_l \tag{16a}$$

where x is the direction normal to the endothelium along the junction (Figure 3.2),

$$Pe_l = \frac{f_l L_l W_l^*}{D_l^*},\ q_l = \frac{q_l^*}{D_l^* C_L^* / L_l},\ C_l = \frac{C_l^*}{C_L^*},\ x = \frac{x^*}{L_l}\,. \tag{16b}$$

L_l, Pe_l, f_l, and D_l^* are the height of the leaky junction, Peclet number, retardation coefficient, and effective diffusion coefficient in the leaky junction, respectively, for this local model whose output is an expression for q_l, which we then use in the model in (11)-(12). In the local model, the solute concentration, C_l, depends on x. The water velocity, W_l^*, in the leaky junction is uniform in the junction (from the continuity equation), which makes the Peclet number Pe_l well-defined. With the assumption of q_l independent of x, Eq. (16a) integrates directly to yield a relationship between q_l and the dimensionless solute concentration, C_{ls}, at the subendothelial side of the leaky junction. For the leaky junction with boundary conditions, $C_l = 1$ at x=0, $C_l = C_{ls}$ at x=1, this gives

$$q_l = Pe_l \frac{\exp(Pe_l) - C_{ls}}{\exp(Pe_l) - 1}; \tag{17}$$

Note the global Eq. (12) and local Eq. (16) models nondimensionalize q_l differently.

We return to the z-boundary conditions. If there is an endothelial ($z = 1+L_i/L_m$) leak,

$$q_{iz} = q_l, \ \frac{C_i}{\gamma_i} = C_{ls} \ for \ R_1 < r < R_2 \ and \ z = 1+L_i/L_m, \tag{18a}$$

$$q_{iz} = Bi(\gamma_i - C_i) \ for \ 0 < r < R_1, \ R_2 < r < \xi, \ and \ z = 1+L_i/L_m \, . \tag{18b}$$

where q_l is given by Eq. (17), the Biot number is $Bi := k_j L_m/D_m^*$ in which k_j is the endothelial mass transfer coefficient for diffusive transport across the endothelia. If there is no endothelial leak, then (18b) holds for $0 < r < \xi$, and $z = 1+L_i/L_m$.

The continuity of flux condition at the IEL-media interface leads to the local average tracer flux through the IEL(31) that matches the flux in media (q_m) and the flux in the intima(31):

$$q_i(z=1) = q_m(z=1-L_I/L_m) = q_I \tag{19}$$

where $q_m = \frac{\partial c_m}{\partial z} + Pe_{m,z} c_m$ and $Pe_{m,z} = w_m^* L_m / D$.

We assume q_I is proportional to the fractional area ϕ_f of the fenestrae and equals

$$q_I = \phi_f \, q_f, \tag{20}$$

where q_f is the tracer flux in the fenestra

$$q_f = d_1 C_i(t) - d_2 C_m(t), \tag{21}$$

where $d_1 = Pe_1 / (1-\exp(-Pe_1))$, $d_2 = d_1 \exp(-Pe_1)$, and $Pe_I = w_I^* L_m / D_I$, which is in terms of the diffusivity D_I in the fenestra.

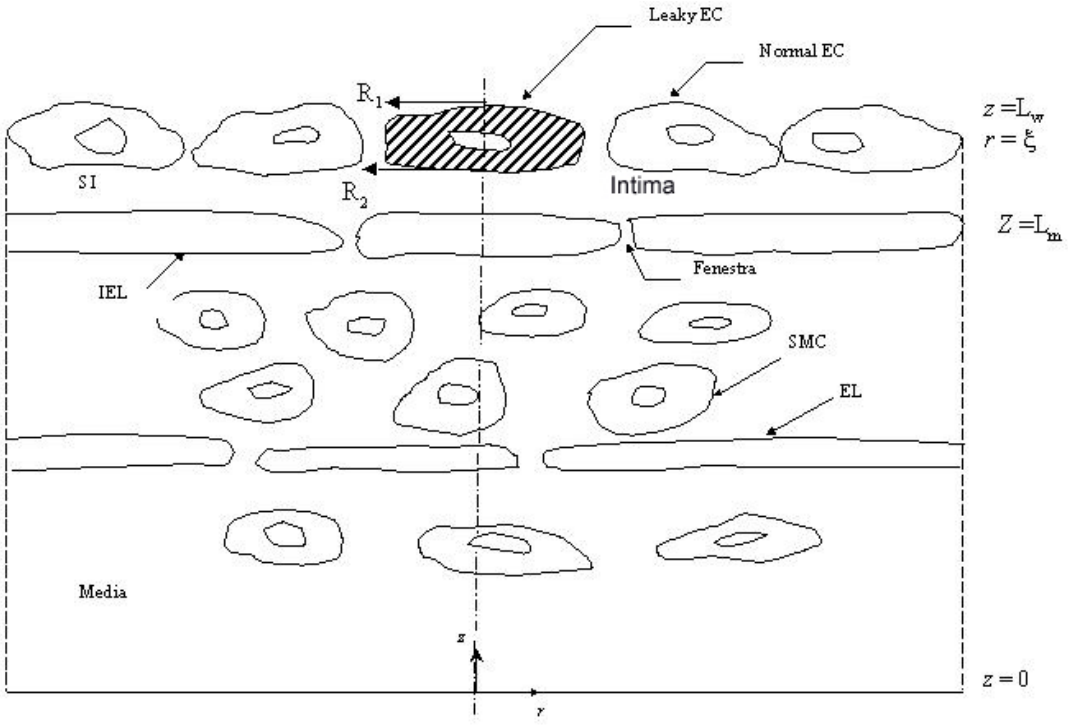

Figure 3.2 Schematic model for the aorta.

The solutions for the concentration distribution can be obtained numerically. As described in Zeng's paper, we choose a direct discretization, finite differences approach for both models. The discretized filtration model becomes a (large) number of

simultaneous linear algebraic equations equal to the total number of mesh points, which can be solved with MATLAB (The MathWorks, Inc.). For the macromolecular transport model, we choose the Hopscotch Method, a fast second order partial differential equation solver. This method, a type of finite difference technique described in(22), is fast, efficient, and unconditionally stable.

To determine the edge of HRP spot size from the numerical solutions, we calculated the HRP concentration profile $C_i(r, z, r)$ for various times and integrated them dz across the vessel wall. After comparison we just use C_i to decide the HRP reaction visibility because HRP mainly exists in the intima. We can achieve consistent HRP spot size even by using C_i and integrated concentration in z for the HRP reaction visibility. We used a threshold C_i of 0.1 to repeat Huang's prediction, as Huang used.

Parameter values

Table 3.1 gives Huang's and Zeng's parameters used for HRP spot size growth without intima compaction, along with the references for these values.

Table 3.1 Baseline values of constants and parameters

L_i (nm) Ref.(12, 25)	500	γ_m Ref(63).	0.08 (albumin)
L_{IEL} (μm) Ref.(82)	1	γ_i Ref.(25)	0.92 (HRP)
Lm (μm) Ref.(75)	200	f_j Ref.(25)	1.0
R_l (μm) Ref(66, 75).	15		
ΔR (nm) Ref.(75)	20	f_i Ref.(25)	1.0 (HRP)
ϕ Ref.(33)	0.0005	f_m Ref.(25, 85)	0.3 (HRP)
Lp_e(cm/s•mmHg) Ref.(64)	18.0×10^{-8}	D_i (cm^2/s) Ref.(25)	4.09×10^{-7} (HRP)

Lp_m(cm/s•mmHg) Ref.(64)	11.0×10^{-8}	D_{zm}(cm^2/s) Ref.(25)	8.4×10^{-9} (HRP)
Kp_i (cm^2) Ref.(25)	2.20×10^{-12}	D_{rm}/D_{zm} Ref.(82)	3.0
Kp_m (cm^2) Ref.(69)	11.97×10^{-15}	μ (g/cm•s) Ref.(24)	7.2×10^{-3}

In the introduction we quote Huang et al.'s(79) measurements for intima thickness, transmural pressure and wall hydraulic conductivities(53, 64) and the Darcy permeability(25). Table 3.2 shows the parameters that we have taken from Huang et al.(26) to predict HRP spot size growth with intima compaction.

Table 3.2 Parameters used in HRP spot growth curves with intima compaction

Pressure(mmHg)	50	70	100
L_i(nm) Ref.(79)	245	150	85
$K_p \times 10^{12}$(cm^2/S) Ref.(25)	0.82	0.4	0.18
$Lp_{IEL} \times 10^8$ (cm/s/mmHg) Ref.(26, 64)	10	9	6.2

3.2.2 Experimental:

Lp measurements, first without, then with a dissolved agent

Experimental Setup and Measurement Technique

Fig 3.3 shows the experimental setup. Two mercury sphygmomanometers control the pressure of two large volume air reservoirs that are connected to two separate solution reservoirs (A and B). Reservoir A1 & B1 contain phosphate buffered saline (PBS) solution with 4% (w/v) bovine serum albumin (BSA, Fraction V, Fisher Scientific), 20μM of $NaNO_3$ (Sigma, MO) and 0.03% (w/v) trypan blue. Reservoir A2 contains a

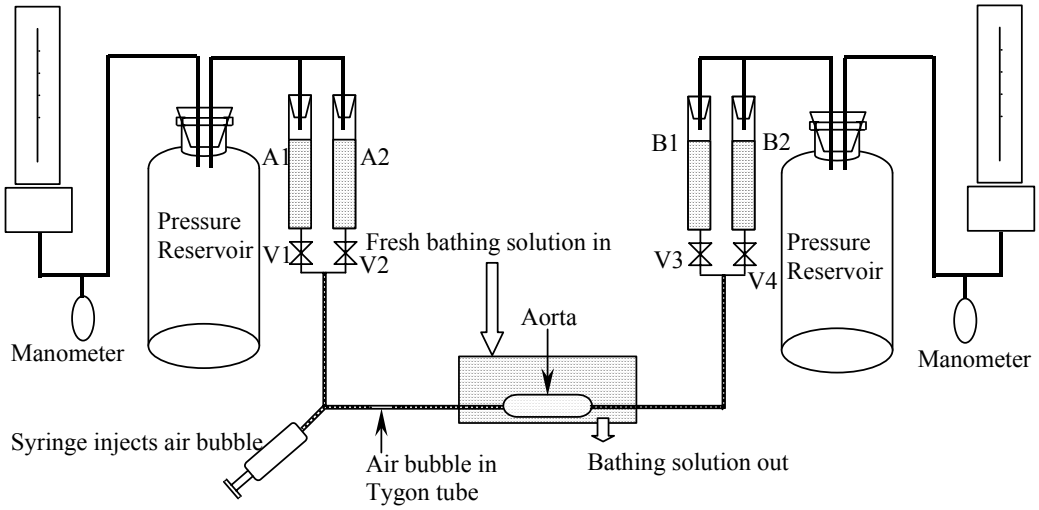

Figure 3.3 Schematic drawing of the pressurized setup. Two pressure reservoirs (A & B) are connected to the solution reservoirs (Res A1, A2, B1, B2). Res A1 and B1 contains trypan blue in PBS solution. Res B2 contains chemicals(norepinphrine, nitroprusside or labetalol) in PBS solution. The flows of each reservoir are controlled by the valves (v1, v2, v3 and v4).

chemical that can adjust blood pressure (norepinephrine, nitroprusside or labetalol) at the appropriate concentration (5μg/mL for norepinephrine, 2μg/mL for nitroprusside, 0.3mg/mL for labetalol) with 4% BSA in PBS solution. Reservoir B2 is a waste container. A three-way connector connects the solution reservoir A, a 5ml syringe and a horizontal, 120 mm Tygon catheter of inner diameter 0.5 mm mounted on a finely graduated ruler. The catheters are inserted into the two ends of the isolated aorta that is immersed in a bathing solution. The syringe injects an air bubble into the catheter and, once its velocity reaches steady state (~30 min), the position of its leading meniscus is recorded 9-10 times at 0.5 mm intervals. Solution incompressibility implies that the volume that it traces out per unit time (bubble velocity times catheter cross section) equals the flow rate through the vessel wall.

All chemicals are obtained from Sigma (St. Louis, MO) unless otherwise stated. Trypan blue serves two purposes. Blue dye appearing in the adventitia means the vessel has a leak (the dye's intensity relative to the clear bathing solution made even minute leaks easily visible), which we try to secure with surgical thread. If this is not successful, we discard the vessel. Also trypan blue is a vital stain that penetrates the membrane of non-viable cells (3, 63). The bathing solution (PBS with 4%BSA and 20μM $NaNO_3$, is identical to the perfusate, (except for the absence of trypan blue), so as to keep the osmotic pressures on both sides of the wall the same. (The concentration of trypan blue used does makes a negligible contribution to the osmotic pressure(53).) As in all previous similar studies (2, 64), we used a digital caliper (accurate to ±0.01 mm) to measure diameters and lengths from tie to tie of pressurized, excised vessels.

All protocols below were IACUC-approved.

Twenty-two healthy male Sprague-Dawley (SD) rats (Charles River, CT) that weigh between 350 and 400 g on a normal diet were used. Seven of the rats were given norepinephrine (experiments for four intact and three denuded aortas), six nitroprusside (three intact and three denuded aortas), seven labetalol (four intact and three denuded aortas) and the two controls only the drug-free perfusate (both with intact aortas to make sure the technology of changing solution has no effect on Lp). After anesthesia with 1% pentobarbital sodium (15 mg/500 g rat) we injected ~0.5 ml of heparin (1,000 units) intravenously to prevent blood coagulation. A rodent respirator kept the rat ventilated. After opening the chest and carefully dissecting the fat, we exposed the aorta from the rest of the fat and connective tissue and ligated the first three pairs of intercostal arteries. The aorta was cannulated with the solution from Reservoir A1 from the distal end and the

lumen side was rinsed with the same solution, pressurized at 60 mmHg to prevent vessel collapse. For the denuded aorta experiment the intact vessel was deendothelialized by inserting a glass rod with an Epon polymer tip of diameter 2.5 mm and working it back and forth. We then inserted a second cannulation from Reservoirs B right below the aortic arch, excised the vessel. The segment of the aorta was immersed in a solution bath as described above at 37^{o}C. The solution bath was changed every 30 min and air was continuously bubbled through it to keep the vessel oxygenated.

To begin the measurement, we closed valves 2, 3 &4, introduced a bubble into the horizontal catheter leading from Reservoir A1 at 40 mmHg, and then increased the pressure to the desired value. The experimental pressure is 180mmHg for norepinphrine, 45mmHg for nitroprusside and labetalol, and 45, 100, 180mmHg for the control. We determined the flow rate through the vessel wall by monitoring the movement of the bubble's front meniscus after it became steady, as described. The outer dimensions (length and diameter) of the vessel were measured. After completing the reference measurement on the vessel, we close valve 1 and opened valves 2 &4, and adjusted the pressure of Reservoirs B to 10mmHg less than that of Reservoirs A. Reservoir A2 perfused the vessel with pharmaceutical (norepinephrine, nitroprusside or labetalol)-containing (for control, same solution as in Reservoir A1) medium for 10 min. We then closed valves 2, 3 &4 and repeated the Lp measurement as the same pressure as before the introduction of the medium in Reservoir A2. After finishing the flow rate measurements, the vessel was fixed with 2% glutaraldehyde under pressure, stained with Harris' hematoxylin and examined under the light microscope to ensure that the endothelium had been totally removed or remained intact.

Calculations

We assume the aorta is cylindrical, and thus its outer surface area $A_S=\pi(36)L$, where OD and L are the vessel outer diameter and length, respectively. The bubble velocity V was determined as V= distance traveled/ time t of travel. Let ID be the inner diameter of the catheter. Since the solution is incompressible, the flow rate Q at steady-state through the vessel wall equals that traced out by the bubble in the tube, i.e., $Q=\pi(ID)^2V/4$. $Q=Lp \times A_S \times \Delta P$, where ΔP is the transmural pressure and A_S the vessel surface area $\pi((\text{vessel diameter})^2/4)(\text{vessel length})$, allowed us to determine the hydraulic conductivity Lp as function of ΔP. For the intact vessel, it represents the total Lp_t; for the deendothelialized vessels, it represents $Lp_{media+IEL}$ of Lp_{m+I}. If, as is standard in the field (16, 64), one assumes that Lps adds like linear capacitances in series, one calculates $Lp_{endothelium+intima}$ or Lp_wi from $1/Lp_t=1/ Lp_{m+I}+1/Lp_{e+i}$. To calculate the percentage resistance of the endothelium+intima, we take the average intact-vessel hydraulic conductivity Lp_t for a particular rat at a particular pressure, do the same for Lp_{m+I} and then use this formula to calculate Lp_{e+i} for that rat at that pressure.

HRP spot growth experiments:

To measure the rate of HRP spot growth, we follow the protocols used by Stemerman et al.(59) and Chuang et al.(14), repeated in brief below. All protocols below were IACUC-approved.

Experiments are reported on 16 male Sprague Dawley rats with acute hypertension (mean blood pressure 180mmHg measured from the right carotid artery), 16 male Sprague Dawley rats with normal blood pressure (mean blood pressure about 100mmHg measured from left femoral artery), 16 male Sprague Dawley rats with acute

hypotension induced by the hook method – see below (mean blood pressure 45mmHg measured from left femoral artery), 12 male Sprague Dawley rats with acute hypotension induced with nitroprusside, and 12 male Sprague Dawley rats with acute hypotension induced by labetalol. We monitored blood pressure during the entire experiments by using a blood transducer connected to a Powerlab/4SP (ADInstruments) with a real-time readout of the blood pressure from the computer.

Hypertension: We use a norepinephrine infusion to create acute hypertension in rats. Norepinphrine is dissolved in 5% dextrose in water to make 0.2mg/mL solution and infused intravenously through the right femoral vein during the spot size experiments on 16 rats in order to maintain their elevated (~1800 mmHg) blood pressure.

Hypotension: Method 1. With the rat's chest open, we use a metal hook to pull the heart and lungs to the right side, thereby limiting the range of motion of the beating heart. Adjusting the hook allow us to lower the rat's blood pressure to the desired value of 45 mmHg in 16 rats. Methods 2 and 3. Nitroprusside (Labetalol) was dissolved in 5% dextrose in water to make 75 μg/mL solution that we infused through the femoral vein (rates given below) of 12 rats (we use high concentration75 μg/mL. after infusion into the vein by micropump about 0.6mL we can achieve pressure of 45mmHg. In Lp experiment we use the diluted concentration 2μg/mL in the whole rat blood volume(about 24mL).) Both pharmaceuticals resulted in mean rat blood pressures of ~45 mmHg.

To prepare the HRP solution, we dissolve 0.58g NaCl in 100 ml distilled water to make normal saline; we then add 8mg HRP/100g rat in 1mL normal saline.

For the reference experiment under normal blood pressure, we anesthetize the rat with 1% Pentobarbital (30 mg Pentobarbital/kg body weight of rat) by intraperitoneal

injection. This solution is made by dissolving 100 mg Pentobarbital Sodium in 10 ml of distilled water and gently shaking the solution until the solute dissolves. We then shave the left leg, dissect it and find the femoral artery and vein. We separate the left femoral artery/vein, cannulate the vein for HRP and Heparin injection and canulate the artery for blood pressure measurement. For the pharmaceutical-induced hypertensive rats we intubate the trachea to a rodent respirator and cannulate the right carotid artery for blood pressure measurement. For the acute hypotensive rats we use the same method as in reference experiment to measure the blood pressure. We used a KDS100 micropump (KD scientific) to introduce the chemical through the femoral vein to adjust the blood pressure. The amount of the chemicals is: norepinephrine (10μg/hr for a 300g rat), nitroprusside (4μg/hr for a 300g rat) and labetalol (0.6mg/hr for a 300g rat). In the hook-induced acute hypoternsive rat experiment, we intubate the trachea to a rodent respirator and split the sternum longitudinally to expose the heart and lung and use the hook as described above. When the blood pressure reaches the desired value (norepinephrine: 180mmHg; nitroprusside, labetalol and hook: 45mmHg) for at least 15 mins, we inject 1ml HRP and 0.5 - 1ml Heparin (5000 units/ml, Elkins-Sinn Inc. NJ) through the cannulated microtubing. At 0.5, 1, 2, or 4 min blood circulation, we sacrifice the rat with an overdose of Pentobarbital and excise the thoracic aorta.

We prepare the excised vessel for examination by peeling away the connective tissues and the adventitia and fixing in Glutaraldehyde (Sigma)1% for 1 hour. Glutaraldehyde (1%) is prepared by adding 1 ml 50% Glutataldehyde to 50 ml PBS (Phosphate Buffered Saline) solution. We then rinse with PBS solution three time to wash out the fixative and use the HRP-DAB reaction to develop the tracer spot. The leakage

site will be brown the color of the reaction DAB production. The DAB solution is made by adding 5 ml 0.3M Tris (0.182 g Tris (MW=121.1) with 5 ml H_2O) to 25 g distilled water. After dissolving 0.045 g DAB, we add 20 μl of 30% H_2O_2. Finally, we add 1M HCl solution to adjust the pH to 7.0~7.4. The DAB reaction takes one hour. For best results, the DAB solution is changed at 30 min. After the reaction, we wash the tissue with PBS solution to clear any remaining residue from the reaction. Finally, we prepare the tissue slides for *en face* observation under the light microscope (Olympus BX51).

Typically one observes that small spots and regions of diffuse HRP staining regions coexist in the same aorta sample after all circulation times, i.e., 1/2, 1, 2 and 4 minute. Using NIH ImageJ (software from the NIH website), we measure the area of each observed spot from each of the vessels and calculate the radius of a circle having that area. A plot of the average spot size data for the aorta vs HRP circulation summarizes the data for each of five different conditions: 180mmHg (norepinephrine), 100mmHg (control), 45mmHg (hook method), 45mmHg (nitroprusside) and 45mmHg (labetalol).

Statistics Analysis

Paired Student' *t*-tests are used for comparison between tracer spot sizes for the different pressures at different times or between different pressures. ($P<0.05$, statistically significant)

3.3 Results:

We begin by successfully repeating Huang' prediction of time-dependent HRP spot sizes for different transmural pressures in rabbit arterial intima using their parameters. We then use the now-available experimental intima thickness, fraction area and diameter of fenestral pores in rats, Shou's Lp(ΔP) data localized HRP spot size as a

function of ΔP. For the blood pressure-altering pharmaceuticals that change Lp we calculate HRP spot sizes subject to Lp measured in the presence of those agents and compare theory with experiment.

3.3.1 Experiments:

The effect of pharmaceuticals used on Lp of intact and denuded aorta of rats:

As a control (Fig. 3.4), we measured Lp(ΔP), flushed with pharmaceutical-free perfusate, and remeasured Lp(ΔP) on the same vessel at the same pressures. The remeasured values were well within the standard deviation of measuring Lp(ΔP) on the same vessel without intermediate flushing. So the technique introduced no artifacts.

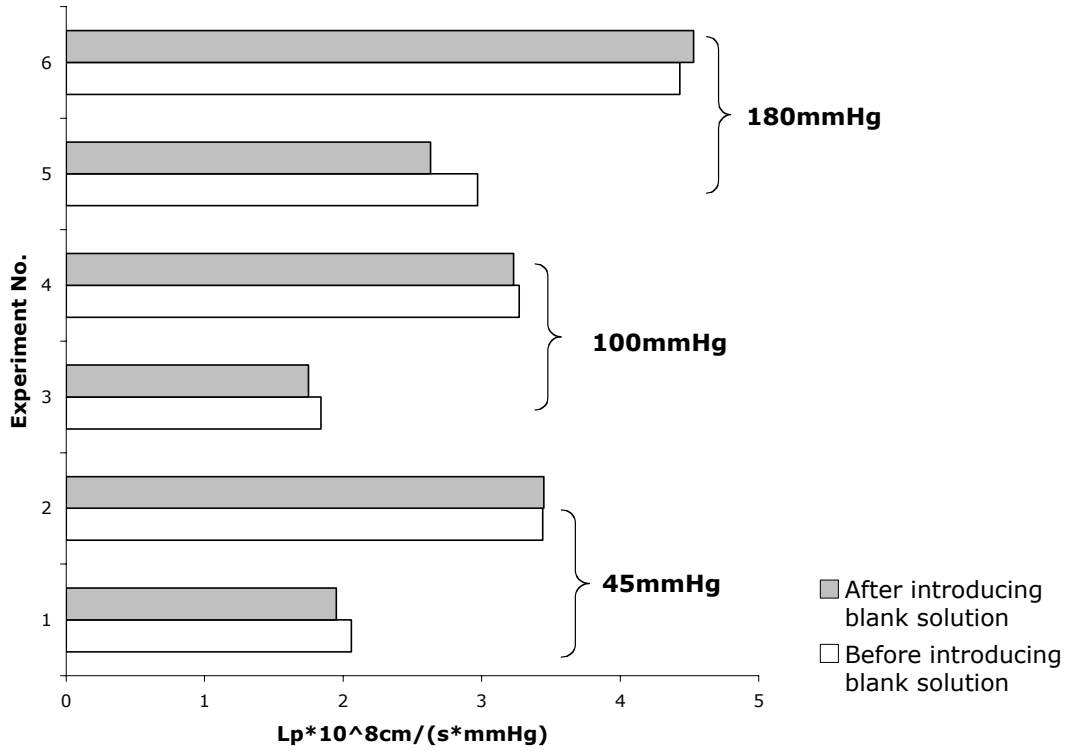

Figure 3.4 Control experiment of Lp on intact aorta.

Fig. 3.5 shows the Lp value of intact and denuded aorta (Lp and Lp_{I+m}) before and after norepinephrine introduction at 180mmHg(we are only interested in the Lp at

180mmHg). The difference is within the error bars of multiple drug-free measurements on the same vessel. In contrast, Fig. 3.6 (7) show the Lp of intact and denuded aorta (Lp and Lp_{I+m}) before and after introducing nitroprusside (labetalol) at 45mmHg. Both nitroprusside and labetalol cause similar substantial Lp increases both for intact and for denuded aortas, despite their different mechanism of action.

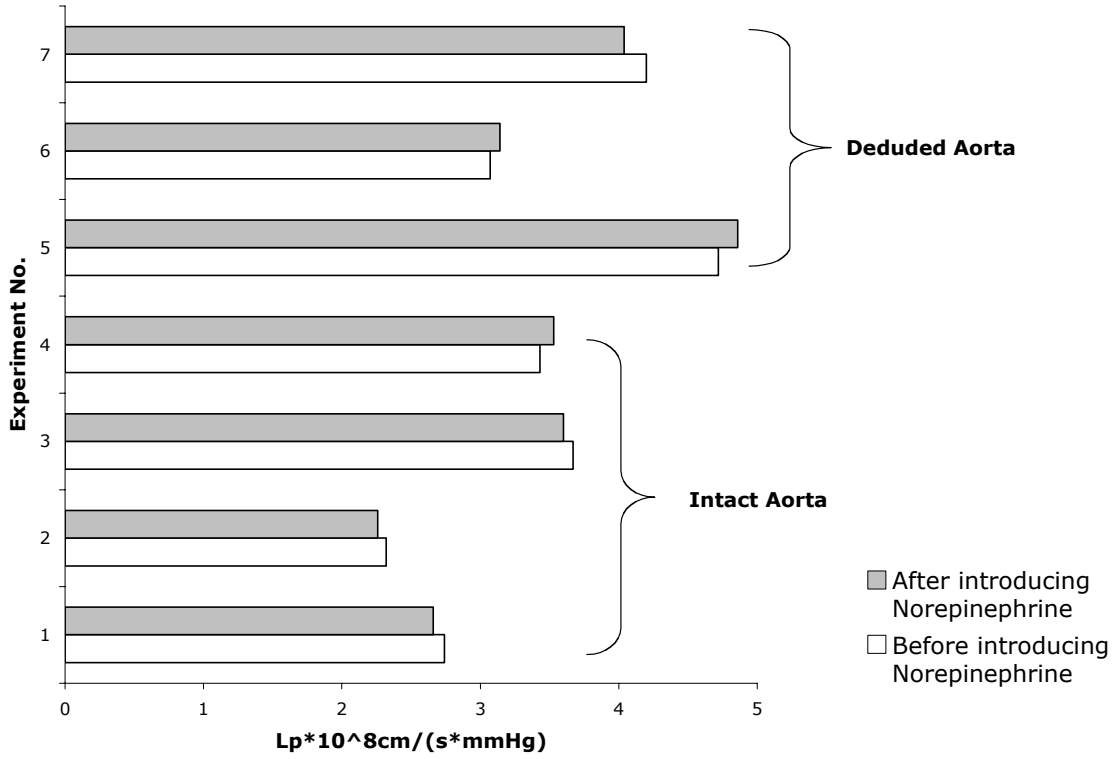

Figure 3.5 The effect of norepinephrine on Lp of aorta at 180mmHg.

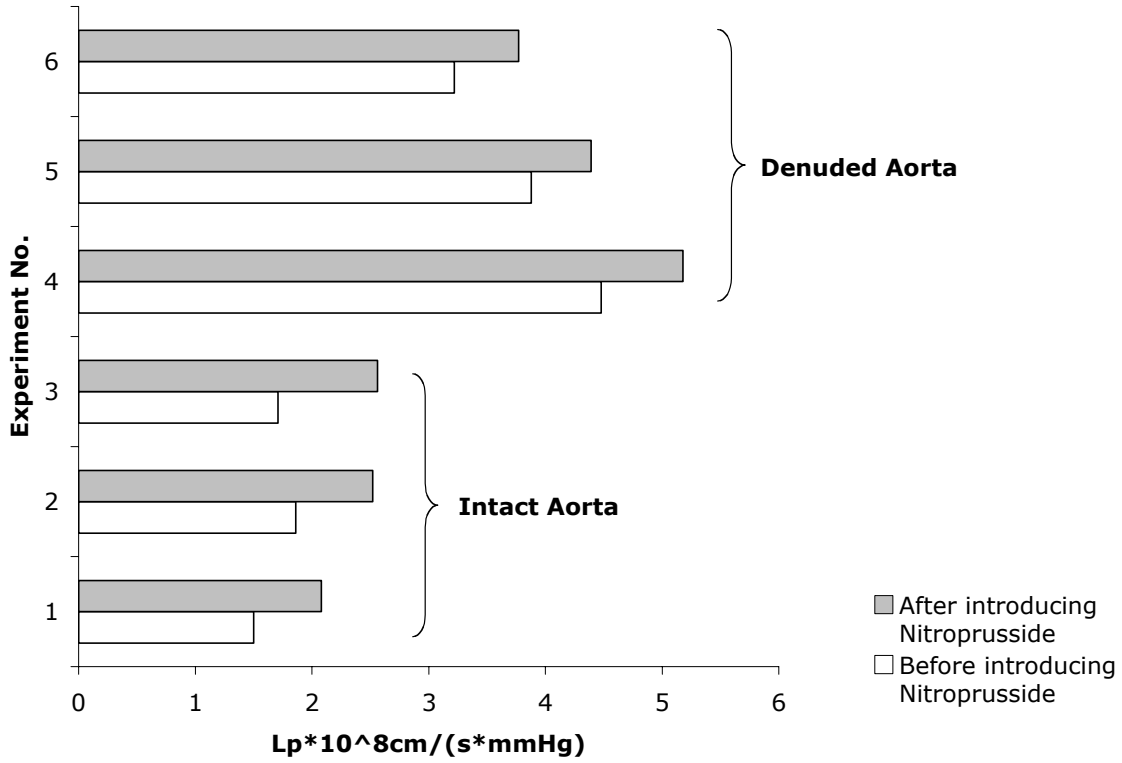

Figure 3.6 The effect of nitroprusside on Lp of aorta at 45mmHg.

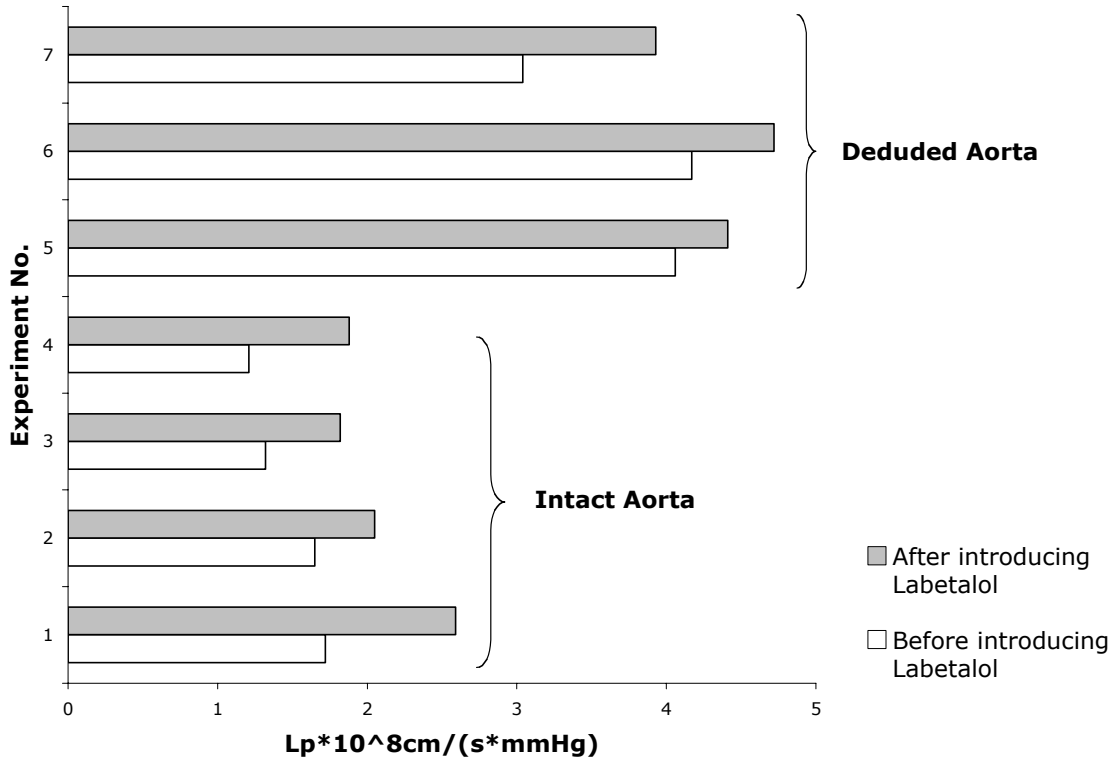

Figure 3.7 The effect of labetalol on Lp of aorta at 45mmHg.

3.3.2 Theoretical predictions for HRP spot growth as a function of ΔP:

We first use Huang et al's(79) parameters about intima thickness vs. ΔP and our Lp results in Fig. 4 to successfully reproduce Huang et al.'s prediction; see Fig. 3.8. We then included Huang et al.'s data for rat aortic intima thickness, fractional fenestral area and diameter, Shou's rat Lp(ΔP) as in Zeng et al.(85), and again reproduced earlier results for HRP spot size vs time for different ΔPs; see Fig. 3.8 again.

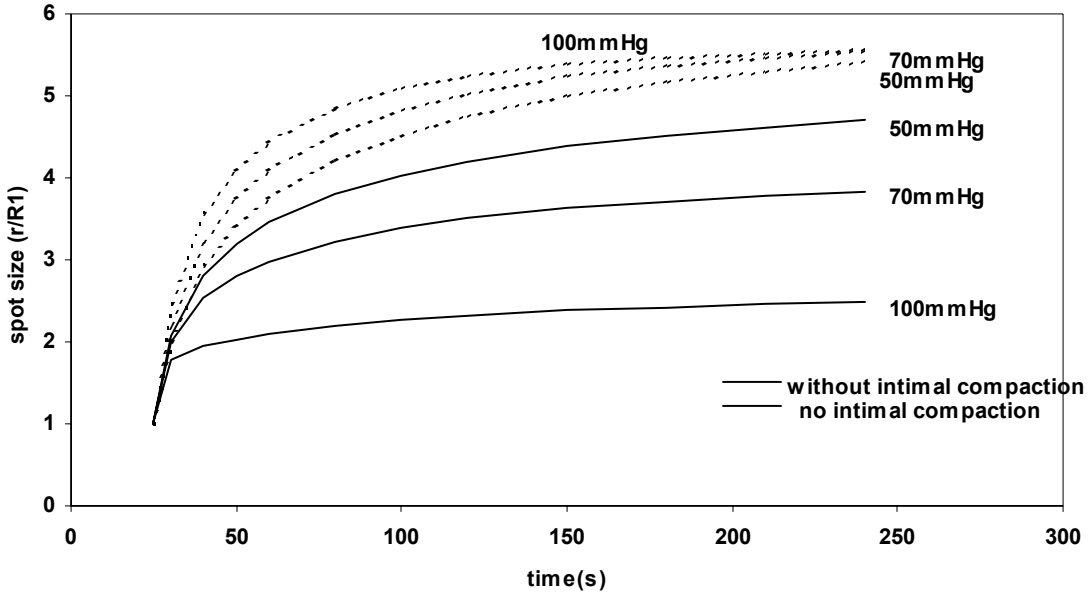

Figure 3.8 Predicted time-dependent HRP spot sizes for several different transmural pressures by repeating Huang's prediction.

Fig. 3.9 shows the theoretical predictions with our measured Lp values in the presence of nitroprusside and labetalol and compares with pharmaceutical-free curves at various ΔPs. These calculations show that the maximum predicted difference between HRP spot sizes with and without the agents nitroprusside and labetalol occurs at the lowest pressure (45mmHg) used at the longest circulation time (4 min). Both nitroprusside and labetalol increase aortic Lp, which increases transmural water velocities and therefore the Peclet number in the intima $Pe_i=f_irU_i/(\gamma_iD_i)$. The smaller mismatch in intima to media Lp generated smaller HRP spots. To fit the experimental and theoretical HRP growths below, we choose a threshold value of Ci =0.022 and use this absolute cutoff throughout.

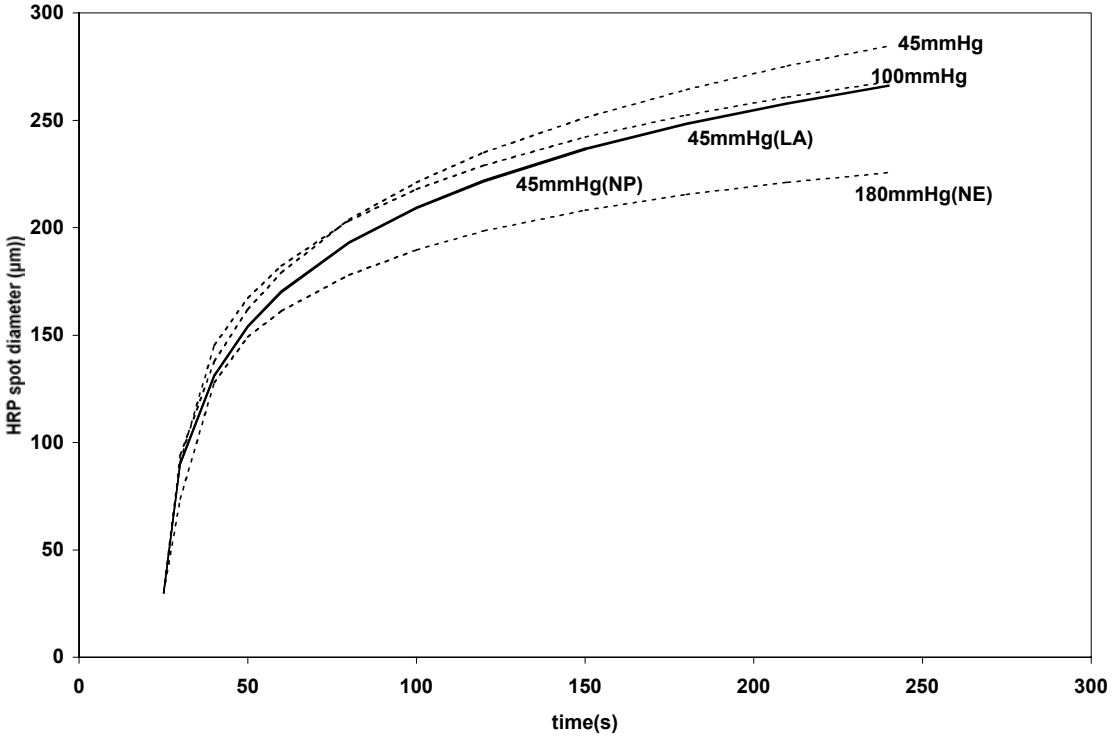

Figure 3.9 Predicted HRP spot size growth in the compressible intima at different pressures. (NP: Nitroprusside; LA: Labetalol; NE: Norepinephrine)

3.3.3 Experimenal results of HRP spot growth

For normal rats (mean arterial blood pressure ~100mmHg), Figure 3.10 shows that HRP spot sizes increase rapidly in the aorta with increasing circulation time, consistent with Chuang *et al*. and others(14, 51). At 30s the diameter of the HRP spots is already ~100μm. From 30s to 1min, the spot diameter increases an additional 60%($P<0.05$), reaching 165μm. Beyond 1min, spot growth slows, increasing only 45%($P<0.05$) from 1min to 2min and 11%($P<0.05$) from 2min to 4min. In norepinephrine-induced acute hypertensive (mean arterial blood pressure ~180mmHg), the HRP spot size (Fig. 3.10) at 4 min is about 19%($P<0.05$) less than at normal blood pressure and the spots needs less time to reach its asymptotic size – it is nearly complete

by 30 s - at hgh than at normal pressures. In hook method-induced acute hypotensive rats (mean arterial blood pressure ~45mmHg), the HRP spot size at 4min is ~6%($P<0.05$) larger than at normal pressure. Fig. 3.10 compares these data with our earlier theoretical predictions and shows very good agreement. In particular, the predicted differences in spot size are indeed significant and in good agreement with the model.

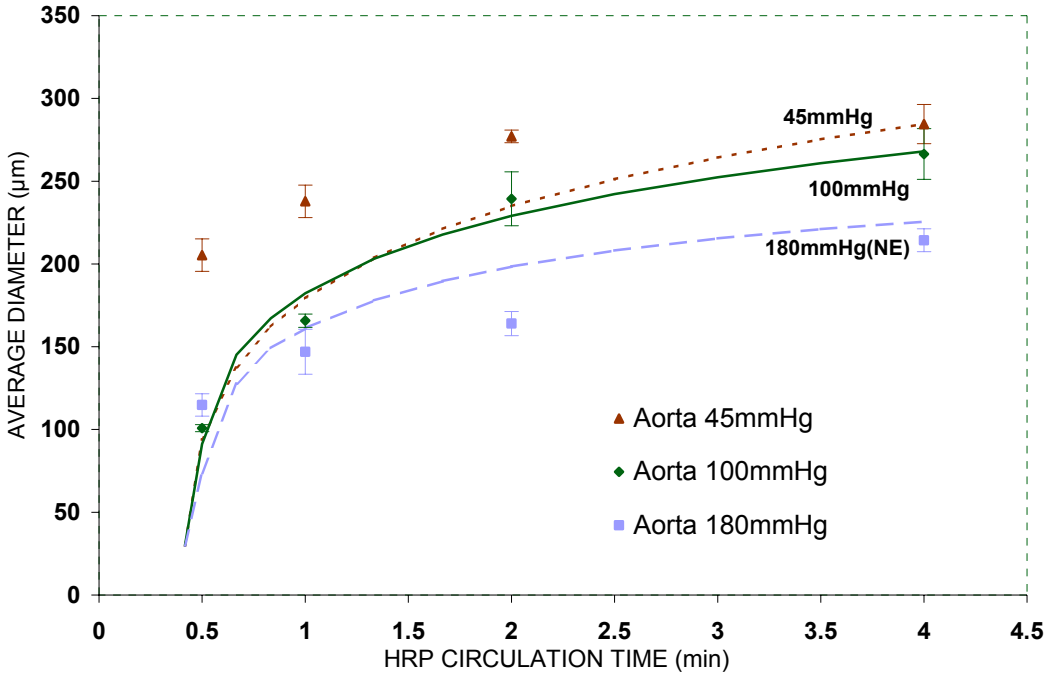

Figure 3.10 HRP spot growth in the aorta of normal rats, acute hypertensive rats (norepinephrine method) and acute hypotensive rats (hook method).

Both the theoretical predictions and the experimental results for HRP spot growth as a function of circulation time in the presence of labetalol or of nitroprusside show (Fig. 3.11) 45 mmHg HRP spots that grow very similarly($P>0.1$) to spots in pharmaceutical-free normotensive rat aortas, which are smaller($P<0.05$) than for hook-induced hypotensive rats.

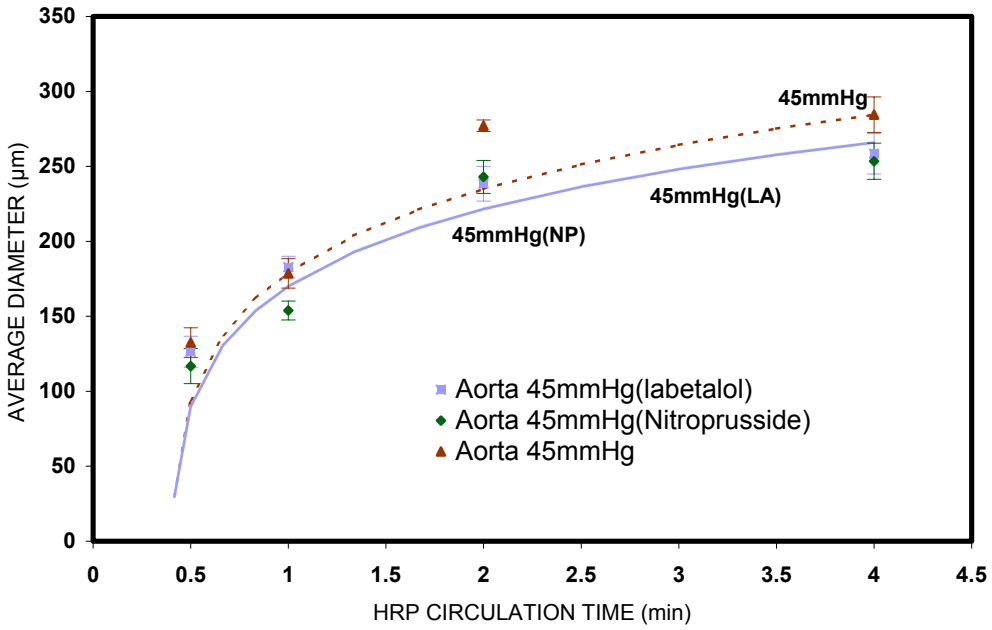

Figure 3.11 HRP spot growth in the aorta of acute hypotensive rats at 45mmHg: hook method, chemical methods (Laberalol and Nitroprusside), compared with baseline and hook method.

3.4 Discussion

In recent years our group has come out with a number of theories on different length scales for water and macromolecular transport in the artery wall. Until the present work, these theories have, with the exception of Huang et al.'s intimal compaction predictions(26), mainly been used to explain pre-existing data. Yet, when combined, these theories indeed make some intriguing, testable predictions. The motivation for this of this paper is to use it to make such predictions for HRP spot size growth in an artery with a compressible intima and to perform such experimental tests. These predictions initially assume that only ΔP, and not other wall transport parameters, change, and therefore we tested each method of adjusting ΔP for its potential effect on vessel Lp.

When there is no effect, we use the theory as is; otherwise we used the altered Lps for new predictions.

In the aorta the tracer HRP (~5nm diameter, (11)) transports across the endothelium at rare isolated leaks, rather than uniformly, for short circulation times <~5min. It follows, given the difficulty of albumin (~8nm diameter) in traversing EC tight junctions, that the much larger LDL (~22nm diameter) should follow the same trend, likely at even at much longer circulation times. Our HRP spot growth measurements for normotensive rats are consistent with Chuang et al.(14) and Shou et al(52) in our lab. Our results are slightly larger than Chuang's HRP spot growth results, but the error bars overlap. This slight difference may be due to the judgement of the person doing the analysis as to defining the precise spot border. All of these papers verify that HRP transport in the aorta is focal at these circulation times. Once across the intima, HRP spot spread is fast and, as Huang et al showed(25), convection dominated. Our new program reproduces Huang et al's spot growth predictions when using Huang et al's parameters. Interestingly, Zeng et al (85) found that replacing Huang et al's guessed parameters with those from Huang et al's(25) structure-derived ones (e.g., fenestral fractional area) and Shou et al's rat Lp data(53) (which agree with Tedgui and Lever''s rabbit values(64)) and correcting those that were incorrectly estimated (including the methods for extracting Lp for the endothelium, IEL and media from Lp of the intact and denuded vessel), can also reproduce those predictions (their Fig. 3.1 & our Fig. 3.8) with only minor alterations of certain internal parameters that are very hard to measure and in the threshold value of Ci for HRP reaction product's visibility.

Both theory and experiment agree that HRP spots in norepinephrine-induced acute hypertensive rat aortas are smaller and have faster rise times than in normotensives. As the transmural pressure increases, the intima compresses. This reduces intimal Lp and the tracer's hindered diffusivity. The driving pressure pushing HRP across the endothelium increases but so does the wall's flow resistance. The combined effect is that HRP has a harder time spreading in the intima. Ignoring intimal compaction leads to spots of nearly the same asymptotic size as normotensives, contrary to observation, but with the hypertensives reaching their asymptotic sizes far faster. The reason for this is that Darcy filtration is a potential flow. When the geometry, i.e., intimal thickness, is independent of ΔP, the stream lines are pressure independent. Increasing the pressure simply increases the velocities along the stream lines without changing their shapes. Except for diffusion effects, which are small at large Pe, the long-time asymptotic spot size are independent of pressure; higher pressure only shortens the time needed to reach its asymptotic size.

Lower transmural pressure yields the opposite trends, i.e., larger spots that rise more slowly, and the reasoning is the same: lower ΔP means thicker intima, leading to larger intima Lp, tracer diffusivity, available volume for HRP and retardation coefficient that give larger, more slowly growing spots (Note that it is the phenomenological parameter Lp_{e+i} calculated as the difference of resistances, that reflects the lumped effects of intmal compaction.) The HRP growth experiments in the aortas of hook-induced hypotensive rats also agree with our theoretical predictions with intimal compaction and disagree with those that do not.

What does all this mean physiologically? What we have seen is that at higher acute transmural pressures, the spot growth, reflecting the rate at which blood-borne

tracer enters the vessel wall, where it can wreak havoc, decreases. This would seem to be a good thing with respect to atherogenesis. However, it is well-known that the vessel's media remodels in response to chronic hypertension, becoming thicker and more cellular(36), which can change the entire picture of transport. Moreover, as two of my labmates, Tieuvi Nguyen and Jimmy Toussaint, have been showing the intima appears to also adjust its Lp over time in response to chronic change sin blood pressure. As such, it is very hard to extrapolate regarding the mass transfer situation from acute to chronic hypertension

Another question is what are the effects of antihypertensive drugs on mass transfer into the vessel wall. Nitroprusside and labetalol relax the aorta vessel wall by acting on the smooth muscle cells in the media through different mechanism. The relaxation of smooth muscle cells increases Lp of the media, which lowers the mismatch of intima to media Lp. This can partially redirect intimal flow that would otherwise be parallel to the endothelium toward the media, leading to smaller spots, as tracer is more quickly pushed from the intima into the media by this flow. Note that, in contrast to the intimal compaction that lowers overall wall Lp, this decrease in spot size is not due less tracer entering the wall, but to its quicker exit from, i.e., lower concentration in, the intima.

3.5 Conclusions

The present investigation provides experimental evidence in support of Huang et al's(26) hypothesis that the intima compresses under transmural pressure loading. We have followed Zeng et al(85) by combining Huang et al's two dimensional, convective-diffusive transport model in the intima(25) with Huang et al's theory of intima

compaction under pressure loading(26) and modified them for the parameters that have since been measured (Huang et al's(79) measurement of structural changes vs ΔP, Shou et al's Lp measurement as a function of ΔP(53), both in the rat aorta) to predict effect of intimal compaction on spot size growth as a function of ΔP. The theory predicts that, as ΔP rises, the rise time and the asymptotic size of HRP spot growth in the intima decrease. With an eye towards testing the theory experimentally, since the theory assumes that only the pressure, and not the wall transport properties, change, we test various pharmaceuticals for their effects on intact and denuded wall Lp. Having settled on methods that leave wall properties unchanged, we then experimentally test the predictions by doing HRP spot growth experiments in the aorta of acute hypertensive, hypotensive and normal rats. The results agree well with theory for both acute hyper and acute hypotensive rats. Moreover, adjusting the theory for the measured changes in intact and denuded wall Lp of other blood-pressure altering agents, led to predictions for spot growth that also agreed well with experiment. In aggregate, these results lend further support to the theory of intimal compaction and its effect on transport in the artery wall. The short-term effects of *acute* hypertension appear to be positive, i,e., to decrease mass transfer into the wall. However, this study says nothing about the long term effects of chronic hypertension, since the wall remodels severely in such cases, thereby radically changing the mass transfer problem.

This and previous HRP spot growth studies do, however, suffer from an obvious drawback. The theory makes predictions for the axisymmetric, three-dimensional tracer concentration as a function of time, but the experiments by nature represent the integration dz of the tracer concentration over the vessel wall. Wouldn't it be a far better

and more stringent test of the theory if one could measure the three-dimensional spot growth, without integrating dz? Using confocal microscopy and a fluorescent HRP reaction product his will be the subject of Chapter 4.

Chapter 4. 3-D imaging and the theory of HRP leakage spots in rat aorta

4.1 Introduction

Atherosclerosis is a disease mainly of large arteries, becoming evident when the arterial wall thickens near the lumen(68). Atherosclerosis appears to begin with the delivery of low-density lipoprotein (LDL) from the blood into the vessel wall, where it accumulates. Blood-borne monocytes enter the arterial intima in regions with high subendothelial lipid concentration, becoming macrophages that attempt to scavenge the extracellular cholesterol lodged in the intima. When overwhelmed, they, along with other smooth muscle-derived scavenger cells, progress to form foam cells. This accumulation of lipid and necrotic cells appears to comprise the earliest lesions (55, 58) that can develop into stenoses leading to blockage, rupture or clot formation.

Since the aorta is the largest major vessels where the disease develops, other large arteries, such as the corotid, are much more likely to clog first. Yet its size and consequent relative ease of handling has made the aorta the focus of numerous studies. The aorta typically consists of a monolayer of endothelial cells (10) at the luminal side, a sub-endothelial intima and an internal elastic laminar (IEL), below which is the tunica media that comprises circa 99% of the total vessel wall thickness. The media have a repeated structure of elastin and smooth muscle cells (SMC). Stemerman *et al*. (59) found that large macromolecular tracers do not cross the endothelium uniformly at short circulation times, but rather focally. Weinbaum *et al* (73) proposed a mathematical model for macromolecular leakage assuming that it proceeds through transiently open or poorly formed endothelial cell junctions, many of which are associated with cells in mitosis or

with dying cells. The normal endothelial cell junction is ~7 nm wide (5, 6, 35, 40, 57), which is far smaller than the size of an LDL molecule (22 nm). Lin *et al*. (33) observed the association of both Evans Blue albumin and Lucifer-Yellow LDL crossing of the endothelium with cells in M-phase of mitosis. Various measurements (33, 34, 66) have associated a fraction of these leaky cells with mitotic and dying cells. Lin *et al*. found that 99% of cell in mitosis leaked, while Truskey *et al*. found 25% of the leakage sites were associated with cells in mitosis.

Chuang *et al*. (14) studied the growth of horseradish peroxidase (HRP) tracer spots around such an isolated leak as a function of tracer circulation time and found spot growth that, in retrospect, was too fast to be consistent with a purely diffusive transport for any reasonable diffusivity. Various mathematic models have since attempted to explain this tracer spot growth. Early mathematical models of macromolecular transport in the vessel wall (20, 21, 65) were one-dimensional – with variation only in the direction normal to the endothelium – and were thus unable to address the issue of isolated spot growth. Early two dimensional models (67, 73, 74, 76) incorporated only limited structural information about the wall (generally they considered the endothelium and lumped the rest of the wall into a uniform medium) and considered diffusion alone, or convection/diffusion mainly in the direction normal to the endothelial surface, and could not describe the observed spot growth. Yuan *et al*. (82) proposed a two-dimension convection/diffusion model that included the intima region and the IEL explicitly, with the IEL assumed to be an appreciable transport barrier so as to encourage the transport parallel to the endothelium evident from the experiments. By assuming that the porosities

and characteristic transport parameters of intima and media were the same, they were, however, also unable to account for the observed spot growth.

Since convection clearly plays a leading role in this spot growth, it is important to understand the fluid filtration problem before attacking the mass transport. Tedgui and Lever (64) measured the transmural flow at 70 mmHg and 180 mmHg on the same vessel by observing the velocity of an air bubble in a horizontal catheter connecting the pressurized water reservoir with the rabbit's isolated vessel's lumen. Baldwin and Wilson (2) extended the pressure range of this experiment on rabbit aorta from 50 mmHg to 150 mmHg and performed it at 25 mmHg increments on the same vessel, first in its intact state and then denuded of its endothelium. The aorta's low pressure value decreased by over 40% as the transmural pressure increased from 50 to 90 mm Hg and then remained constant thereafter up to the edge (180 mm Hg) of the physiological range. Huang *et al*. (25) noticed that Frank and Fogelman's ultra-rapid freezing/rotary shadow etching study (18) revealed that the structure of the subendothelial intima was ultra-porous. Their *ab initio* theory for the intimal transport parameters showed that the intima provided almost two orders of magnitude less flow resistance than did the media. Huang *et al* 's model incorporated these radically different, structure-based parameters for the intima and media into a two-dimensional convection/diffusion model similar to Yuan, but with modeling errors corrected. With all of the major model parameters now fixed and not free to be adjusted to fit the experiments, their results predicted that a convective flow in the intima, mainly in the direction parallel to the endothelium, spread tracer that had been advected into the aortic intima through a leaky junction, thereby quickly forming large spots that agreed with experiment. Eventually, the overall transmural–pressure driven

flow caused the tracer to seep into the media. Thus, on the basis of the theory's ability to explain the radius of HRP spots vs circulation time, it appears that the early time filtration and macromolecular transport into the aortic wall is reasonably well understood, i.e., theory and experiment agree. Huang et al.(26) developed a theory of intimal compaction under transmural pressure loading to explain Tedgui and Lever and Baldwin and Wilson's findings about the variation of the rabbit aorta's hydraulic conductivity with transmural pressure. In Chapter 3 and Chapter 5, we combine their results with the convection-diffusion theory for macromolecular transport in the vessel wall to predict the effect of changing tansmural pressure on HRP spot growth and use such spot size measurements to test Huang's intima compaction theory at different transmural pressures and by altering wall conductivity through the blocking of a water channel molecule called aquaporin 1.

Until now all tracer distribution experiments viewed spots by illumination below the tissue and observation from above. This resulted in experimental integration of the tracer absorption intensity across the tissue perpendicular to the endothelium. Our 2-D filtration and convection-diffusion model in cylindrical coordinate, axisymmetric about the z axis yields the tracer concentration as a function of r (in the endothelial plane) and z (normal to it) in the vessel wall. Comparison with previous experiments required one of two methods. One was to assume that most of the tracer was in the intima and then compare the theoretical intima concentration profile with experiment(26). This method ignored tracer in the media. The second method was to integrate the theoretical result across the tissue and then to compare with experiment(85, 89). Clearly integration is error

smoothing. A more demanding test of the theory would be a comparison of theory with a spot experiment that resolved the tracer in the z-direction as well.

Confocal microscopy (41) is an optical imaging technique used to increase micrograph contrast and/or to reconstruct three-dimensional images by using a spatial pinhole to eliminate out-of-focus light or flare in specimens that are thicker than the focal plane. The confocal microscope images only molecules that fluoresce. Computer control directs the system to scan sequential planes in the Z-direction for the fluorescing species, stores them, and creates overlays of the various in-focus Z sections. This information can also be used to create three-dimensional images, or movie rotations of specimens. The confocal microscope has become an invaluable tool for a wide range of investigations in the biological and medical sciences for imaging thin optical sections in living and fixed specimens ranging in thickness up to 100 micrometers. In our case, one can either use a tracer that itself fluoresces or, given the use of horseradish peroxidase as a tracer, to choose a substrate for developing the HRP whose reaction product fluoresces. 10-Acetyl-3,7-dihydroxyphenoxazine (ADHP, or Amplex Red) is just such a substrate for HRP. ADHP is not fluorescent, but its HRP-catalyzed oxidation product, Resorufin (red fluorescent compound), does. ADHP is widely used to detect both H_2O_2 and HRP(28, 62, 77).

Below we carry out HRP tracer experiments on rat aortas at different circulation times and, after development with ADHP, take confocal images of the resulting HRP spots. In order to compare these results with the theoretical predictions, there is one remaining issue: one must locate the theoretical cylindrical coordinate in the vessel wall. The problem becomes to determine where the origin is and to tilt the specimen so that the

experimental and theoretical endothelial planes coincide as best as possible. That is, we use an optimization approach to adjust the positions of the origin and the tilt angles of the endothelial planet so as to minimize the least square error between experiment and theory. We choose Bremermann's method(7) of unconstrained global optimization for this six parameters optimization. This method is based on the chemotactic behavior of bacteria and efficiently and rapidly finds very good approximations for the global maximum or minimum of a real-valued function of many variables, even when the function has many local maxima or minima.

4.2 Methods

4.2.1 Experiments

Sample preparation for confocal microscoye

All protocols below were IACUC-approved.

We anesthetize 2 male SD rats with 1% pentobarbital (30 mg/kg) i.p. and cannulate both the left femoral vein (for infusions) and artery (to monitor the blood pressure). We inject 1ml HRP (8mg/100g rat weight in normal saline) and 0.5 ~ 1ml Heparin (5000 units/ml, Elkins-Sinn Inc. NJ) through the cannulated microtubing. At 0.5 min (one rat), 1 min (the other rat) blood circulation, we sacrifice the rat with an overdose of Pentobarbital. We perfuse the aorta with PBS solution to wash out the blood for 10min before perfusion-fixing the aorta with Bouin's solution. We excise the thoracic aorta, place it in Bouin's solution overnight in the refrigerator, then rinse it with PBS three times and 70% ethanol three times (5min every time) to wash out the fixative. We cut the aorta open longitudinally along the ventral curvature, section it into several segments and run the ADHP-H_2O_2 reaction to produce fluorescent resorufin which links to HRP. To do

this, one mixes fresh 25μM ADHP in PBS solution with 11.6μM H_2O_2, places the aorta into the ADHP solution and lets it react for 1hr. One washes the aorta with PBS 6 times (5min every time) and make slides for investigation under the confocal microscope. We put one segment of vessel onto each slide with endothelium layer facing up. We use vectashield (Fisher Scientific) as mounting media, cover the segment with cover glass. At last we use nail polish to locate the edge of the cover glass on the slide.

3-D imaging of HRP spot in the aorta with confocal microscope

We use a Zeiss LSM 510 confocal laser scanning system to do the 3-D imaging of the tracer spots. The laser filter is LP560, green light. The objective magnification is 20X. We do Z-stack scan for each HRP spot. We scan part of sample with thickness ranging from 20 to 80μM. The number of slices ranges from around 30 to 100 since the thickness of each slice is 1.7μM. After each scan, the position of the slide will move 0.85μM in z direction and then the confocal microscope scans the next 1.7μM thick slice. The confocal microscope records the image in 512 by 512 pixels. From the 20 times objective magnification we know the size of each image is 420μM by 420μM. We can set the x-y dimension according to these information. One pixel means around 0.8μM by 0.8μM in x-y plane.

4.2.2Theory

As described in Chapter 3, we use a 2-D filtration and convection-diffusion transport models to describe the transport process in the aorta.

Water Filtration and its Boundary Conditions

The aorta has a continuous, quiescent layer of endothelium that covers the lumen side of the vessel wall. A very thin layer of extracellular matrix called the sub-endothelial

intima separates the endothelium and the IEL. The media, which is beneath the IEL, consists mainly of proteoglycans, elastic fibers and smooth muscle cells.

As in Chapter 3, for a slab of the aorta wall we define a cylindrical coordinate system whose origin is at the center of a leaky cell and whose z-axis is perpendicular to the endothelium. The r coordinate is, in the context of the whole artery wall, a radial position in the "plane" "parallel" to the endothelium and we assume the problem is axisymmetric. Note, the wall's radius of curvature is negligible (the radius of the aorta is around 1.5mm) with respect to its thickness (less than 0.1mm) and thus we take the endothelial "plane" to be flat. By abuse of geometry (since circles do not tile the plane) we take a cylindrical slab of radius ξ (defined below) to be periodic. Let us begin with the fluid filtration problem. The lumen pressure is higher than the extravascular pressure and this transmural pressure drives a transmural flow. We assume that water (by which we mean the cell-free portion of the blood) enters the artery wall through all of the inter-endothelial junctions, but fluid that bears large solute molecules can only enter through rare, isolated leaky junctions. Since both the intima and the media are porous media, the transport through them is a Darcy (potential) flow, rather than a Navier-Stokes flow, i.e., for each of the intima and the media, one has

$$0 = \nabla^2 p_k^*, \text{ i.e., } \frac{\partial^2 P_i}{\partial r^2} + \frac{1}{r}\frac{\partial P_i}{\partial r} + \frac{\partial^2 P_i}{\partial z^2} = 0$$

$$u_k^* = -\frac{Kp_k}{\mu}\frac{\partial p_k^*}{\partial r}, \text{ and } w_k^* = -\frac{Kp_k}{\mu}\frac{\partial p_k^*}{\partial z}, \text{ k= i(intima), m(media), (4.1a-c)}$$

where u^* and w^* are the horizontal (r direction) and vertical (z direction) velocities, respectively. K_{p_k} (different for the k=intima and for the k=media) is the Darcy's permeability, μ is the fluid viscosity and p^* is the pressure. The asterisk represents a

dimensional variable. The continuity equation, which expresses conservation of mass, for each of the intima and the media, is:

$$\frac{1}{r^*}\frac{\partial}{\partial r^*}\left(r^* u_k^*\right)+\frac{\partial w_k^*}{\partial z}=0,\ \text{k= i(intima), m(media). (4.2)}$$

The non-dimensionalizations are the following:

$$r=\frac{r^*}{L_m},\ z=\frac{z^*}{L_m},\ P=\frac{p^*-p_o^*}{p_L^*-p_o^*},\ Kp=\frac{Kp^*}{Kp_m},\ U=\frac{u^*}{Lp_m\Delta P^*},\ \text{and}\ W=\frac{w^*}{Lp_m\Delta P^*},$$

where L_m is the thickness of the media. P_L^* is the lumen pressure and, P_o^* is the pressure outside of the aorta. Kp_m and Lp_m are the Darcy permeability and hydraulic conductivity of the media, respectively. So, the nondimensional forms of the governing equations, after normalization, become:

$$U_k=-\frac{\partial P_k}{\partial r},\ W_k=-\frac{\partial P_k}{\partial z},\ \text{(4.3a, b)}$$

$$\frac{1}{r}\frac{\partial}{\partial r}\left(rU_k\right)+\frac{\partial W_k}{\partial z}=0,\ \text{k=i(intima),m(media).}\qquad (4.4)$$

Boundary conditions are needed at the three z-surfaces, the endothelium, the IEL (both assumed here to be infinitely thin) and the media-adventitial boundary, as well as at the centerline r=0 and at the edge r=ξ of the periodic unit. At r=0 and ξ, symmetry and the periodicity conditions lead to no flow in the r-direction:

$$U=0 \text{ at } r=0,\ \xi. \qquad (4.5)$$

At the media-adventitia boundary, the pressure is the fixed adventital (reference) value:

$$P_m(z=0)=0. \qquad (4.6)$$

At the IEL, W is continuous and the IEL is a barrier characterized by a hydraulic conductivity Lp, i.e., the W is linearly related to the pressure difference across the IEL. Thus

$W_I(z=1)=W_m(z=1-L_I/L_m)=Lp_I(P_i(z=1)-P_m(z=1-L_I/L_m))$ (4.7)

Where L_I is the IEL thickness. Huang et al.(25), by using a simplified one-dimensional model for the fenestral pore interaction, found the hydraulic conductivity of the IEL to be

$$L_{p_I} = \frac{W_f \phi_I}{1 - W_f \phi_I} \tag{4.7a}$$

where $\phi_I = a_f^2 / \xi_I^2$ is the fractional area of the fenestra in the IEL, a_f the mean radius of the fenestra, and $2\xi_I$ is the mean distance between adjacent fenestrae. This local model yields the water velocity, W_f, through the fenestra as

$$W_f = \frac{(L_m/L_I)(K_{p_1}/K_{p_2})}{1 + G_0(L_m/L_I)(K_{p_1}/K_{p_2})}, \tag{4.7b}$$

$$G_0 = \Phi_I + \sum_{n=2}^{\infty} \frac{2a_f J_1(\mu_n a_f)}{\mu_n^2 \coth(\mu_n) \xi_I^2 J_0^2(\mu_n \xi_I)}$$

where $J_0(x)$ and $J_1(x)$ are the zeroth and first order Bessel functions, and μ_n (n = 1, 2, 3, …) are the roots of the eigenvalue equation $J_1(\mu_n \xi_I) = 0$ in increasing order.

The nondimensional lumen pressure is 1. Let the subscripts I, nj, j correspond to the IEL, the normal endothelial junctions and the leaky junctions, respectively. Except at the endothelium's leaky junctions, we treat the endothelium as a continuous surface that presents a barrier to water transport that is characterized by an otherwise uniform hydraulic conductivity Lp_{nj}:

$W_i=Lp_{nj}(1-P_i)$ at $R_2 < r < \xi$ and $z=1+L_i/L_m$, (4.8)

where L_i is the thickness of the intima. The hydraulic conductivity Lp_j of the endothelium's leaky junctions is far higher than Lp_{nj}, and therefore in the leaky junction , one has

$W_i=Lp_j(1-P_i)$, at $R_1 < r < R_2$ and $z=1+L_i/L_m$. (4.9)

Finally, we assume there is no flow across the endothelial cell whose junctions leak, although this assumption can easily be relaxed(89). Thus,

$W_i = 0$ at $0 < r < R_1$ and $z = 1+L_i/L_m$ (4.10)

Yuan et al.(82) used a one-dimensional Poisseuille flow model for the hydraulic conductivity of the leaky junction, normalized by L_{pm}^{*}, to get

$$L_{p_j} = \frac{(\Delta R)^2}{12\mu L_l L_{p_m}^{*}} \tag{4.9a}$$

where L_l is the length of the leaky junction and μ the fluid viscosity, $\Delta R=R_2-R_1$, is the average width of the leaky junction.

The Macromolecular Transport Problem and its Boundary Conditions

In a similar manner, one can define the convection-diffusion problem in this geometry, using as an input the velocity distribution from the above solution. Due to the complexity of the velocity field, this problem, subject to an initial condition of zero tracer (i.e., HRP) concentration in the wall and a lumen boundary condition of a fixed, non-zero lumen concentration corresponding to the above-mentioned experiment for time t>0, requires a numerical solution. The solutions give the tracer concentration in the artery wall as a function of position (r,z) and time t. The nondimensional convection-diffusion equation for the tracer transport is:

$$\frac{\partial C_k}{\partial \tau} = \underline{\nabla} \bullet \underline{q_k}\text{ , k= i(intima), m(media).} \tag{4.11}$$

where $\underline{q_k} = (q_{kr}, q_{kz})$ is the nondimensional vector of solute flux in the r and z directions.

$$q_{kr} = -D_k \frac{\partial C_k}{\partial r} + Pe_{kr} C_k\text{ , } q_{kz} = -D_k \frac{\partial C_k}{\partial z} + Pe_{kz} C_k\text{ ,} \tag{4.12}$$

$$C_k = \frac{C_k^*}{C_L^*}, \tau = \frac{D_m^* t}{L_m^{*2}}, \; D_k = \frac{D_k^*}{D_m^*} \tag{4.12a}$$

$$Pe_{kr} := \frac{f_k L_m^* U_k^*}{\gamma_k D_m^*}, \; Pe_{kz} := \frac{f_k L_m^* W_k^*}{\gamma_k D_m^*}, \; q_{kr} = \frac{q_{kr}^*}{D_m^* C_L^* / L_m^*}, \; q_{kz} = \frac{q_{kz}^*}{D_m^* C_L^* / L_m^*}. \tag{4.12b}$$

C_k^* is the dimensional macromolecular concentration, locally averaged over all phases present in the tissue in each of the intima or media. C_k for the region k is normalized by the lumen concentration C_L^*. Pe_{kr} and Pe_{kz} are the local Peclet numbers in the r and z directions that include the retardation coefficients f_k in their definitions. τ is the nondimensional time and D_k is the nondimensional diffusivity. f_k and γ_k are the retardation coefficient, representing the ratio of the solute velocity to water velocity, and volume fraction for macromolecules, representing the fractional volume available for macromolecules per unit total tissue volume.

We begin with the initial condition that the wall is tracer-free, i.e..,

$$C_k(t=0)=0. \tag{4.13}$$

At the intima-media interface, the solute concentration in the fluid is continuous,

$$\frac{C_i}{\gamma_i} = \frac{C_m}{\gamma_m} \; at \; z = 1 \tag{4.14}$$

The boundary conditions in r are simple. At r=0, ξ, symmetry and periodicity for both the intima and IEL require no flux:

$$\left.\frac{\partial C_k}{\partial r}\right|_{r=0,\xi} = 0. \tag{4.15}$$

Before moving to the z-boundary conditions, we note that both the endothelium and the IEL have significant transport through holes of far smaller dimension than the other scales of that surface and the holes that occupy a small fraction of that surface's

area. The nondimensional tracer flux q_l through such a hole requires a local model on that scale. Ref (67) posits such a local, one-dimensional quasi-steady, convection-diffusion junctional model, which yields

$$q_l = -\frac{\partial C_l}{\partial x} + Pe_l C_l \tag{4.16a}$$

where x is the direction normal to the endothelium along the junction,

$$Pe_l = \frac{f_l L_l W_l^*}{D_l^*},\ q_l = \frac{q_l^*}{D_l^* C_L^* / L_l},\ C_l = \frac{C_l^*}{C_L^*},\ x = \frac{x^*}{L_l}. \tag{4.16b}$$

L_l, Pe_l, f_l, and D_l^* are the height of the leaky junction, Peclet number, retardation coefficient, and effective diffusion coefficient in the leaky junction, respectively, for this local model whose output is an expression for q_l, which we then use in the model in (4.10)-(4.12). In the local model, the solute concentration, C_l, depends on x. The water velocity, W_l^*, in the leaky junction is uniform in the junction (from the continuity equation), which makes the Peclet number Pe_l well-defined. With the assumption of q_l independent of x, Eq. (4.16a) integrates directly to yield a relationship between q_l and the dimensionless solute concentration, C_{ls}, at the subendothelial side of the leaky junction. For the leaky junction with boundary conditions, $C_l = 1$ at x=0, $C_l = C_{ls}$ at x=1, this gives

$$q_l = Pe_l \frac{\exp(Pe_l) - C_{ls}}{\exp(Pe_l) - 1}; \tag{4.17}$$

Note the global Eq. (4.12) and local Eq. (4.16) models nondimensionalize q_l differently.

We return to the z-boundary conditions. If there is an endothelial ($z = 1+L_i/L_m$) leak,

$$q_{iz} = q_l,\ \frac{C_i}{\gamma_i} = C_{ls}\ for\ R_1 < r < R_2\ and\ z = 1+L_i/L_m, \tag{4.18a}$$

$$q_{iz} = Bi(\gamma_i - C_i) \text{ for } 0 < r < R_1,\ R_2 < r < \xi, \text{ and } z = 1+L_i/L_m\,. \qquad (4.18b)$$

where q_l is given by Eq. (4.17), the Biot number is Bi := $k_j L_m/D_m^*$ in which k_j is the endothelial mass transfer coefficient for diffusive transport across the endothelia. If there is no endothelial leak, then (4.18b) holds for $0< r < \xi$, and $z = 1+L_i/L_m$.

The continuity of flux condition at the IEL-media interface leads to the local average tracer flux (31) through the IEL that matches the flux (q_m) in media and the flux (31) in the intima:

$$q_i\,(z=1)=q_m(z=1-L_I/L_m) = q_I \qquad (4.19)$$

where $q_m = \dfrac{\partial c_m}{\partial z} + Pe_{m,z}c_m$ and $Pe_{m,z} = w_m^* L_m \big/ D$.

We assume q_I is proportional to the fractional area ϕ_f of the fenestrae and equals

$$q_I = \phi_f\, q_f, \qquad (4.20)$$

where q_f is the tracer flux in the fenestra

$$q_f = d_1\, C_i(t) - d_2\, C_m(t), \qquad (4.21)$$

where $d_1 = Pe_1/(1-\exp(-Pe_1))$, $d_2 = d_1\exp(-Pe_1)$, and $Pe_I = w_I^* L_m \big/ D_I$, which is in terms of the diffusivity D_I in the fenestra.

The solutions for the concentration distribution can be obtained numerically. As described in Zeng et al(85), we choose a direct discretization, finite differences approach for both models. In order to integrate the filtration and the convection-diffusion problems and to simplify the calculations, one should use a single set of grid points for both. The central difference formulae for the first and second order derivatives for variable grid sizes are different from those under the classical uniform grid sizes and are defined as

$$f'(u) = \frac{f(u+h_2) - f(u-h_1)}{h_1 + h_2} \tag{4.22a}$$

$$f''(u) = \frac{h_1 f(u+h_2) + h_2 f(u-h_1) - (h_1+h_2) f(u)}{\frac{1}{2} h_1 h_2 (h_1 + h_2)} \tag{4.22b}$$

where $f'(u)$ and $f''(u)$ are the first and second order derivatives of $f(u)$ and h_1 and h_2 are the backward and forward differences of point u.

The numerical procedure for the filtration model is relatively simple. The discretization of the filtration model leads to a linear system consisting of a (large) number of linear algebraic equations equal to the total number of mesh points. MATLAB 6.5 (The MathWorks, Inc.) can solve this linear system in seconds. During discretization, one must treat the point at r = 0 carefully since Eq. (4.1) contains $\frac{1}{r}\frac{\partial P_k}{\partial r}$ which takes indeterminate form $\frac{0}{0}$ there. By Maclaurin's expansion,

$$\frac{\partial P_k}{\partial r} = \left.\frac{\partial P_k}{\partial r}\right|_{r=0} + r\left.\frac{\partial^2 P_k}{\partial r^2}\right|_{r=0} + \frac{1}{2} r^2 \left.\frac{\partial^3 P_k}{\partial r^3}\right|_{r=0} + \ldots, \tag{4.22c}$$

but according to Eq. (4.5), $\left.\frac{\partial P_k}{\partial r}\right|_{r=0} = 0$. So

$$\lim_{r\to 0} \frac{1}{r}\frac{\partial P_k}{\partial r} = \left.\frac{\partial^2 P_k}{\partial r^2}\right|_{r=0} \tag{4.22d}$$

Thus Eq. (4.1) at $r = 0$ can be replaced by

$$2\frac{\partial^2 P_k}{\partial r^2} + \frac{\partial^2 P_k}{\partial z^2} = 0 \tag{4.22e}$$

After solving the filtration model, one substitutes the velocity fields' solutions into the macromolecular transport Eq. (4.11). Just as Eq. (4.1), Eq. (4.11) contains two terms, $\frac{1}{r}\frac{\partial C_k}{\partial r}$ and $\frac{U_k}{r}$, that are singular at $r = 0$, and which resolve to

$$\lim_{r\to 0}\frac{1}{r}\frac{\partial C_k}{\partial r} = \left.\frac{\partial^2 C_k}{\partial r^2}\right|_{r=0} \tag{4.22f}$$

$$\lim_{r\to 0}\frac{U_k}{r} = -K_{p_k}\lim_{r\to 0}\frac{1}{r}\frac{\partial P_k}{\partial r} = -K_{p_k}\left.\frac{\partial^2 P_k}{\partial r^2}\right|_{r=0} \tag{4.22g}$$

where the solution to the filtration model has determined $\frac{\partial^2 P_k}{\partial r^2}$.

The discretized filtration model becomes a (large) number of simultaneous linear algebraic equations equal to the total number of mesh points, which can be solved with MATLAB (The MathWorks, Inc.). For the macromolecular transport model, we choose the Hopscotch Method, a fast second order partial differential equation solver. This method, a type of finite difference technique described in (22), is fast, efficient, and unconditionally stable. Based on the computational algorithm described in detail in(15), Eq. (4.11) can be written as

$$\frac{\partial C}{\partial \tau} = L(C) \tag{4.23}$$

where L is a convection-diffusion differential operator. With the forward difference in time and simple explicit and implicit approximations, Eq. (4.23) can be replaced by

$$C_{mn}^{k+1} = C_{mn}^{k} + \Delta\tau L_h(C_{mn}^{k}),\ \textit{if } m+n+k = \textit{odd} \tag{4.24}$$

$$C_{mn}^{k+1} = C_{mn}^{k} + \Delta\tau L_h(C_{mn}^{k+1}),\ \textit{if } m+n+k = \textit{even}, \tag{4.25}$$

where L_h is the finite difference replacement of the operator L and C_{mn}^{k}, the concentration at $\tau = \sum_{k=1}^{k} \tau_k$, $r = \sum_{m=1}^{m} r_m$, and $z = \sum_{n=1}^{n} z_n$, where τ_k, r_m, and z_n, k, m, and n = 1, 2, 3, …, are the changing intervals of τ, r, and z. Combining Eq. (4.24) with (4.25) gives

$$C_{mn}^{k+2} = 2C_{mn}^{k+1} - C_{mn}^{k},\ if\ \ m+n+k = even \tag{4.26}$$

which helps define the fast and efficient hopscotch algorithm as follows:

1) When k = 1, for all i, j satisfying m+n+k = odd, Eq. (4.24) is used to get C_{mn}^{2}.

2) For any k, m, and n satisfying m+n+k = even, Eq. (4.25) is used to get C_{mn}^{k+1}. If the computation is required to stop, print out the result; otherwise go to step 3).

3) For any k, m, and n satisfying m+n+k = even, Eq. (4.26) is used to get C_{mn}^{k+2}.

4) Increase k by 1, repeat steps 2) and 3).

The Hopscotch Method is unconditionally stable and converges for the linear differential operator L. Since the exact analytic or an *a priori* accurate solution is unknown, one adopts different refinements/sets of mesh points with decreasing grid sizes to test the accuracy until the differences between two sequential computations are small enough. The 2-D model for the case of no leaks in either endothelial aspect reduces to a 1-D model whose mass transport solution more easily lends itself to the standard Crank-Nicolson implicit finite difference method(56).

Using the above theory to predict outcome of above experiment

Unlike the experiments in previous works(14, 52, 59) that used the DAB reaction to detect HRP concentration, our methods involves the use of Bouin's fixative in order to minimized the native tissue's auto-fluorescence. This fixative is very strong, and, unlike in earlier works that use the DAB reaction, it is critical to thoroughly flush the blood

from the aorta with PBS for 10 min before perfusion fixing it with Bouin's solution. This wash period before fixation allows some of the HRP that entered the vessel wall during the time between HRP infusion and animal sacrifice to back-diffuse out of the tissue and into the PBS solution. Thus we model the initial period by an initial value problem whose initial condition is $C(r,z,t=0)=0$ and whose lumen concentration $C_L=C_0$ and integrate from $t=0$ to the HRP circulation time t_c. Then we solve a second initial value problem using the same equations, but where its initial condition is $C(r,z,t_c)$ from the first problem and its lumen concentration $C_L=0$, and integrate forward in time for the 10 min period of the washing at 100mmHg. It is this final concentration profile that we compare with experiment.

The confocal microscope scans the sample layer by layer. It would be convenient if the endothelium were the first layer, the layer beneath the second, etc. Unfortunately, the confocal microscope only tells us the exact position (in the direction perpendicular to the scan plane) of the image slices relative to the first image. Each image is comprised of values at automatically chosen sets of grid points ((r,z) or (x,y)) in n sequential planes. That is, the confocal microscope does not know where in the tissue the first layer that it scans actually is, i.e., we do not know where z=0 is. Neither do we know a priori, where r=0, i.e., the center of the leaky cell, is. Moreover, we do not know if the scan planes are exactly parallel to the endothelium. In fact, the geometry is an idealization of the true situation, e.g., the endothelium is in fact not really flat, and therefore it is not a priori clear what parallel to the endothelium really means. Thus, in order to compare with experiment, it is necessary to locate the coordinate origin in the tissue and to orient the axes with the tissue in an optimal manner.

Our approach is to allow these unknown parameters to be chosen as those that minimize the least square error between the theoretical prediction and the experimental results. The six unknown parameters are Δx, Δy, Δz, β, γ and c. The first three parameters are used to adjust the origin of the coordinate system. The fourth and fifth are the tilt angles by which we rotate the x and y axes in the tissue. The last parameter, c, is the unknown ratio of the concentration that derives from the theory to the experimental fluorescence intensity. Our approach is to begin by choosing (by eye) an alignment of the tissue with the theoretical coordinates and by guessing a rough value of c. The program then calculates the initial least square error by summing, over all confocal-microscope-generated grid points, the square of the difference of the experimental concentration values at each grid point minus the theoretical concentration at that grid point. We then use Bremermann's optimization(7) based on how chemotactic bacteria search for their chemotatic agent, to generate random guesses for these six parameters and to search for a global minimum of the least square error function. First the optimizer estimates error function for the initial estimate of the six parameters (X_0). Then it chooses a random direction r from a multivariate Gaussian distribution with a zero mean and a unit standard deviation. On the line determined by initial estimation of parameters and r the optimizer approximates the restriction of error function to this line by five-point Lagrangian interpolation, which is a fourth-degree polynomial. The derivative of the interpolation polynomial is a third-degree polynomial. It has one (λ_0) or three real roots (λ_1, λ_2, λ_3). Once the error function at the position of ($X_0+ \lambda_0$) or ($X_0+\lambda_1$, $X_0+ \lambda_2$, $X_0+ \lambda_3$) is no more than the initial error function value, the tentative changes in the direction are retained. Otherwise,

the system reverts to its original configuration. A new random direction is then chosen, and the process is repeated. For each such guess, we use 3-D interpolation to adjust the location of the origin and the tilt of the endothelial plane of the experimental 3-D images and to then calculate a new set of interpolated experimental values at a set of grid points in this new coordinate system. The transformation matrix is(43):

$$\begin{bmatrix} \cos\beta\cos\gamma & \sin\gamma & -\sin\beta\cos\gamma \\ -\cos\beta\sin\gamma & \cos\gamma & \sin\beta\sin\gamma \\ \sin\beta & 0 & \cos\beta \end{bmatrix} \qquad (4.27)$$

We have coded this algorithm in Fortran. We run Bremermann's optimizer for 500 iterations before accepting its final answer, and we compare the final results by plotting the experiment and the theory to assure ourselves of the adequacy of the fit. We choose this number of iteration in order to make sure we achieve the good optimized parameters. The heuristic given in Bremermann's paper(7) is less than 100 iterations.

4.3 Results

4.3.1 Theoretical predictions

Figure 4.1 and Figure 4.2 show the HRP concentration as a function of r and z in cylindrical coordinate for one spot from an aorta after 30s and one form an aorta after 1min HRP circulation. For fixed r=0, both figures exhibit a peak in the HRP concentration in z in the media roughly 10-15μm from the adventitia. At the z position corresponding to the maximum HRP concentration, the HRP maximum is highest at r=0 and decreases montonically for r>0. Interestingly, the r-dependence of the HRP concentration adjacent to the endothelium is opposite, being lowest at r=0 and rising for increasing r. Naturally, this is only true for r distances that are relatively small. Our calculations show that this value in fact begins to decrease at r= 22 at 0.5 min and 1 min

circulation time. The HRP concentration maximum in z for r=0 at 1 min circulation is about double that at 30s HRP circulation, whereas the endothelial value is ~4 times as high at 1 min than at 30 s.

The maximum intima concentrations are around 10^{-3}. It is usually quite different from the media value adjacent to it (about 10^{-4}). Remember that the concentrations are in per-unit-total volume units – and since the intima has far more void space than the media, the value in the media's interstices is far higher than the calculated value, whereas the value in the intima interstices is very close to the calculated value.

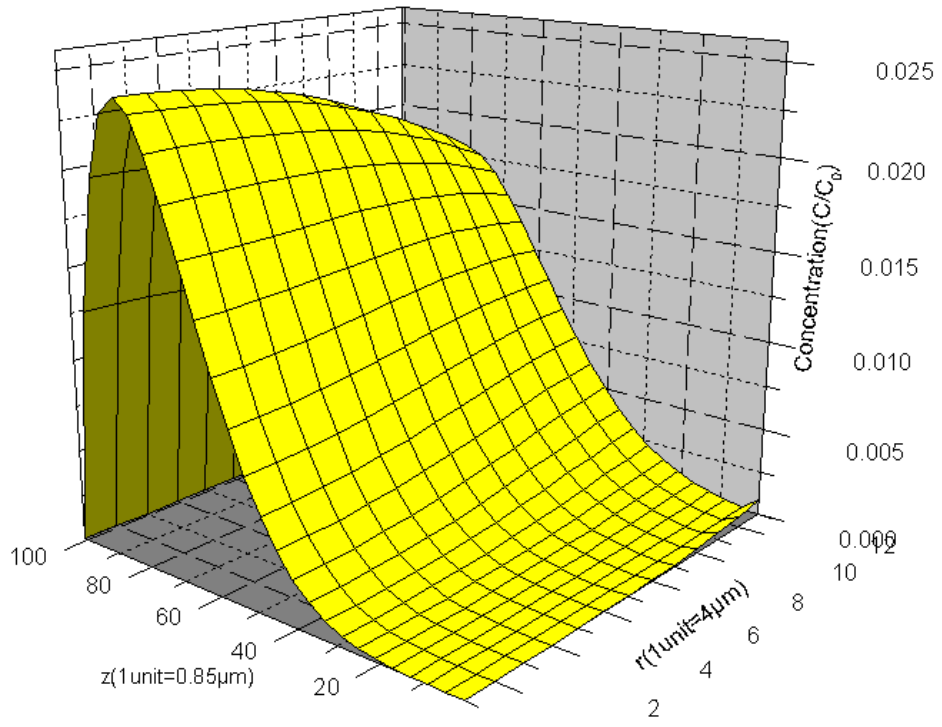

Figure 4.1 Theoretical prediction of HRP distribution after 30s HRP circulation time. R=0 is the center of leaky cell. Z=0 is the endothelium layer. Z=100 is the plane between media and adventitia.

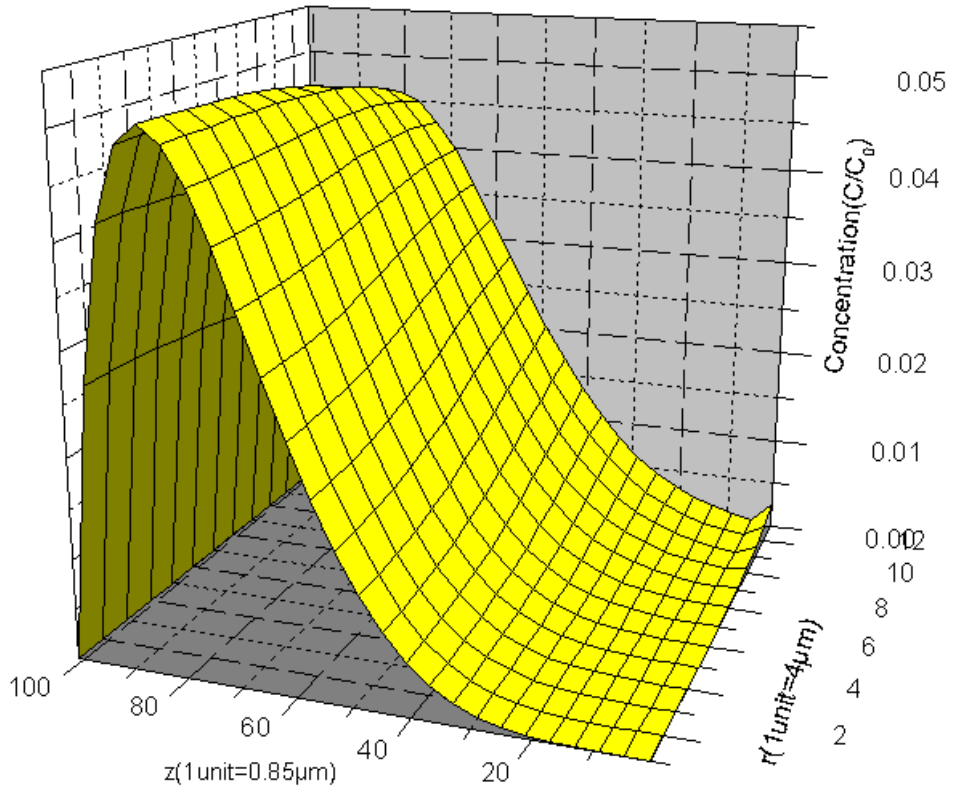

Figure 4.2 Theoretical prediction of HRP distribution after 1min HRP circulation time. R=0 is the center of leaky cell. Z=0 is the endothelium layer. Z=100 is the plane between media and adventitia.

4.3.2 Experiment results

Figure 4.3 and Figure 4.4 show the experiment results from 13 spots after the optimization procedure described above for 30s and 1min HRP circulation time. All of the figures exhibit a peak in the HRP concentration in the z direction near the adventitia side of the media. In the r direction, this maximum HRP concentration is highest at r=0 and decreases for increasing r. These trends agree qualitatively with the theoretical predictions. Adjacent to the endothelium the concentration of HRP is so low that confocal microscope cannot detect any signal. That's why all the experiment results only show the

images in the media. Compared with theoretical prediction the experiment results are far less smooth, which is not unexpected. We made an assumption that the media is uniform. While the actual media has layered structure, it's very difficult to achieve a smooth distribution of concentration in the vessel wall, especially in z direction.

The concentration is over 0.015 at z=45 in experiment result of Figure 4.3. Compared with the corresponding value of theoretical prediction in Figure 4.1 (around 0.005), experimental result 0.015 is much higher. While at z=100, the experiment results exhibit concentration only around 0.005, which is larger than the theoretical concentration of 0. At the peak plane (z~80), the maximum and minimum of concentration in r direction are about 0.0275 and 0.015 for experiment, 0.023 and 0.018 for theory.

When we compare Figure 4.4A and Figure 4.2, we find at z=66 experiment shows concentration of about 0.03 that is similar to theoretical value. The concentration of experimental results at z=95 is around 0.01, which is smaller than the theoretical result ~0.02. In addition, the peak plane (z~83) shows the maximum and minimum of concentration in r direction are about 0.065 and less then 0.04 for experiment, 0.051 and 0.045 for theory. Figure 4.4B gives very similar information. At z=66 the concentration is about 0.03, which is very similar to theory. The concentration at z=100 is not the theoretical value of 0. The peak plane exhibits concentration is in the range of 0.04 to 0.05 in experimental results.

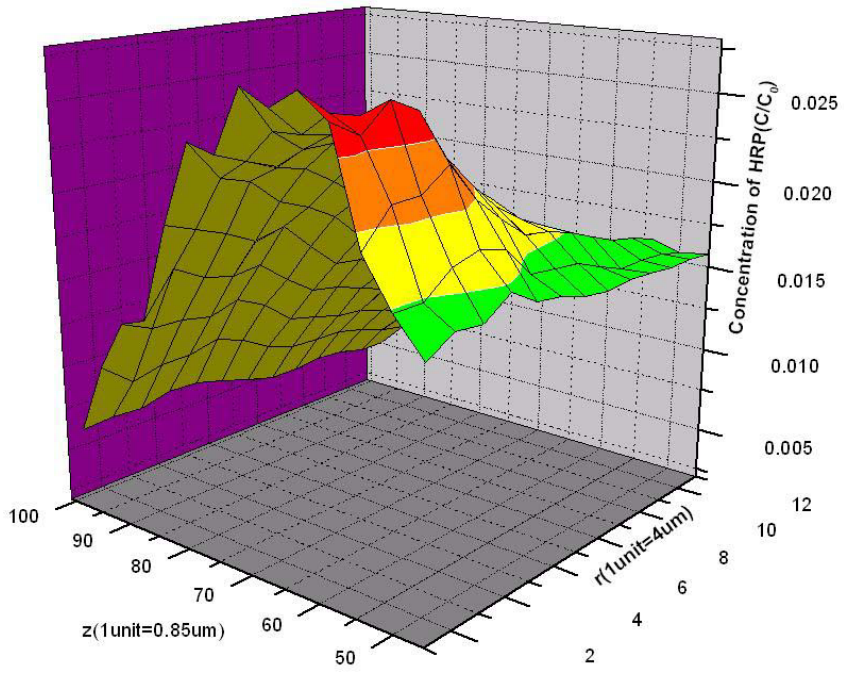

Figure 4.3 Experiment result of HRP distribution in the aorta after 30s HRP circulation time

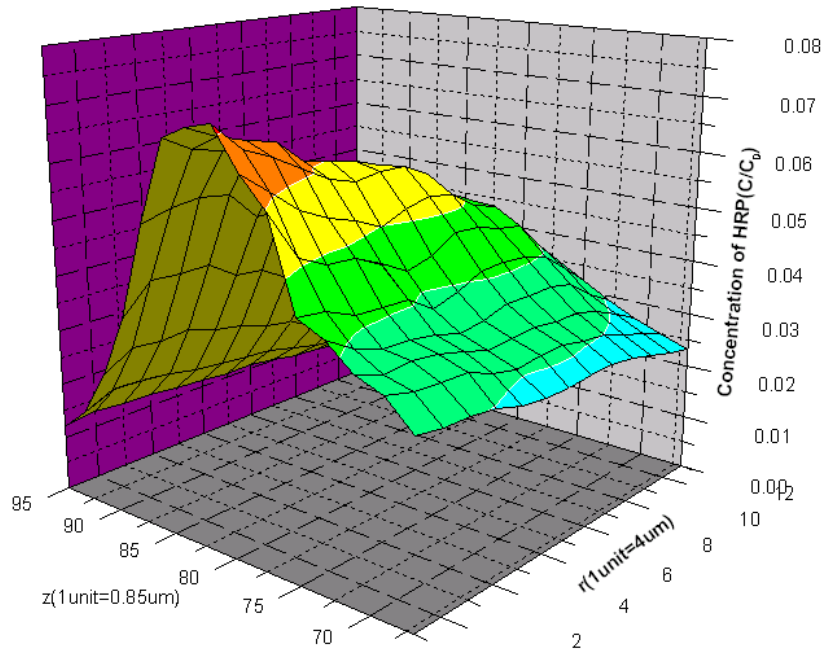

(4.4A)

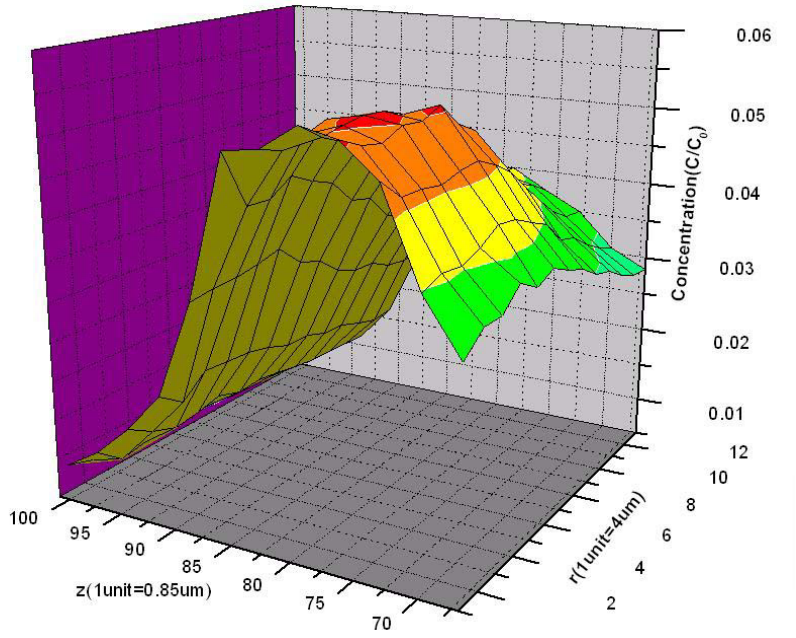

(4.4B)

Figure 4.4 (4.4A) and (4.4B) are experiment results of HRP distribution in the aorta after 1min HRP circulation time

4.3.4 Note regarding comparison of theory and experiment

We note that before conducting the quantitative 6-paramter optimization of the fit of the theory to the experimental results, we first did a rough comparison by eye to make sure they have basic similarities. We found that even the qualitative the shape of the theoretical curve depended non-trivially on the value chosen for the tracer retardation coefficient in the media (f_m). For example, it strongly affects the location of the peak in HRP concentration peak with z direction. Previous studies by Huang et al(25) and Zeng et al(85) used f_m=0.3. The calculation of f_m, is given here:

$$f_m = 1 - (1 - \psi_m)^2 \tag{4.28}$$

where $\psi_m = \gamma_m/\gamma_{wm}$ is the partition coefficient and γ_m and γ_{wm} are the fractional volumes available for macromolecules and water, respectively. γ_m =0.08(63), an

experimental value for albumin, here used for HRP and γ_{wm} =0.5 give f_m the value of 0.3. When we use f_m=0.3 our theory predicts the position of the HRP concentration maximum as being far closer to the endothelium than in the experiments. Actually HRP is smaller than albumin. γ_m for HRP should be larger than 0.08. By increasing it to γ_m =0.13, that is, f_m =0.45, the theoretical maximum is far closer to the experimental values at both 30s and 1min HRP circulation time. From $Pe_{mr} := \frac{f_m L_m^* U_m^*}{\gamma_m D_m^*}$, $Pe_{mz} := \frac{f_m L_m^* W_m^*}{\gamma_m D_m^*}$, we know increase f_m will increase Pe_m, which means convection plays more important role here. The water flow will carry more tracer into media. That pushes the HRP concentration maximum far away from the endothelium. Thus we fix this parameter before proceeding to the optimum comparison of theory with experiment.

4.4 Discussion

In this chapter we investigate the 3-D concentration of HRP in the rat aorta after HRP circulation and PBS rinsing before vessel fixation, both experimentally and theoretically. This appears to be the first study that resolves the HRP concentration in the. z direction experimentally.

Our 2-D filtration and diffusion-convection model did an excellent job for the investigation HRP spot growth with pressure and pharmaceuticals in chapter 3 and 5. These experiments corresponded to setting the lumen HRP concentration to a fixed value for the given circulation time at a fixed mean transmural pressure and then fixing the vessel. We only consider the HRP circulation process since we fix the tissue right after sacrifice the rat. The results generally showed very high concentration of HRP near the

leaky junctions (near r=0) both in the r and z directions. The concentration of HRP decreased sharply from leaky site both in r and z directions.

In contrast, as noted in the methods, the sample preparation for the confocal microscope study required a 10 min PBS flush before using Bouin's solution, which was needed to reduce the tissue's broad spectrum autofluorescence. Upon modeling this entire procedure as described, we find, for r=0, the maximum of HRP concentration is shifted from z=0 to a z value deep in the media. The reason for this is clear: After HRP circulation the HRP distribution is as it was in Chapters 3 and 5. However, during the PBS washing at 100mmHg, HRP has the opportunity to back-diffuse from the tissue into the PBS. Since there was a transmural pressure of 100mmHg, then, rather than the HRP diffusing into the PBS wash, the HRP-free PBS washed the HRP from the part of the wall close to the endothelium and washed it further into the tissue. The HRP concentration change in the intima is huge during the washing. First, the maximum concentration decreases from over 1 to 10^{-3}. Second, the position of the maximum concentration shifts from r=15μm to r~90μm.The mass transfer process is convection-dominated. In the intima, the water velocity in the z direction (W), and thus the tracer advection, is smaller than that in the r direction (U): W/U is in the range of 10^{-1} to 10^{-3}. The concentration change in the r direction is more than z direction. The media values of W/U is in the range of 10^{2} to 10^{7}, which accounts for the more change in z direction than r direction.

We also notice the experiment concentration at the boundary of the media and adventitia z=100 is not the theoretical value 0. That's because we use a thickness value of 85μm(79), each vessel wall's thickness is different and the wall thickness is different at

different place even in the same vessel. Those spots happened to be at a place with wall thickness larger than 85μm.

As noted above our theory used a larger value for the media's tracer retardation coefficient than two previous studies of transport in the aorta. In both of those studies, both of which modeled HRP spots after HRP circulation, but without PBS wash, most of the HRP in the wall was in the intima due to its far larger porosity than the media's. Therefore the media's tracer retardation coefficient, which reflects the efficiency of tracer transport through the media, is very insensitive to its precise value. As such, this change should not affect their results, and we have verified that it does not affect our results in chapters 3 and 5. Figure 4.5 shows the effect of f_m on the HRP spot growth at 100mmHg. When f_m increases the HRP spot radius increased a little. At 4 min circulation time the HRP spot radius is increased by about 4% when f_m changes from 0.3 to 0.45. The theoretical prediction of HRP spot size when f_m is 0.45 is still in the experiment error.

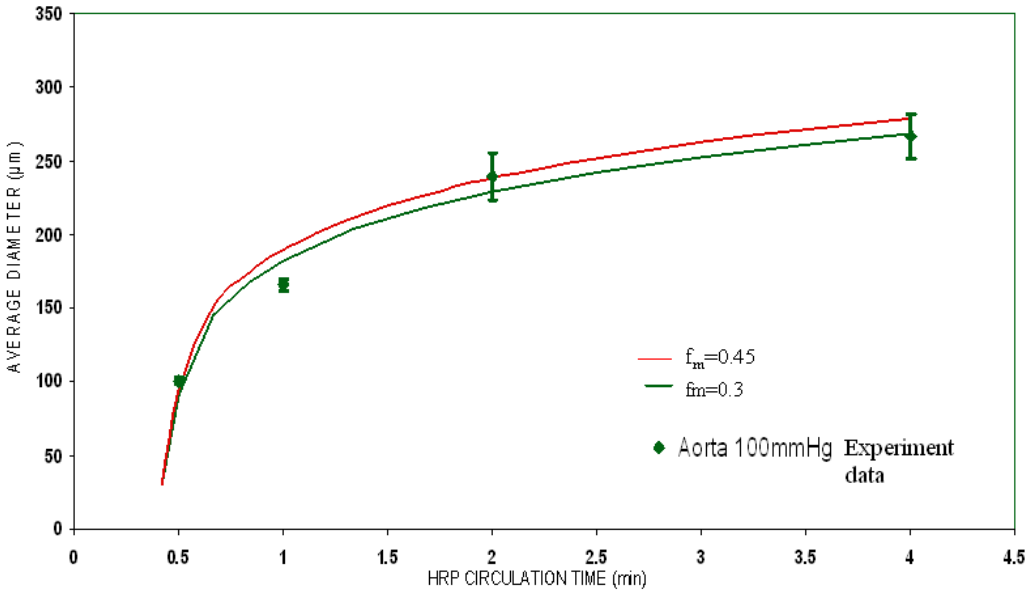

Figure 4.5 The effect of f_m on the HRP spot growth at 100mmHg.

The fitted values of c for the three curves are: 0.036 for 30s HRP circulation time(Figure 4.3), 0.0882 for Figure 4.4A and 0.0935 for Figure 4.4B (1min HRP circulation time). We adjust confocal microscope's gain to image sample in 8-bit picture (the intensity of each pixel is in the range of 0-255). Every scan has its own gain value. When we use the software to adjust the gain we can always find almost same gain for same sample. From optimized value of c of the two one-minute spots we can tell they are really similar. Theoretically the concentration distribution is same for them so we should get exactly same optimized value. While from experiment we can only achieve similar results since the animal tissue is non- homogeneous even in the same animal. We can tell the two optimized value of c of the two 1min spots are consistent. The optimized value of c of 30s circulation time should be about half 1min circulation since the HRP concentration maximum in z for r=0 at 1 min circulation is about double that at 30s HRP

circulation. In this case our optimized value of c at 30s circulation is about 0.4 that at 1min circulation, which is not bad compared with 0.5. In a whole, the optimized values of c at different circulation times appear consistent.

Our experiment results agree qualitatively with the theoretical prediction for HRP concentration vs. z and r. The experiment results are, naturally, not as smooth as the theory and fits are not perfect because our theory contains many simplifications. Some of these are particularly sever in the media. For example, despite the fact that the media has repeated layers of elastin separated by smooth muscle cells and proteoglycans, we have treated it as a uniform medium in z. Thus one would expect the experimental z-profiles to be far less smooth than the theoretical predictions. From our comparison in results part, the concentration at the specific positions is always more or less different between experiment and theory. Despite this difference, the theory appears to do quite well.

4.5 Conclusion

This investigation for the first time provides the HRP tracer concentration as a function of distance from a localized leak, both in the endothelial plane as well as normal to it. Due to the necessity of using a substrate with fluorescent reaction product to enable study by confocal microscopy, it was necessary to follow HRP circulation with a 10min of washout of blood by PBS. Modeling of both HRP circulation and this wash-out yields curves that are quite consistent with experiment. In the z direction both theory and experiment show a peak of concentration in the media near the adventitia. HRP concentration in the r direction decreases slowly from the center of the leaky cell close to the cell, but falls off farther from it. This chapter provides further evidence to support

Huang's 2-D convection-diffusion model for the transport of water and macromolecular into the aortic wall, one of the earliest events in atherogenesis.

Chapter 5. The Role of Aquaporin1 in HRP Spot Growth in Rat Aorta

5.1 Introduction

Atherosclerosis is the leading cause of death in all Western countries, both above and below age 65(68). It afflicts large arteries such as the aorta (68)and is triggered by low-density lipoprotein (LDL) transport from the blood into the arterial wall where it accumulates. Blood-borne monocytes enter the lipid-laden subendothelial intimal arterial regions and transform into macrophages as they and media-derived smooth muscle cells scavenge extracellular cholesterol(44, 47). When overwhelmed, they form foam cells, which appear to start the formation of the earliest lesions. These eventually thicken the arterial wall, narrowing the cross section for blood flow, making arterial wall less complaint and increasing the risk of a lesion rupture and/or of blockages.

A monolayer of the endothelial cells separates the lumen from the thin, sparse subendothelial intima. An internal elastic laminar (IEL) borders the intima, followed by the dense tunica of media comprised of a repeated structure of elastin sheets separated by extracellular matrix and smooth muscle cells (SMC). Beyond the media is the loose adventitial layer. Stemerman et al (59) showed that macromolecules rapidly cross the endothelium focally through isolated hot spots, and not uniformly. Weinbaum and co-workers (73, 76) suggested that such leaks correspond to dying or mitotic endothelial cells that consequently have temporarily widened or not-yet-formed intercellular junctions, and therefore allow macromolecules too large to pass through intact tight junctions to leak into the arterial wall. Lin et al. (33, 34)showed that 99% of the cells in mitotic (M) phase are associated with Evans blue albumin conjugate (EBA) leakage and that 80% of cells in M-phase leaked Lucifer yellow-LDL (LY-LDL). Truskey et al.

(66)used autoradiography to measure the permeability of 125I-LDL and found approximately 25% of the leakage sites were associated with mitotic cells.

Chuang et al. (14) studied the rapid subendothelial spread of HRP with increasing tracer circulation time. They found that localized HRP spots in the aorta initially grew very rapidly and then appeared to slow down, reaching almost ~200 μm in diameter after 4 min circulation time. Such growth was not consistent with a diffusion-dominated mechanism for any reasonable diffusivity. Yuan et al's (82) unsuccessfully tried to explain this data in terms of a mathematical model that included some ultrastructural details of the vessel wall. Huang et al. (25) used the observed extremely sparse subendothelial intima matrix structure to construct an ab initio theory for the intimal transport parameters that could not be measured directly. By incorporating these values into a two-dimensional, convection-diffusion mathematical model, they were able to explain the HRP spot growth data. These studies show that transendothelial convection plays a crucial role in tracer transport into the vessel wall. When there is no osmotic pressure gradient across the wall, Starling's law, $Q = LpA\Delta P$, describes the flow rate Q across a section of wall of outer surface area A, where the transmural pressure ΔP is the driving force and Lp is the hydraulic conductivity of the wall. Its reciprocal reflects the specific flow resistance. Lp of the wall and of its individual layers are critical transport parameters for the filtration/convection pattern, which depends on the wall's detailed ultrastructure. Tedgui and Lever (63, 64) and Baldwin and Wilson (2, 3) each showed that the overall Lp of the rabbit's aortic wall displayed anomalous behavior with increasing transmural pressure. Its low pressure value decreased by over 40% as the transmural pressure increased from 50 to 90 mm Hg and then remained constant

thereafter up to the edge (180 mm Hg) of the physiological range. Endothelial denudation roughly doubled Lp and rendered it pressure-insensitive. Shou *et al.* (52, 53)measured a complete set of Lp on various rat vessels, with their endothelia both intact and denuded, and the rat aorta's Lp vs ΔP agrees well with Tedgui and Lever's rabbit Lp vs ΔP. In order to explain the above-mentioned behavior, our group's insight into the aorta's and, in particular, the intima's, structure was crucial. Huang(27) postulated that under high transmural pressures, the intima would compress, typically up to a factor of five, from its unstressed value. (Once compressed to a certain extent, the strong collagen fibers in the intima would resist further compression.) This compression would decrease the intima's inter-fiber spacing, thereby decreasing its transport parameters and, more importantly, cause the endothelium to partially block some of the IEL's fenestra. This latter effect could lower wall hydraulic conductivity drastically. To check this theory, our group developed a model for the local flow into an IEL fenestra (26). The result of this theory confirmed the alteration of the flow due to fenestral plugging and provided, as an output, values of the effective IEL conductivity Lp_I as a function of ΔP to be used in the convection-diffusion model above. They also predicted the time-dependent HRP spot growth for several different transmural pressures in the arterial intima (with parameters taken from both rat and rabbit data) shown with and without the effect of intimal compaction – with each showing different trends. In Chapter 3 we tested these predictions by measuring HRP spot growth in rat aorta at different acute transmural pressures. The results agree very well with the predictions of the theory that incorporates intimal compaction under ΔP.

Until now it has been assumed that the endothelial hydraulic conductivity represents transport through the tight inter-endothelial junctions(21, 25, 65), through which water is small enough (1.2 Å) to pass. Another known pathway for water transport is diffusion through pure lipid bilayers of the cells (54). The last decade has brought about the identification of a ubiquitous class of extremely specific water channel membrane proteins called aquaporins (AQP) (70). Aquaporins 0-9 have so far been identified in various cell types from humans, and many others have been found in cells from plants (17, 29) and animals, including erythrocytes (13), smooth muscle (48) and epithelial and endothelial (39) cells, among others. Endothelial cells from the nephron have been observed to contain type 1 AQP (AQP-1) (39), also known as CHIP28 (channel forming integral protein, 28 kDa). An AQP-1 unit is a tetramer with each of its four circa 60 Å long monomers providing a water pore. The AQP-1 pore has a dumbbell shape with a wide opening of about 15 Å to the extracellular space. About 20 Å from the opening, the pore constricts down to 2.8 Å in diameter, hence giving rise to AQP-1's high selectivity (37, 60). The sulphhydryl group of Cysteine189 (Cys189) of AQP-1 plays a critical role in the functioning of the water channel. It is located in the pore near the extracellular side of the constriction (60) and is sensitive to mercury (42). A mercury ion (Hg^{2+}) (with a size of 2.2 Å) can bind to the Cys189 and block the narrow pore's neck (~2.8 Å), thereby blocking the channel's ability to transport water. A number of studies have used mercuric chloride ($HgCl_2$) as the blocker of water permeability in isolated cells deriving from the lung (45)and the kidney (90). Waltz *et al*. (72) used a transmural osmotic gradient in the absence of a transmural pressure to swell aquaporin-containing synthetic membrane vesicles, and from the swelling rate calculated the hydraulic

conductivity l_p=3.85x10^{-18} cm^5/N·s for a single water channel. Tricky detailed molecular dynamics simulation (91) of single water channel also calculated l_p and found the value 2.0±0.3x10^{-17} cm^5/N·s.

J. Toussaint in our lab has used immunohistochemistry with anti-aquaporin-1 antibodies to show that rat aortic endothelial cells express this protein in their cell membrane and in their interior. Shou *et al.* (51, 53)did the first pilot Lp measurements that used $HgCl_2$ to modify Lp of a vessel, rather than of a single cell. Without $HgCl_2$ Lp has a high value at 60 mmHg, drops about 40% at 100 mmHg and remains flat to 140 mmHg. Introduction of 10 μM $HgCl_2$ to the same vessel depresses Lp over the entire range 60-140 mmHg, but mostly (27.5%) at 60 mmHg. Tieuvi Nguyen in our group made various improvements to Shou's technique and redid these experiments, first on the intact aorta, then again after treatment with $HgCl_2$, and then again after endothelial denudation, all on the same vessel. Among the controls she did, Nguyen confirmed that any effect that the blocking AQP1 with $HgCl_2$ had on Lp of aorta media was well within the measurement noise despite the fact that the media contains ample smooth muscle cells (SMCs) that avidly express AQP1. Evidently, water transport through the media is mainly around these SMCs and not through them. This leaves only the endothelium, subendothelium intima and IEL to explain the pressure-dependent effect of $HgCl_2$ on vessel wall Lp. It is conceivable that blocking EC AQP1 can change the percentage of transmural ΔP acting on the endothelium the portion of ΔP that can compress the intima. To test this possibility, we shall combine many of the results quoted above to make a testable prediction. In particular, Huang *et al*'s(26) theory for a compressible intima predicts that HRP spots in rat aorta will grow very differently if the aortic intima is

compressed than if it is uncompressed and that the aortic intima is significantly uncompressed at pressures below 60 mmHg. If blocking AQPs indeed shifts enough of this ΔP to the endothelium to compress it without changing overall ΔP, then the nature of the spot growth in a rat aorta should indicate this compression. We shall use Huang *et al*'s(26) 2-D filtration and convection/ diffusion model to predict HRP spot growth before and after blocking AQP1 by $HgCl_2$. We shall then test this prediction *in vivo*.

Before embarking on an experimental protocol to test this, we note a few facts. Since, with no aquaporin blocker, the arterial intima would be maximally compressed at somewhere between 80-100 mmHg, the intima is normally always compressed. In addition, given experimental standard errors, one would want to pick a transmural pressure to test the theory's predictions at which the theory predicts a maximal effect. Shou *et al.*(51) have calculated that one can expect a maximal difference in spot size between untreated and $HgCl_2$-treated aortas at the lowest pressures where the animal can function. As such, we choose a blood pressure of 45 mmHg.

The predictive theory requires as an input the Lp value at 45mmHg in both untreated and $HgCl_2$-treated aortas, which we measure *ex vivo* on the same vessel. However we must make sure $HgCl_2$-treatment *ex vivo* has the same effect on Lp as such treatment *in vivo*. Mercuric chloride, a common inhibitor for AQP-1 (45, 90) and 2-mercaptoethanol unbinds $HgCl_2$ from AQP-1. We first measure Lp(ΔP) *ex vivo*, treat with with $HgCl_2$ and remeasure Lp(ΔP), treat with 2-mercaptoethanol (at a titrated concentration) to remove the $HgCl_2$ and then remeasure Lp(ΔP). If the latter Lp(ΔP) agrees with the untreated Lp(ΔP), we conclude that the changes in Lp upon $HgCl_2$ administration are due to AQP1 blockage, and not to any irreversible toxicity. We shall

then treat the rat to a (titrated) amount of $HgCl_2$, sacrifice the animal, remove its aorta and measure its Lp(ΔP) *ex vivo*, then treat the vessel with the titrated concentration of 2-mercaptoethanol and remeasure Lp (ΔP), Only if the final Lp(ΔP) agrees with the untreated Lp(ΔP) measured *ex vivo* will we use these Lps to predict the HRP spot growth.

5.2 Methods:

5.2.1 Theory

Water Filtration and its Boundary Conditions

The aorta has a continuous quiescent layer of endothelium covering the lumen side of its wall. A very thin layer of extracellular matrix called the subendothelial intima separates the endothelium from the internal elastic lamina (IEL). The media, which is beneath the IEL, consists much of proteoglycans, elastic fibers and smooth muscle cells.

As in Chapter 3, following Huang(26) and Zeng(85), for a slab of the aorta wall we define a cylindrical coordinate system whose origin is at the center of a leaky cell and whose z-axis is perpendicular to the endothelium. The r coordinate is, in the context of the whole artery wall, a radial position in the "plane" "parallel" to the endothelium and we assume the problem is axisymmetric. Note, the wall's radius of curvature is negligible with respect to its thickness and thus we take the endothelial "plane" to be flat. By abuse of geometry (since circles do not tile the plane) we take a cylindrical slab of radius ξ (defined below) to be periodic. Let us begin with the fluid filtration problem. The lumen pressure is higher than the extravascular pressure and this transmural pressure drives a transmural flow. We assume that water (by which we mean the cell-free portion of the blood) enters the artery wall through all of the inter-endothelial junctions, but fluid that bears large solute molecules can only enter through rare, isolated leaky junctions. Since

both the intima and the media are porous media, the transport through them is Darcy (potential), rather than Navier-Stokes flow, i.e., for the intima and the media, one has

$$0 = \nabla^2 p_k^*,$$

$$u_k^* = -\frac{Kp_k}{\mu}\frac{\partial p_k^*}{\partial r}, \text{ and } w_k^* = -\frac{Kp_k}{\mu}\frac{\partial p_k^*}{\partial z}, \text{ k= i(intima), m(media), (1a-c)}$$

where u^* and w^* are the horizontal (r direction) and vertical (z direction) velocities, respectively. K_p (different for the intima and for the media) is the Darcy's permeability, μ is the fluid viscosity and p^* is the pressure. The asterisk represents a dimensional variable. The continuity equation, which expresses conservation of mass, for each of the intima and the media, is:

$$\frac{1}{r^*}\frac{\partial}{\partial r^*}\left(r^* u_k^*\right) + \frac{\partial w_k^*}{\partial z} = 0, \text{ k= i(intima), m(media). (2)}$$

The non-dimensionalizations are the following:

$$r = \frac{r^*}{L_m},\ z = \frac{z^*}{L_m},\ P = \frac{p^* - p_o^*}{p_L^* - p_o^*},\ Kp = \frac{Kp^*}{Kp_m},\ U = \frac{u^*}{Lp_m(P_L^* - P_o^*)}, \text{ and } W = \frac{w^*}{Lp_m(P_L^* - P_o^*)},$$

where L_m is the thickness of the media. P_L^* is the lumen pressure and, P_o^* is the pressure outside of the aorta. Kp_m and Lp_m are the Darcy permeability and hydraulic conductivity of the media, respectively. The nondimensional forms of the governing equations, after normalization, become:

$$U_k = -\frac{\partial P_k}{\partial r},\ W_k = -\frac{\partial P_k}{\partial z}, \text{ (3a, b)}$$

$$\frac{1}{r}\frac{\partial}{\partial r}\left(rU_k\right) + \frac{\partial W_k}{\partial z} = 0, \text{ k=i(intima),m(media).} \qquad (4)$$

Boundary conditions are needed at the three z-surfaces, the endothelium, the IEL (both assumed here to be infinitely thin) and the media-adventitial boundary, as well as at

the centerline r=0 and at the edge r=ξ of the periodic unit. At r=0 and ξ, symmetry and the periodicity conditions lead to no flow in the r-direction:

$$U=0 \text{ at } r=0, \xi. \tag{5}$$

At the media-adventitia boundary, the pressure is the fixed adventital pressure:

$$P_m(z=0) =0. \tag{6}$$

At the IEL, W is continuous and the IEL is a barrier characterized by a hydraulic conductivity Lp i.e., the W is linearly related to the pressure difference. Thus

$$W_I(z=1)=W_m(z=1-L_I/L_m)=Lp_I(P_i(z=1)-P_m(z=1-L_I/L_m)), \tag{7}$$

where L_I is the thickness of IEL. Huang et al.(25), by using a simplified model for the fenestral pore interaction, found the hydraulic conductivity of the IEL to be

$$L_{p_I} = \frac{W_f \phi_I}{1 - W_f \phi_I} \tag{7a}$$

where $\phi_I = a_f^2 / \xi_I^2$ is the fractional area of the fenestra in the IEL, a_f the mean radius of the fenestra, and $2\xi_I$ the mean distance between the neighboring fenestrae. Their model calculated the water velocity, W_f, through the fenestra to be

$$W_f = \frac{(L_m/L_I)(K_{p_1}/K_{p_2})}{1 + G_0(L_m/L_I)(K_{p_1}/K_{p_2})}, \tag{7b}$$

$$G_0 = \Phi_I + \sum_{n=2}^{\infty} \frac{2a_f J_1(\mu_n a_f)}{\mu_n^2 \coth(\mu_n) \xi_I^2 J_0^2(\mu_n \xi_I)}$$

where $J_0(x)$ and $J_1(x)$ are the zeroth and the first order Bessel functions, and μ_n (n = 1, 2, 3, …) are the roots in nondecreasing order of the eigenvalue equation $J_1(\mu_n \xi_I) = 0$.

At the endothelium's normal junctions (the nondimensional lumen pressure is 1),

$$W_i=Lp_{nj}(1-P_i) \text{ at } R_2 < r < \xi \text{ and } z=1+L_i/L_m, \tag{8}$$

where L_i is the thickness of the intima. At the endothelium's leaky junctions,

$W_i=Lp_j(1-P_i)$, at $R_1 < r < R_2$ and $z=1+L_i/L_m$; (9)

$W_i = 0$ at $0 < r < R_1$ and $z = 1+L_i/L_m$ (10)

where the subscripts I, nj, j correspond to the IEL, the normal endothelial junctions and the leaky junctions, respectively. Yuan et al.(82) used a 1D Poiseuille flow model to find the hydraulic conductivity of the leaky junction, normalized by L_{pm}^{*}, as

$$L_{p_j} = \frac{(\Delta R)^2}{12\mu L_l L_{p_m}^{*}} \tag{9a}$$

where L_l is the length of the leaky junction and μ the fluid viscosity, $\Delta R=R_2-R_1$, is the average width of the leaky junction.

The Macromolecular Transport Problem and its Boundary Conditions

In a similar manner, one can define the convection-diffusion problem in this geometry, using as an input the velocity distribution from the above solution. Due to the complexity of the velocity field, this problem, subject to an initial condition of zero tracer (i.e., HRP) concentration in the wall and a lumen boundary condition of a fixed, non-zero lumen concentration corresponding to the above-mentioned experiment, requires a numerical solution. The solutions give tracer concentrations in the artery wall as a function of position (r,z) and time t. The nondimensional convection-diffusion equation for the tracer transport is:

$$\frac{\partial C_k}{\partial \tau} = \underline{\nabla} \bullet \underline{q_k}\text{ , k= i(intima), m(media).} \tag{11}$$

Here $\underline{q_k} = (q_{kr,} q_{kz})$ is the nondimensional vector of solute flux in the r and z directions.

$$q_{kr} = -D_k \frac{\partial C_k}{\partial r} + Pe_{kr} C_k \,,\; q_{kz} = -D_k \frac{\partial C_k}{\partial z} + Pe_{kz} C_k \,, \tag{12}$$

$$C_k = \frac{C_k^*}{C_L^*}, \tau = \frac{D_m^* t}{L_m^{*\,2}},\; D_k = \frac{D_k^*}{D_m^*} \tag{12a}$$

$$Pe_{kr} := \frac{f_k L_m^* U_k^*}{\gamma_k D_m^*},\; Pe_{kz} := \frac{f_k L_m^* W_k^*}{\gamma_k D_m^*},\; q_{kr} = \frac{q_{kr}^*}{D_m^* C_L^* / L_m^*},\; q_{kz} = \frac{q_{kz}^*}{D_m^* C_L^* / L_m^*}. \tag{12b}$$

C_k^* is the dimensional macromolecular concentration locally averaged over all phases present in the tissue in each of the intima or media. C_k for the region k is normalized by the lumen concentration C_L^*. Pe_{kr} and Pe_{kz} are the local Peclet numbers in the r and z directions that include the retardation coefficients f_k in their definitions. τ is the dimensionless time and D_k is the dimensionless diffusivity. f_k and γ_k are the retardation coefficient, representing the ratio of the solute velocity to water velocity, and volume fraction for macromolecules, representing the fractional volume available for macromolecules per unit total tissue volume.

We begin with the initial condition that the wall is tracer-free, i.e..,

$$C_k(t=0)=0. \tag{13}$$

The boundary conditions in r are simple. At r=0, ξ, symmetry and periodicity for both the intima and IEL require no flux:

$$\left.\frac{\partial C_k}{\partial r}\right|_{r=0,\xi} = 0\,. \tag{14}$$

At the intima-media interface, the solute concentration in the fluid is continuous,

$$\frac{C_i}{\gamma_i} = \frac{C_m}{\gamma_m} \;\; at\; z = 1. \tag{14}$$

Before moving to the other z-boundary conditions, we note that both the endothelium and the IEL have significant transport through holes of far smaller dimension than the other scales of that surface and these holes occupy only a small fraction of that surface's area. The nondimensional tracer flux q_l through such a hole requires a local model on that scale. Ref (67) posits such a local, one-dimensional quasi-steady, convection-diffusion junctional model:

$$q_l = -\frac{\partial C_l}{\partial x} + Pe_l C_l \tag{16a}$$

where x is the direction normal to the endothelium along the junction,

$$Pe_l = \frac{f_l L_l W_l^*}{D_l^*},\ q_l = \frac{q_l^*}{D_l^* C_L^* / L_l},\ C_l = \frac{C_l^*}{C_L^*},\ x = \frac{x^*}{L_l}. \tag{16b}$$

L_l, Pe_l, f_l, and D_l^* are the height of the leaky junction, the Peclet number, retardation coefficient, and effective diffusion coefficient in the leaky junction, respectively, for this local model whose output is an expression for q_l, which we then use in the model in Eq. (11)-(12). In the local model, the solute concentration, C_l, depends on x. The water velocity, W_l^*, in the leaky junction is uniform in the junction (from the continuity equation), which makes the Peclet number Pe_l well-defined. With the assumption of q_l independent of x, Eq. (16a) integrates directly to yield a relationship between q_l and the dimensionless solute concentration, C_{ls}, at the subendothelial side of the leaky junction. For the leaky junction with boundary conditions, $C_l = 1$ at x=0, $C_l = C_{ls}$ at x=1, this gives

$$q_l = Pe_l \frac{\exp(Pe_l) - C_{ls}}{\exp(Pe_l) - 1}; \tag{17}$$

Note the global Eq. (12) and local Eq. (16) models nondimensionalize q_l differently.

We return to the z-boundary conditions. If there is an endothelial ($z = 1+L_i/L_m$) leak,

$$q_{iz} = q_I,\ \frac{C_i}{\gamma_i} = C_{ls}\ for\ R_I < r < R_2\ and\ z = 1+L_i/L_m, \tag{18a}$$

$$q_{iz} = Bi(\gamma_i - C_i)\ for\ 0 < r < R_I,\ R_2 < r < \xi,\ and\ z = 1+L_i/L_m\,. \tag{18b}$$

where q_I is given by Eq. (17), the Biot number is $Bi := k_j L_m/D_m^*$ in which k_j is the endothelial mass transfer coefficient for diffusive transport across the endothelia. If there is no endothelial leak, then Eq. (18b) holds for $0 < r < \xi$, and $z = 1+L_i/L_m$.

The continuity of flux condition at the IEL-media interface leads to the local average tracer flux through the IEL(31) that matches the flux in media (q_m) and the flux in the intima(31):

$$q_i(z=1) = q_m(z=1-L_I/L_m) = q_I \tag{19}$$

where $q_m = \frac{\partial c_m}{\partial z} + Pe_{m,z} c_m$ and $Pe_{m,z} = w_m^* L_m / D$.

We assume q_I is proportional to the fractional area ϕ_f of the fenestrae and equals

$$q_I = \phi_f\, q_f, \tag{20}$$

where q_f is the tracer flux in the fenestra

$$q_f = d_1\, C_i(t) - d_2\, C_m(t), \tag{21}$$

where $d_1 = Pe_I/(1-\exp(-Pe_I))$, $d_2 = d_1 \exp(-Pe_I)$, and $Pe_I = w_I^* L_m / D_I$, which is in terms of the diffusivity D_I in the fenestra.

The solutions for the concentration distribution can be obtained numerically. As described in Zeng *et al*REF, we choose a direct discretization, finite differences approach for both models. The discretized steady state filtration model becomes a (large) number of simultaneous linear algebraic equations equal to the total number of mesh points,

which can be solved with MATLAB (The MathWorks, Inc.). For the macromolecular transport model, an initial value problem, we choose the Hopscotch Method, a fast second order partial differential equation solver. This method, a type of finite difference technique described in detail in (22), is fast, efficient, and unconditionally stable.

To determine the edge of HRP spot size from the numerical solutions, we calculated the HRP concentration profile, both in the intima, where $C_i(r, z, r)$ is nearly independent of z, and also integrated dz across the vessel wall, for various HRP circulation times. Both methods give consistent HRP spot sizes. As in our earlier studies of the aorta(25, 85) , it is adequate to just use a cutoff (we choose Ci as 0.022, as in chapter 3) based on Ci(r,t) to decide the HRP reaction visibility because, in the aorta, the bulk of the HRP in the wall is in its intima.

Table 5.1 gives the parameters we use for our theoretical predictions.

Table 5.1 Baseline values of constants and parameters

L_{IEL} (μm) Ref.(82)	1	f_i Ref.(25)	1.0 (HRP)
R_1 (μm) Ref(66, 75).	15	f_j Ref.(25)	1.0
ΔR (nm) Ref.(75)	20	f_m Ref.(25)	0.3 (HRP)
ϕ Ref.(33)	0.0005		
Kp_i (cm^2) Ref.(25)	2.20×10^{-12}	D_i (cm^2/s) Ref.(25)	4.09×10^{-7} (HRP)
Kp_m (cm^2) Ref.(69)	11.97×10^{-15}	D_{zm}(cm^2/s) Ref.(25)	8.4×10^{-9} (HRP)
γ_m Ref(63).	0.08 (albumin)	D_{rm}/D_{zm} Ref.(82)	3.0

γ_i Ref.(25)	0.92 (HRP)	μ (g/cm•s) Ref.(24)	7.2×10^{-3}

Theoretical prediction of HRP spot growth experiments before and after blocking the AQP1 with $HgCl_2$

In Chapter 3, we briefly describe Huang et al's(26) intima compaction theory and successfully test it *in vivo* at different acute transmural pressures. In this chapter, we use the results of Lp experiments without and with AQP1 blocking as inputs to the above model so as to predict HRP spot growth without and with the endothelium AQP1 blocking. Note that a change in the Lp of the endothelium strongly affects the pressure distribution – and its gradient, the velocity field, in the vessel wall, which advects the HRP. It thus changes the predicted spot growth. We then compare the prediction with the results of the HRP spot growth experiments described below.

5.2.2 Lp measurement

Experimental Setup and Measurement Technique

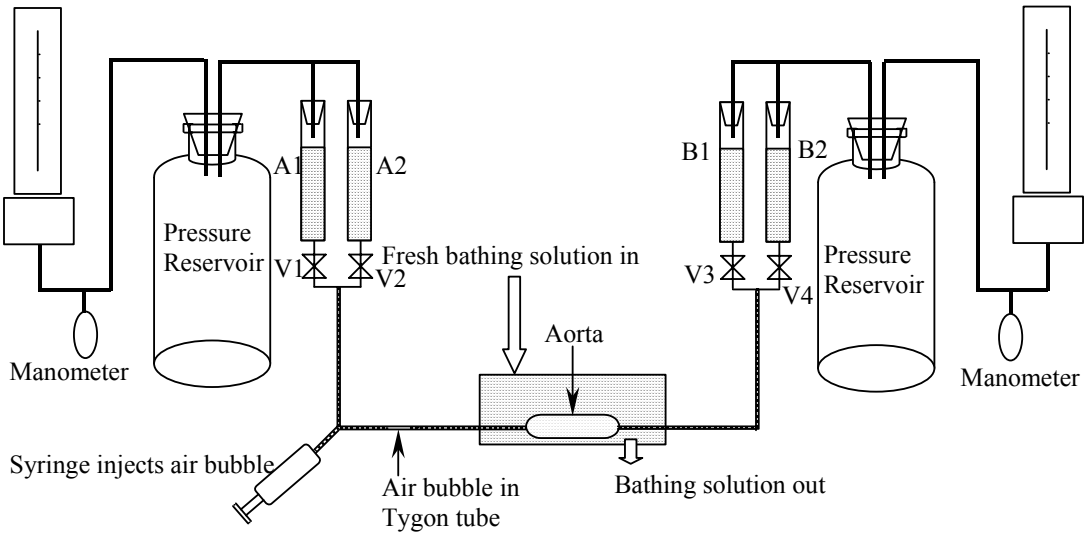

Figure 5.1 Schematic drawing of the pressurized setup. Two pressure reservoirs (A & B) are connected to the solution reservoirs (Res A1, A2, B1, B2). Res A1 and B1 contains trypan blue in PBS solution. Res B2 contains the chemical (norepinphrine, nitroprusside or labetalol) to be administered in PBS solution. The flows of each reservoir are controlled by the valves (v1, v2, v3 and v4).

Fig. 5.1 shows the experimental setup. Two mercury sphygmomanometers control the pressure of two large volume air reservoirs that are connected to two separate solution reservoirs (A and B). Reservoir A1 & B1 contain phosphate buffered saline (PBS) solution with 4% (w/v) bovine serum albumin (BSA, Fraction V, Fisher Scientific), 20μM of $NaNO_3$ (Sigma, MO) and 0.03% (w/v) trypan blue. Reservoir A2 contains 5μM $HgCl_2$ or 2μM 2-mercaptoethanol with 4% BSA in PBS solution. Reservoir B2 is a waste container. A three-way connector connects the solution reservoir A, a 5ml syringe and a horizontal, 120 mm Tygon catheter of inner diameter 0.5 mm mounted on a finely graduated ruler. The catheters are inserted into the two ends of the isolated aorta that is

immersed in a bathing solution. The syringe injects an air bubble into the catheter and, once its velocity reaches steady state (~30 min), its time is recorded 9-10 times at 0.5 mm intervals. Solution incompressibility implies that the volume (bubble velocity times catheter cross section) that it traces out per unit time equals the flow rate through the vessel wall.

All chemicals are obtained from Sigma (St. Louis, MO) unless otherwise stated. Trypan blue serves two purposes. Blue dye appearing in the adventitia means the vessel has a leak (the dye's intensity relative to the clear bathing solution made even minute leaks easily visible), which we try to secure with string. If this is not successful, we discard vessel. Around half aortas are successful. Also trypan blue is a vital stain that penetrates the membranes of non-viable cells (3, 63). The bathing solution (PBS solution with 4%BSA and 20μM $NaNO_3$) is identical to the perfusate, but absent trypan blue (whose osmotic contribution here is negligible(53)), so as to keep the osmotic pressures on both sides of the wall the same. As in all previous similar studies (2, 64), we used a digital caliper (accurate to ±0.01 mm) to measure diameters and lengths from tie to tie of pressurized, excised vessels.

All protocols below were IACUC-approved.

Four healthy male Sprague-Dawley (SD) rats (Charles River, CT) that weigh between 350 and 400 g on a normal diet are used. We subject two of them to $HgCl_2$-treatment *in vivo* before sacrifice and vessel excision. We sacrifice the other two and exposed their excised aortas to $HgCl_2$ *ex vivo*.

Vessels treated with $HgCl_2$ ex vivo

After anesthesia with 1% pentobarbital sodium (15 mg/500 g rat) we inject ~0.5 ml of heparin (1,000 units) intravenously to prevent blood coagulation. A rodent respirator keeps the rat ventilated. After opening the chest and carefully dissecting the fat, we expose the aorta from the rest of the fat and connective tissue and ligate the first three pairs of intercostal arteries. The aorta is cannulated with the solution from Reservoir A1 from the distal end and the lumen side is rinsed with the same solution, pressurized at 60 mmHg to prevent vessel collapse. We then insert a second cannulation from Reservoirs B right below the aortic arch and excise the vessel. The segment of the aorta is immersed in a solution bath a described above at 37^{o}C. The solution bath is changed every 30 min and air is continuously bubbled through it to keep the vessel oxygenated.

We first precondition the aorta by raising and lowering its pressure to its minimum and maximum physiological values 3 times, each for less than a minute. We close valves 2, 3 &4, introduce a bubble into the horizontal catheter leading from Reservoir A1 at 40 mmHg, and then increase the pressure to the desired value. The experimental pressure is 45mmHg. We determine the flow rate through the vessel wall by monitoring the movement of the bubble's front meniscus after it becomes steady, as described. The outer dimensions (length and diameter) of the vessel are measured. After completing the reference measurement on the vessel, we close valve 1, open valves 2 &4 and adjust the pressure of Reservoirs B to 10mmHg less than that of Reservoirs A. Reservoir A2 perfuses the vessel with 5μM HgCl2-containing medium for 10 min. The vessel is washed with the trypan blue solution from Reservoir B1 for 10 min by switching from valve 4 to 3. Reservoir A2 collects the waste solutions. We then close valves 2, 3 &4 and repeat the Lp measurement as the same pressure as before the introduction of the

medium in Reservoir A2. We then perfuse the vessel with 2μM 2-mercaptoethanol containing medium for 10min. We wash the vessel with trypan blue solution for 10min. After finishing the flow rate measurements, the vessel is fixed with 2% glutaraldehyde under pressure, stained with Harris' hematoxylin and examined under the light microscope to ensure that the endothelium has been intact throughout the experiment.

$HgCl_2$-treated in vivo

The dissection is same as the $HgCl_2$-treated *in vitro* except that we inject the $HgCl_2$-PBS solution (We begin with the concentration 5μM titrated in our *ex vivo* study(38, 51) , with the concentration based on the rat's total blood volume and modify this value if necessary) through left femoral vein and let it circulate for 10min before cannulating the aorta. Clearly it is not possible to do the reference (untreated) *ex vivo* measurement on the same vessel as the treated one here. Thus we measure Lp(ΔP) *ex vivo* right after excision ($HgCl_2$-treated) and then again after 2-mercaptoethanol treatment.

Calculations

As in Chapter 3, we take the aorta to be cylindrical in shape. The outer surface area of the vessel (AS) is then AS= π (36)L, where OD and L are the outer diameter and length of the vessel, respectively. The bubble velocity V=*l*/t, where *l* is the distance bubble travels in a time t. Let ID be the inner diameter of the catheter. At steady-state, the flow rate Q through the vessel wall equals that $Q= \pi (ID)^2V/4$, which is traced out by the bubble. The hydraulic conductivity Lp=Q/(AS*ΔP), where ΔP is the transmural pressure.

5.2.3 HRP spot growth experiments:

To measure the rate of HRP spot growth in untreated and in $HgCl_2$-treated aortas *in vivo*, we follow the protocols used by Stemerman *et al.*(59) and Chuang *et al*.(14), repeated in brief below. All protocols below were IACUC-approved.

The HgCl2-treated experiments

We anesthetize 12 male SD rats with 1% pentobarbital (30 mg/kg) i.p. and cannulate both the left femoral artery (to measure blood pressure) and vein. We monitor blood pressure during the entire part of the experiment prior to sacrifice by a blood transducer connected to a Powerlab/4SP (ADInstruments) and read the value of blood pressure from a computer. After a tracheotomy, we connect the rat to a rodent respirator, split the sternum longitudinally to expose the heart and lungs and use a hook to pull them to the right side, thereby restricting the extent of motion of the heart until the blood pressure stabilizes at 45 mmHg. We then inject a titrated (We determine this concentration starting with the 5μM *in vitro* value converted to the rat's total blood volume) concentration of $HgCl_2$ into the rat through the femoral vein and allow it to circulate for 10-15 min. We then inject 1ml HRP (8mg/100g rat weight in normal saline) and 0.5 ~ 1ml Heparin (5000 units/ml, Elkins-Sinn Inc. NJ) through the cannulated microtubing. At 0.5, 1, 2, or 4 min blood circulation, we sacrifice the rat with an overdose of Pentobarbital and excise the thoracic aorta.

After getting the desired tissue, we prepare the tissue for examination by peeling away the connective tissues and the adventitia. We fix in Glutaraldehyde (Sigma)1% for 1 hour. Glutaraldehyde (1%) is prepared by adding 1 ml 50% Glutataldehyde into 50 ml PBS (Phosphate Buffered Saline) solution. We then rinse with PBS solution three time to

wash out the fixative. We use the HRP-DAB reaction to develop the tracer spot. The leakage site will be a brown spot because the reaction production is brown. The DAB solution is made by adding 5 ml 0.3M Tris (0.182 g Tris (MW=121.1) with 5 ml H_2O) to 25 g distilled water. After dissolving 0.045 g DAB, we add 20 μl of 30% H_2O_2. Finally, we add 1M HCl solution to adjust the pH to 7.0~7.4. The DAB reaction takes one hour. For best results, the DAB solution is changed after 30 min. After the reaction, we wash the tissue with PBS solution to clean away any reaction residue. Finally, we prepare the tissue *en face* on slides and observe them under the light microscope (Olympus BX51).

First, we observe if, as in previous studies, in all cases the aorta has small, intense HRP spots coexisting with regions of diffuse background HRP staining after a circulation time as short as 30 sec. We measure the spot sizes as a function of time in each vessel by drawing an outline by eye with the cursor around the spot and then, using ImageJ (software from the NIH website), calculate its area. By compiling these spot size data for the aorta, one can find the spot growth curves for each condition.

Spot growth for animals not treated with $HgCl_2$

We use 12 male SD rats. The control experiments here are identical to the $HgCl_2$-treated experiments at 45mmHg except we do not inject $HgCl_2$ before HRP injection.

Statistics Analysis

Paired Student's *t*-tests are used for comparing tracer spot sizes from $HgCl_2$-treated and untreated rats at the same circulation times and between rats in each group at different circulation times. We choose $P<0.05$ to indicate statistical significance.

5.3 Results

5.3.1 Lp experiments

Fig 5.2 shows the Lp values before after $HgCl_2$-treatment and then after 2-mercaptoethanol-treatment, all on the same vessel *ex vivo* and all at ΔP=45mmHg. Each figure represents two aortas, and the pairs give consistent results. The reference Lp, with only a flush of blank solution between measurements, is ~2×10^{-8}cm/(s*mmHg). $HgCl_2$-treatment *ex vivo* decreases Lp by ~30%. 2-mercaptoethanoltreatment successfully removes the $HgCl_2$ thoroughly and recovers the reference Lp value.

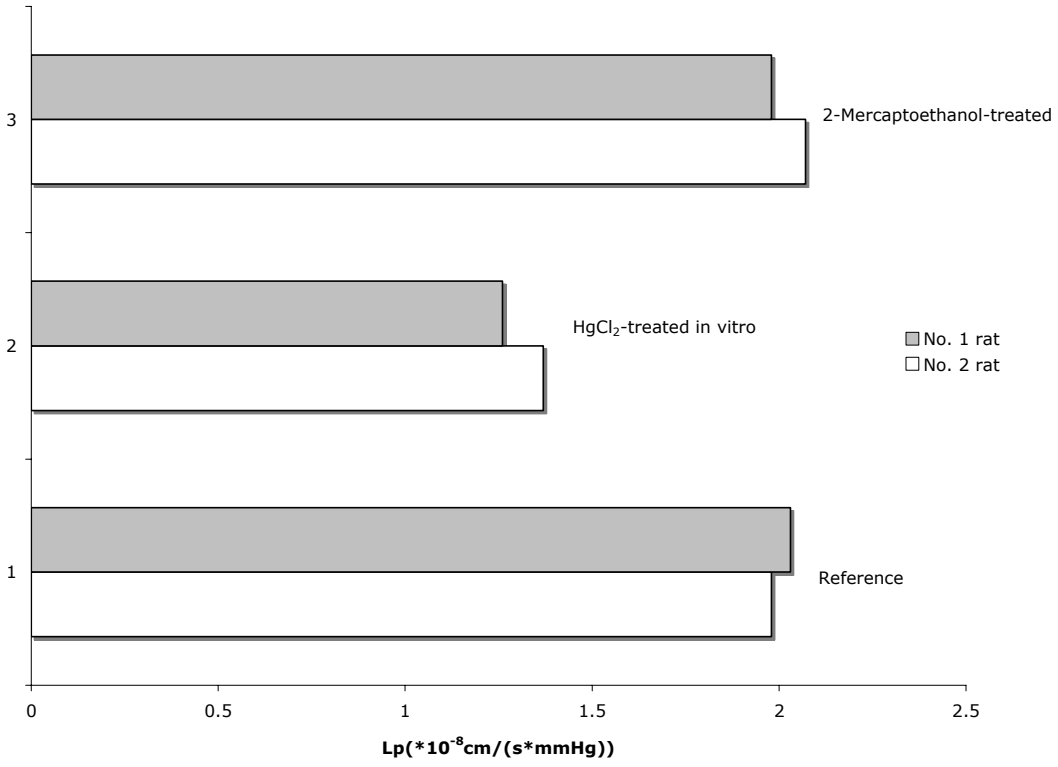

Figure 5.2 The Lps before after $HgCl_2$-treatment *ex vivo* and Lps after 2-mercaptoethanol-treatment at 45mmHg. Reference corresponds to Lp before and after flushing with blank solution containing neither chemical.

Fig 5.3 gives Lp values for the *in vivo* $HgCl_2$-treated rats. These aortas, treated with $HgCl_2$ *in vivo* and then with 2-mercaptoethanol *ex vivo*, show Lp values very similar

to those in the completely *ex vivo* experiments. Thus we can use the reference Lp and Lp after $HgCl_2$-treatment in our theory to predict HRP spot growth curves for these cases.

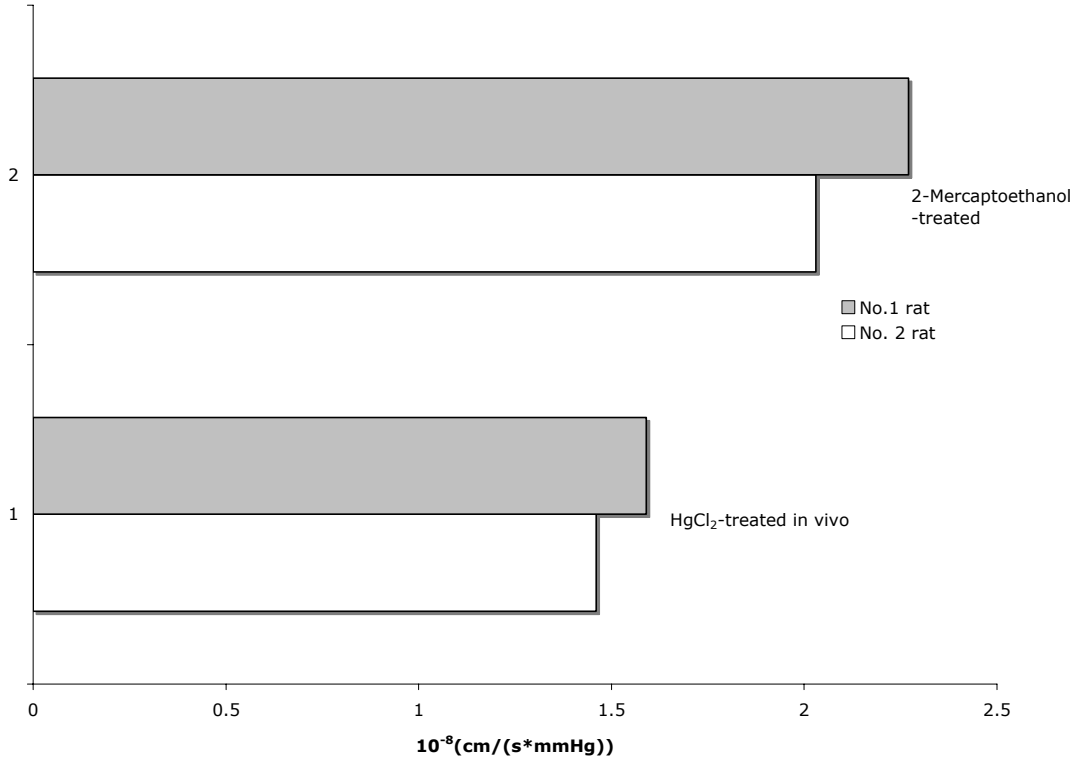

Figure 5.3 The Lps after HgCl2-treated in vivo and Lps after 2-mercaptoethanol-treated at 45mmHg.

5.3.2 Theoretical prediction and HRP spot experiments

Fig 5.4 shows the theoretically predicted and experimentally measured HRP spot growth curves at 45mmHg, both with and without $HgCl_2$-treatment. The HRP spots grow rapidly in the first 30s and grow slower thereafter. At 4min, the theory predicts that $HgCl_2$ blocking of endothelial AQP1 increases the HRP spot size by ~11%, and the experiment confirms this (statistically significant) ($P<0.05$) difference. The theory seems to slightly underpredict spot sizes at 1 and 2 minutes, but the overall trend of AQP blocking yielding larger spots, likely due to intimal compression, agrees with the data.

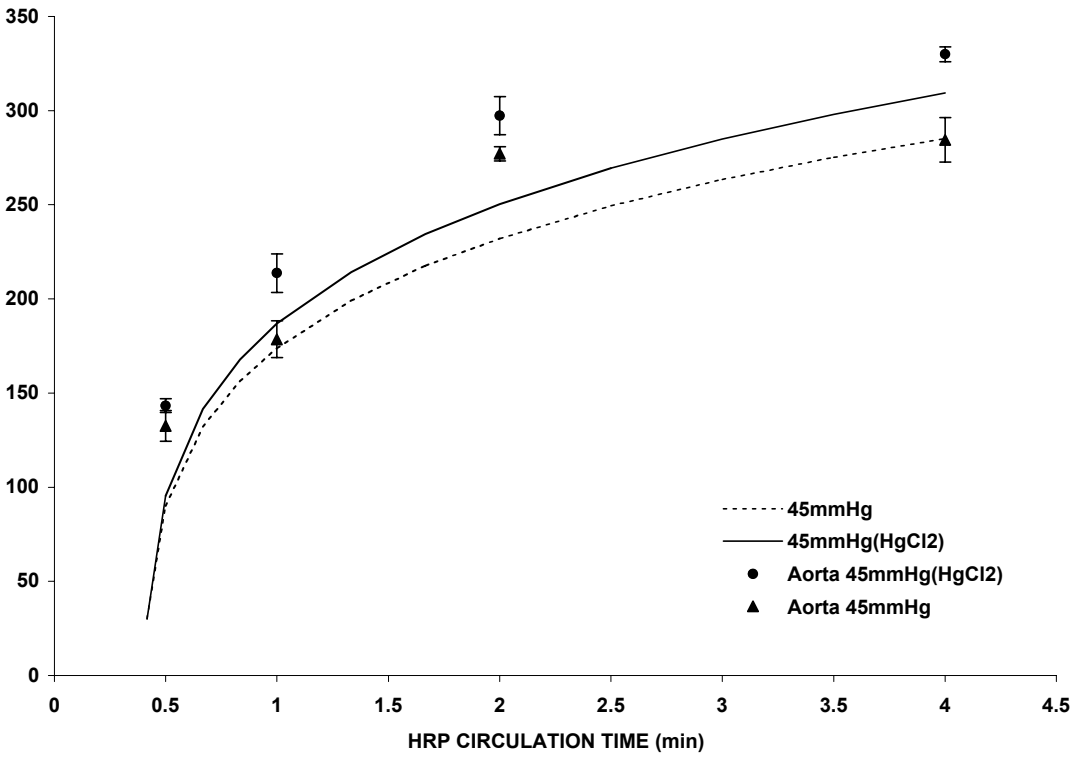

Figure 5.4 The theoretical and experimental HRP spot growth curves in with and without HgCl2-treated aorta at 45mmHg.

5.4 Discussion

The goal of this chapter has been to help explain the anomolous behavior of Lp(ΔP) upon treatment with $HgCl_2$. We guess that AQP blocking induces intimal compaction at lower transmural pressures and that this affects HRP spot growth.

AQP-1 is a highly specific transmembrane water channel protein; even single protons cannot cross through the aquaporin channel, since they associate with a molecule of water to become H_3O^+, which is too large to cross the narrow 2.8Å diameter neck of the channel (60). J. Toussaint, in our group has used immunohisotchemistry with anti-AQP1 antibodies to clearly show that AQP-1 is present in rat aortic endothelial cell membranes. It is thus reasonable to suspect that AQP1 contributes to rat endothelial water permeability and thus affects macromolecular transport. A mercury ion of size 2.2Å can

bind to the Cys189 in the water pore of the AQP-1 and block its narrow neck (60). A titration procedure is required to determine the appropriate concentration of $HgCl_2$. A too low value may not block all (or enough) of the aquaporins in the membrane and a too high value may create artifacts for many reasons, including the fact that $HgCl_2$ is generally toxic to living cells (1). We use 5μM (based on total blood volume) $HgCl_2$ in our experiments, the same value used in our earlier purely *ex vivo* experiments. Similarly, we choose the titrated 2μM concentration of 2-mercaptoethanol. Experiments show that vessel Lp responds the same way to these chemicals *in vivo* and *ex vivo*, and therefore they can be used to make predictions.

As noted in introduction, Huang et al. (26, 79)presented a theory and experimental evidence that the aortic intima compresses under transmural pressure load. The experiments of the latter paper showed that this compaction indeed occurred. However, it did not show any consequences of such compaction in vivo. Shou and Nguyen's experiments strongly suggest that AQP1 plays a nontrivial role in endothelial Lp and since this role appears phenomenologically to be highly pressure-dependent, The prediction that we test here is that, at low transmural pressures where the intima is normally uncompressed, blocking EC AQPs can shift a larger portion of the overall ΔP to the endothelium at fixed ΔP to compress the endothelium. This compression at fixed ΔP and fixed Lpmedia+IEL leads to larger spots. The reason for this is that at constant overall ΔP when AQP blockage lowers Lp (that is, Lpe), the pressure in the intima far from any leak will decrease, as Figure 5.5 shows. Therefore the intimal radial pressure difference between the (non-dimensional) pressure near and far from a leak is higher (0.277 vs 0.189) with $HgCl_2$ than without it at 45mmHg. Fig. 5.6 shows the

corresponding radial intima velocities that advect the tracer faster radially in the intima in the treated cases. Moreover, the unchanged overall ΔP=45 mmHg at lower wall Lp upon $HgCl_2$ treatment lowers the overall transmural flow that dilutes the intima's tracer concentration and flushes it from the intima. Figure 5.7 shows that, as a result, the intima tracer concentration is slightly higher upon $HgCl_2$treatment. Thus the combined effect is slightly larger HRP spots with AQP blockage at constant ΔP. This is in marked contrast to Chapter 3, where intimal compaction due to increased ΔP led to smaller spots. The difference is that at higher ΔP, even though the nondimensional radial pressure gradient in the intima may result in a higher advecting velocity, the higher overall transmural flow dilutes the intima's tracer concentration and more effectively flushes it from the intma, thereby leading to smaller, not larger HRP spots.

The arbiter of these predictions is the experiment, whose results indeed show larger HRP spots in the $HgCl_2$–treated aortas. The theory and experiment agree well for the untreated animals, except at 2 min circulation, where the experiments seem a bit high. Given that we have already checked this agreement with larger n in Chapter 3, it is very likely that the 2 min value is in error. On the other hand, the theory seems to under-predict Lp with AQP blocked over the whole pressure range, despite getting the trend upon AQP blockage correct. In our theory we have used some of the same transport parameters (permeability and diffusivity, but not Lpe) in the intima for both cases. Actually intimal compaction upon AQP1 blocking changes the mean fiber spacing in the intima and thereby should decrease matrix permeability and tracer diffusivity in the intima. As Huang *et* al(26) show, this effect is negligible compared with fenestral blockage; our theory therefore neglects such changes.

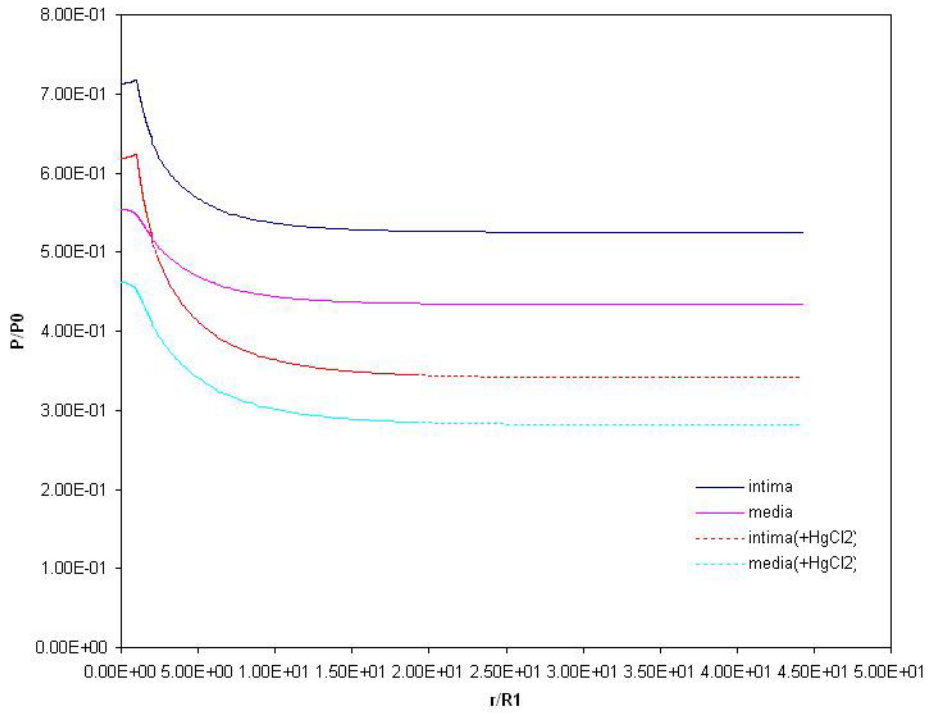

Figure 5.5 The pressure distribution in the intima and the media just beneath the IEL at 45mmHg with or without $HgCl_2$ treatment

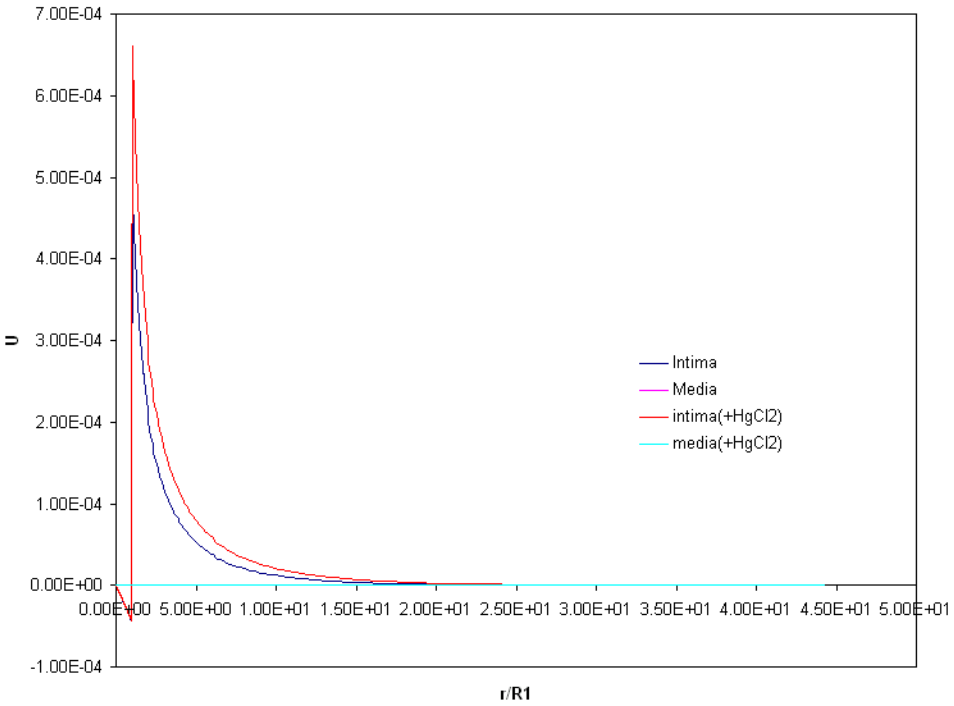

Figure 5.6 The velocity in the r direction in the intima and media just beneath the IEL with or without $HgCl_2$ treatment

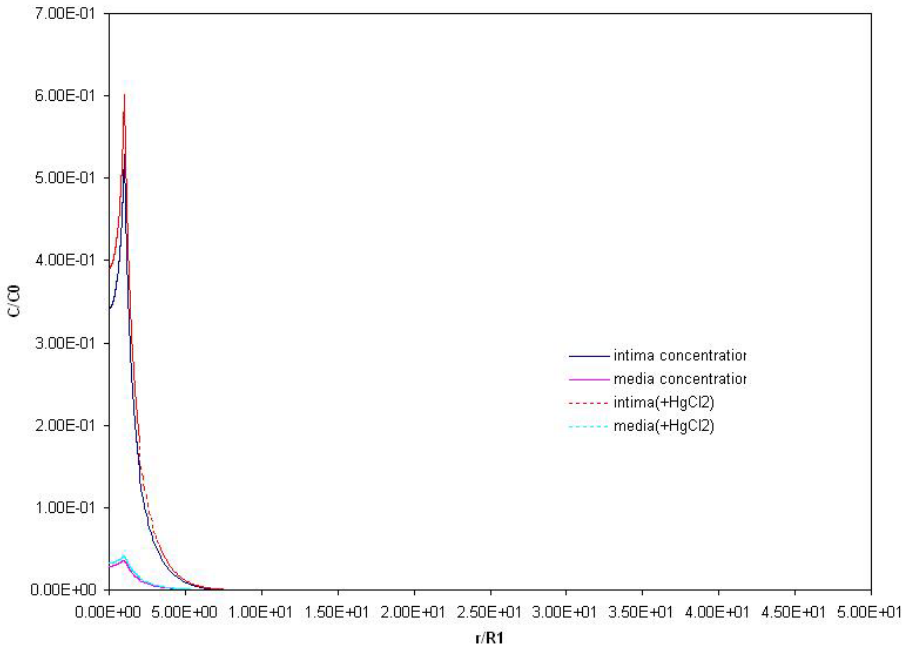

Figure 5.7 The concentration distribution in the intima and the media just beneath the IEL with or without the $HgCl_2$ treatment

5.5 Conclusion

In this chapter, we investigate the role of AQP1, and of its blockage, in HRP spot growth in rat aorta, both theoretically and experimentally. We use $HgCl_2$ to block aquaporin, and use it at concentrations and exposure times that do not show any toxic effects on transport. AQP blocking at constant ΔP shifts enough of ΔP to the endothelium to compress the intima and lower Lp. Alternatively, blocking endothelial AQP1 at the constant transmural pressure of 45 mmHg compacts the intima, which decreases Lp. However, because the overall transmural water flow is decreased, the result is larger, not smaller, HRP spots. This contrasts sharply with intimal compaction due to increased transmural pressure, which, can at the same time decrease wall Lp and still increase overall transmural flow. As we have seen in Chapter 3, that leads to smaller HRP spots.

Our 2D convection/diffusion/mass transfer model gives precise predictions (and enough information to explain them) for the growth of HRP spots with HRP circulation

time. Here we show both theoretically and experimentally that this can happen *in vivo* as well. A change in endothelial AQP expression, for whatever reason, can affect when intimal compaction occurs and, consequently, tracer spot size, i.e., the rate and amount of tracer (e.g., LDL cholesterol) that enters the wall and its concentration distribution there. This may be of importance in understanding the how factors that affect AQP expression can impact atherogenesis.

Chapter 6 Conclusions and future work

The problem of understanding the early events that trigger atherosclerosis is indeed a difficult and important one. It is generally agreed these days that the transendothelial transport of LDL cholesterol and its lodging in the intima's extracellular matrix are critical events in this process. Earlier work focused on showing that mcuh of this transport was via transmural pressure-driven water transport that advects macromolecules around rare endothelial cells whose intercellular junctions leaked. In order to understand why high pressure arteries are susceptible to atherosclerosis, but low pressure arteries and even lower pressure veins are usually resistant, this thesis begins by investigating the frequency of such macromolecular leaks in prototypical vessels of each type, the aorta, pulmonary artery (PA) and the inferior vena cava (IVC). Their relative leakage frequencies are about 20:10:1. These data can be used in the mathematical model in the three different vessels, but this difference alone cannot explain the differeing susceptibilities of these vessels. Zeng's work in our group(85, 86) is addressing these issues with detailed transport models for the PA and IVC.

Huang et al's 2-D filtration and convection-diffusion model(25) and intima compaction theory(26) in the aorta shed some light in understanding transport in the aorta. Experimental confirmation has thus far come in the form of predictions of the integration through the tissue of the tracer (HRP) concentration as a function of radial distance from the center of a localized leak and the observation via sectioning vessels fixed under pressure of intimas of differing thicknesses. These theories are sufficiently complex and postulate sufficiently novel ideas that they call out for more rigorous tests of them individually and of their combined predictions. That is the focus of this thesis. First,

we combine these theories to predict the HRP spot growth as a function of acute transmural pressure, both with and without intimal compaction. These two situations led to prediction of opposite trends, and our experimental study clearly supports the theory that incorporates intimal compaction. The results show when pressure increases the spot size decreases. Chapter 4 then uses confocal microscopy to examine the 3D, axisymmetric tracer (HRP) concentration c*(r,z,t) and compares it to the model predictions, without the need to integrate (i.e., data smooth and loose information). This comparison is for 0.5 or 1 min HRP circulation followed by a 10min washout blood process. This is a far more demanding test of the theories above, and the results seem to be quite positive regarding the theory. A peak of concentration in the z direction exists in the media nearer the adventitia. The concentration in the r direction decreases slowly from the center of the leaky endothelium cell to the edge of the HRP spot.

Finally, our group has determined that aquaporins play an important role in and account for a nontrivial fraction of endothelial hydraulic conductivity. Since transendothelial water transport not only brings LDL into the intima, but also dilutes it and flushes it from the intima, understanding such water transport is vital. By chemically blocking AQP, my colleagues Shou and Nguyen have found that vessel wall hydraulic conductivity drops significantly and that this drop appears to be pressure-dependent. We guess that the blocking of AQP actually shifts a larger fraction of the overall transmural pressure to the endothelium and thereby compresses the intima, thereby reducing wall conductivity, at a lower overall transmural pressure than when the AQPs are not blocked. That means, there should be low pressures where blocking AQPs causes intimal compression without a change in trnasmural pressure, and we use theory to predict the

effect on HRP spot growth *in vivo* for these two circumstances. We design and carry out experiments to test these predictions and the results are very satisfactory. Blocking the AQP of endothelium cells increases HRP spot growth compared with no blocking. We believe the work in this thesis has gone a long way to clarifying and towards validating the theories of Huang et al.(25, 26)

As noted, our model appears very good at describing the mass transfer of macromolecular into the rat aorta. Zeng in our group has developed the models for the PA and the IVC. In the future, we can test the models of the PA and IVC in similar way to those used to test the aortic models, both by making similar theoretical predictions and by testing them experimentally. For example, we can predict and test the effect of acute transmural pressure on the tracer spot growth, the 3-D imaging of tracer spot in these two different vessels as well. We can also investigate if these vessels' endothelia express AQP and, if so, what the roles of AQP in the water and in the mass transfer of macromolecules into their vessel walls are. Is there any AQP1 in the endothelium cells of the PA and IVC? What role does AQP1 play in their Lp measurements? How does blocking AQP1 change tracer spot growth in their vessels? This may help us better understand their disease resistance and may lead to novel strategies to inhibit disease in susceptible vessels.

References

1. **Aleo MF FM, F. Bettoni, S. Tanganelli, A. Vezzola, R. Giuliani, N. Steimberg, Pl Apostoli, and G. Mazzoleni.** Antioxidant poteintial and gap junction-mediated intercellular communication as early biological markers of mercuric chloride toxicity in the MDCK cell line. *Toxicology in Vitro* 16: 457-465, 2002.

2. **Baldwin AL, and Wilson, L. M.** Endothelium increases medial hydraulic conductance of aorta, possibly by release of EDRF. *Am J Physiology* 264: H26-H32, 1993.

3. **Baldwin AL, Wilson, L. M., and Simon, B. R.** Effect of pressure on hydraulic conductance. *Arteriosclerosis and Thrombosis* 12: 163-171, 1992.

4. **Barakat AI UP, Colton CK.** Topographical mapping of sites of enhanced HRP permeability in the normal rabbit aorta. *J Biomech Eng* 114: 283-292, 1992.

5. **Bell FP, Adamson, I.L., and Schwartz, C.** Aortic endothelial permeability to albumin: Focal and regional patterns of uptake and transmural distribution of ^{131}I-albumin in the young pig. *Exp Molec Pathol* 20: 57-68, 1974.

6. **Bell FP ASG, and C. Schwartz.** Focal and regional patterns of uptake and the transmural distribution of 131I-fibrinogen in the pig aorta in vivo. *Exp Mol Pathol* 20: 281-292, 1974.

7. **Bremermann H.** A method of unconstrained global optimization. *Mathematical Biosciences* 9: 1-15, 1970.

8. **Brenda Mrtinez-Nieves JCD.** Vascular dilatatory responses to sodium nitroprusside (SNP) and α-adrenergic antagonism in female and male normal and diabetic rats. *PSEBM* 222: 90-98, 1999.

9. **Brown MS, and Goldstein, J. L.** How LDL receptors influence cholesterol and atherosclerosis. *Scientific Amer* 251: 58-66, 1984.

10. **Bruecke E.** Beitraege zur Lehre von der Difffusion tropftbare Flussigkeiten durch poroese Scheidewaende. *Am Phys Chem* 58: 77-94, 1843.

11. **Chen YL, K.M. Jan, H.S. Lin, and S. Chien.** ultrasructural studies on macromolecular permeability in relation to endothelial cell turnover. *Atherosclerosis* 118: 89-104, 1995.

12. **Chien S, Lin, S., Weinbaum, S., Lee, M. M. L., and Jan, K.,.** The role of Arterial Endothelial Cell Mitosis in Macromolecular Permeablity. *Advances in Experimental Medicine and Biology* 242: 59-73, 1988.

13. **Cho MR DWK, B. L. Smith, J. J. Mooulds, P. Agre, N. Mohandas, and D. E. Golan.** Membrane dynaimcs of the water transport protein Aquaporin-1 in intact human red cells. *Biophysical Journal* 76: 1136-1144, 1999.

14. **Chuang P, Cheng, J., Lin, S., Jan, K., Wang, D., and Chien, S.** Macromolecular transport across arterial and venous endothelium in rats: studies with evans blue-albumin and horseradish peroxidase. *Arteriosclerosis* Arteriosclerosis: 188-197, 1990.

15. **Curry FE.** Mechanics and thermodynamics of transcapillary exchange. In: *Handbook of Physiology, Section 2, The cardiovascular system, Vol. 4, Microcirculation*. Bethesda, MD: American Physiology Society, 1984, p. 309-374.

16. **FF Vargas SP, Osorio H.,and Schulz C.** Hydraulic conductivity of venous endothelium as measured with a volume clamp method. *American Journal of Physiology* 251: H676-H680, 1986.

17. **Fortin MG NAM, and D. P. Verma.** Nodulin-26, a peribacteroid membrane nodulin is expressed independently of the development of the peribacteroid compartment. *Nucleic Acids Res* 15: 813-824, 1987.

18. **Frank JS, and Fogelman, A. M.** Ultrastructure of the intima in WHHL and cholesterol-fed rabbit aortas prepared by ultra-rapid freezing and freeze-etching. *J of Lipld Research* 30: 967-978, 1989.

19. **Frokjaer-Jensen J.** Three dimensional organization of plasmalemmal vesicles in endothelial cells: An analysis by serial sectioning of frog mesenteric capillaries. *J Ultrastruct Res* 73: 9-20, 1980.

20. **Fry DL.** Mass transport, atherogenesis, and risk. *Arteriosclerosis* 7: 88-100, 1987.

21. **Fry DL.** Mathematical models of arterial transmural transport. *Am J of Physiol* 248: H240-H263, 1985.

22. **Gourlay AR.** Hopscotch: A fast second order partial differential equation solver. *J Inst Maths Applics* 6: 375-390, 1970.

23. **Herrmann R, Malinauskas, R., and Truskey, G.** Characterization of sites with elevated LDL permeability at intercostal, celiac, and iliac branches of the normal rabbit aorta. *Arteriosclerosis and Thrombosis* 14: 313-323, 1994.

24. **Holman JP.** *Heat Transfer*. New York: McGraw-Hill, 1986.

25. **Huang Y, Rumschitzki, D., Chien, S., and Weinbaum, S.** A fiber matrix model for the growth of macromolecular leakage spots in the arterial intima. *J Biomedical Engineering* 116: 430-445, 1994.

26. **Huang Y, Rumschitzki, D., Chien, S., and Weinbaum, S.,.** A fiber matrix model for the filtration through fenestral pores in a compressilbe arterial intima. *Am J Physiol* 247: H2023-H2039, 1997.

27. **Huang Y. K-MJ, D. Rumschitzki and S. Weinbaum.** Strucrural changes in rat aortic intima due to transmural pressure. *Journal of Biomechanical Engineering* 120: 476-483, 1998.

28. **J. G. Mohanty JSJ, Edward S. Schulman and Donald G. Raible.** A highly sensitive fluorescent micro-assay of H202 release from activated human leukocytes using a dihydroxyphenoxazine derivative. *J Immunol Methods* 202: 133-141, 1997.

29. **Johanson U MK, I. Johansson, S. Gustavsson, S. Sjovall, L. Fraysse, A. R. Weig, and P. Kjellbom.** The complete set of genes encoding major intrinsic proteins in Arabidopsis provides a framework for a new nomenclature for major intrinsic proteins in plants. *Plant Physiol* 126: 1358-1369, 2001.

30. **Lever MJ, T.J. Mark and P.J.Coleman.** Plasma protein entry and retention in the vascular wall:possible factors in atherogenesis. *Canadian Journal of Physiology and Pharmacology* 74: 818-823, 1996.

31. **Li Qi-fang DA-g.** Hypoxia-inducible factor-1 alpha regulates the role of vascular endothelial growth factor on pulmonary arteries of rats with hypoxia-induced pulmonary hypertension. *Chinese Medical Journal* 117: 1023-1028, 2004.

32. **Lin S, Jan, K. M., and Chien, S.** Role of dying endothelium cells in transendothelial macromolecular transport. *Atherosclerosis* 10: 703-709, 1990.

33. **Lin S, Jan, K. M., Schuessler, G., Weinbam S. and Chien, S.** Enhanced macromolecular permeability of aortic endothelial cells in association with mitosis. *Atherosclerosis* 73: 223-232, 1988.

34. **Lin S, Jan, K.M., Weinbaum, S., and Chien, S.** Transendothelial transport of low denstity liporotein in association with cell mitosis in rat aorta. *Atherosclerosis* 9: 230-235, 1989.

35. **Majno G GEP, and G. L. Schoetl.** Studies in inflammation. II. The site of action of histamine and serotonin along the vascular tree: a topographic study. *J Biophys Biochem Cytol* 11: 567-629, 1961.

36. **MN Hart DHaMB.** Effect of chronic hypertension and sympathetic denervation on wall/lumen ratio of cerebral vessels. *Hypertension* 2: 419-423, 1980.

37. **Murata K, Mitsuoka K, Hirai T, Walz T, Agre P, Heymann JB, Engel A, and Fujiyoshi Y.** Structural determinants of water permeation through aquaporin-1. *Nature* 407: 599-605, 2000.

38. **Nguyen T, Jimmy, Toussaint., Kung-ming, Jan., and David, Rumschitzki.** The functional role of AQP1 on the filtration properties of the aorta. In writing, 2008.

39. **Nielsen S SB, Christensen EI, Knepper MA, Agre P.** CHIP28 water channels are localized in constitutively water-permeable segments of the nephron. *J Cell Biol* 120: 371-383, 1993.

40. **Packham MA, Roswell, H.C., Jorgensen, L., and Mustard, J.F.** Localized protein accumulation in the wall of the aorta. *Exp Molec Pathol* 20: 214-232, 1967.

41. **Pawley JB.** *Handbook of Biological Confocal Microscopy*: New York: Plenum Press, 1995.

42. **Preston GM JSJ, W. B. Guggino and P. Agre.** The mercury-sensitive residue at cysteine 189 in the CHIP28 water channel. *The Journal of Biological Chemistry* 268: 17-20, 1993.

43. **Rose M, E.,.** *Elementary Theory of Angular Momentum*: Wiley: New York, 1957.

44. **Ross R.** The pathogenesis of atherosclerosis - an update. *N Eng J Med* 314: 488-500, 1986.

45. **Schnitzer JE aPO.** Aquaporin-1 in plasma membrane and caveolae provides mercury-sensitive water channels across lung endothelium. *American Journal of Physiology (Heart Circ Physiol)* 270: H416-422, 1996.

46. **Schwenke DC, and Carew, T. E.,.** Initiation of atherosclerosis lesions in cholesterol-fed rabbits. I. Focal increases in arterial LDL concentration precede development of fatty streak lesions. *Arteriosclerosis* 9: 895-907, 1989.

47. **Selzer A.** Changing aspects of the natural histor of valvular aortic stenosis. *N Eng J Med* 317: 91-98, 1987.

48. **Shanahan CM CDL, Thson K. L., Cary Nr., Osbourn J. K., Agre P., and P. L. Weissberg.** Aquaporin-1 is expressed by vascular smooth muscle cells and mediates rapid water transport across vascular cell membranes. *J Vasc Res* 36: 353-362, 1999.

49. **Shlomoh Simchon WMM, Gabriele Blumberg, Jeffrey Brensilver and Stanley Cortell.** Impaired renal vasodilation and urinary cGMP excretion in Dahl salt-sensitive rats. *Hypertension* 27: 653-657, 1996.

50. **Shlomoh Simchon WMM, Guo-Shan Shi and Jeffrey Brensilver.** Impaired renal vascular reactivity in prehypertensive Dahl salt-sensitive rats. *Hypertension* 20: 524-532, 1992.

51. **Shou Y.** Water and Macromolecular Transport into the Walls of Vessels with Differing Atherogenic Susceptibilities. 2005.

52. **Shou Y, Jan, Kung-ming., and Rumschitzki, David.** Transport in rat vessel walls. II. Macromolecular leakage and focal spot size growth in rat arteries and veins. *American Journal of Physiology* 292: H2881–H2890, 2007.

53. **Shou Y, Jan, Kung-ming., and Rumschitzki,David.** Transport in rat vessel walls. I. Hydraulic conductivities of the aorta,pulmonary artery, and inferior vena cava with intact and denuded endothelia. *American Journal of Physiology* 291: H2758–H2771, 2006.

54. **Sidel VW and Solomon AK.** Entrance of water into human red cells under an osmotic pressure gradient. *J Gen Physiol* 41: 243-257, 1957.

55. **Simionescu N, Vasile, E., Lupo, F., Popescu, G., and Simionescu, M.,.** Prelesional events in atherogenesis. Accumulation of extracellular cholesterol-rich liposomes in the arterial intima and cardiac valves of the hyperlopodemic rabbits. *Am J Pathol* 123: 109-125, 1986.

56. **Smith GD.** *Numerical Solution of Partial Differential Equations*. New York and London: Oxford University Press, 1965.

57. **Sprague EA MAF, M. R. Hagens, G. B. Wilhelm, and C. J. Schwartz.** *Observations on vascular surface membrane charge distribution. In Hemodynamics and the arterial wall.*: Houston: Univ. of Houston Press, 1980.

58. **Steinberg D.** Lipoproteins and atherosclerosis: A look back and a look ahead. *Arteriosclerosis* 3: 283-301, 1983.

59. **Stemerman MB, Morre, E.M.,Burke, K.R., Colton, C.K., Smith, K. A., and Lees, R. S.,.** Local variation in arterial wall permeability to Low Density Lipoprotein in normal rabbit aorta. *Atherosclerosis* 6: 64-69, 1986.

60. **Sui HX BH, J. K. Lee., P. Walian and B. K. Jap.** Structural basis of water-specific transport through the AQP1 water channel. *Nature* 414: 872, 2001.

61. **Susan C. Fagan MPB, Patrick D. Lynden, and Justin A.Zivin.** Acute hypertension promotes hemorrhagic transformation in a rabbit embolic stroke model: effect of laberalol. *Experimental Neurology* 150: 153-158, 1997.

62. **Tatyana V. Votyakovaa aIJR.** Detection of hydrogen peroxide with Amplex Red: interference by NADH and reduced glutathione auto-oxidation. *Archives of Biochmistry and Biophysics* 431: 138-144, 2004.

63. **Tedgui A, and Lever, M. J.,.** Effect of pressure and intimal damage on 131I-Albumin and [14C]Sucrose spaces in aorta. *Am J Physiology* 253: H1530-H1539, 1987.

64. **Tedgui A, and Lever, M. J.,.** Filtration through damaged and undamaged rabbit thoracic aorta. *Am J Physiology* 247: H784-H791, 1984.

65. **Truskey GA, Colton, C. K., and Smith, K. A.** Quantitative analysis of protein transport in the arterial wall. In: *Structure and function of the circulation*, edited by Schwartz CJ, Werthessen, J. T., and Wolf, S.,. New York: Plenum Pubilshing Corporation, 1981, p. 287-355.

66. **Truskey GA, Robert, W. L., Herrmann, R. A., and Malinauskas, R. A.,.** Measurement of endothelial permeability to 125I-low density lipoproteins in rabbits arteries by use of en face preparations. *Circ Res* 71: 883-897, 1992.

67. **Tzeghai G, Banatos, P., Pfeffer, R., Weinbaum, S., and Nir, A.,.** A theoretical model to study the effect of convection and leaky junctions on macromolecule transport in artery walls. *J Theor Biol* 121: 141-162, 1986.

68. **Vander A, J. Sherman, and D. Luciano.** *Human Physiology: the Mechanisms of Body Function*. New York: McGraw Hill Companies, Inc., 2001.

69. **Vargas CB, Vargas FF, Pribyl JG, and Blackshear PL.** Hydraulic conductivity of the endothelial and outer layers of the rabbit aorta. *Am J Physiol* 236: H53-60, 1979.

70. **Verkman A.** Water channels in cell membranes. *Annu Rev Physiol* 54: 97-108, 1992.

71. **Wa Mo AKS, Jose A. L. Arruda, and George Dunea.** Role of nitric oxide in cocaine-induced acute hypertension. *American Journal of Hypertension* 11: 708-714, 1998.

72. **Waltz T BLS, M. L. Zeidel, A. Engel, and P. Agre.** Biologically active two-dimensional crystals of Aquaporin CHIP. *J Biol Chem* 269: 1583-1586, 1994.

73. **Weinbaum S, Tzeghai, G., Ganatos, P., Pfeffer, R., and Chien, S.** Effect of cell turnover and leaky junctions on arterial macromolecular transport. *Am J of Physiol* 248: H945-H960, 1985.

74. **Weinbaum. S. W, G., Ganatos, P., Pfeffer, R., Lee, M. M. L., and Chien, S.** On the time-dependent diffusion of macromolecules through transient open junction and their subendothelial spread. I. Short-time model for cleft exit region. *J of Theortical Physiology* 135: 1-30, 1988.

75. **Wen G, Weinbaum, S., Ganatos, P., Pfeffer, R., and Chien, S.** On the time-dependent diffusion of macromolecules through transient open junctions and their subendothelial spread. II. Long-time model for interaction between leakage sites. *J of Theortical Physiology* 135: 219-253, 1988.

76. **Wen GB, S. Weinbaum, P. Ganatos, R. Pfeffer and S. Chien.** On the time dependent diffusion of macromolecules through transient open junctions and their subendothelial spread. 2. Long time model for interaction between leakage sites. *J Theor Biol* 135: 219-253, 1988.

77. **Wenpeng LaW, Jin.** Measurement of peroxidase activity in single neutrophils by combining catalyzed-enzyme reaction and epi-fluorescence microscopy. *Talanta* 70: 251-256, 2006.

78. **Wu C, Chi, J., Jerng, J., Lin, S., Jan, K., Wang, D., and Chien, S.** Transendothelial macromolecular transport in the aorta of spontaneously hypertensive rats. *Hypertension* 16: 154-161, 1990.

79. **Y. Huang K-MJ, D. Rumschitzki and S. Weinbaum.** Strucrural changes in rat aortic intima due to transmural pressure. *Journal of Biomechanical Engineering* 120: 476-483, 1998.

80. **Yin Y.** *The initiation and growth of extracellular lipid liposomes in arteries and valves* (Doctoral Dissertation). New York: The Graduate Center of The City University of New York, 1999.

81. **Yin Y, Lim, K., Weinbaum, S., Chien, S., and Rumschitzki, D.,.** A model for the initiation and growth of extracellular lipid liposomes in arterial intima. *Am J Physiol* 272: H1033-H1064, 1997.

82. **Yuan F, Chien, S., and Weinbaum, S.,.** A new view of convective-diffusive transport processes in the arterial intima. *ASME Journal of Biomechanical Engineering* 113: 314-329, 1991.

83. **Yuh-Lien Chen K-MJ, Huai-San Lin, Shu Chien.** Relationship between endothelial cell turnover and permeability to horseradish peroxidase. *Atherosclerosis* 133: 7-14, 1997.

84. **Yuh-Lien Chen K-MJ, Huai-San Lin, Shu Chien.** Ultrastructural studies on macromolecular permeability in relation to endothelial cell turnover. *Atherosclerosis* 118: 89-104, 1995.

85. **Zeng Z, Jan, K. M. & Rumschitzki, D. S.** Transport in rat vessel walls III: A theory for water and macromolecular transport in the pulmonary artery and its comparison with the aorta. *American Journal of Physiology*: in review, 2008.

86. **Zeng Z, Jan, K. M. & Rumschitzki, D. S.** Transport in rat vessel walls IV: A theory for water and macromolecular transport in the inferior vena cava. *American Journal of Physiology*: in review, 2008.

87. **Zeng Z, Patricia Nievelstein-Post, Y. Yin, K. M. Jan, Joy S. Frank, and D. Rumschitzki.** Macromolecular transport in heart valves. III. Experiment and theory for the size distribution of extracellular liposomes in hyperlipidemic rabbits *Am J Physiol Heart Circ Physiol* 292: H2687-H2697, 2007.

88. **Zeng Z, Y. Yin, A. L. Huang, K. M. Jan, and D. Rumschitzki.** Macromolecular transport in heart valves (I): studies with horseradish peroxidase. *American Journal of Physiology* 292: H2664-H2670, 2007.

89. **Zeng Z, Y. Yin, K. M. Jan, and D. Rumschitzki.** Macromolecular transport in heart valves (II): theoretical models. *American Journal of Physiology* 292: H2671-H2686, 2007.

90. **Zhang R ANvH, J. Biwersi, and A. S. Verkman.** A point mutation at Cysteine 189 blocks the water permeability of rat kidney water channel CHIP28k. *Biochemistry* 32: 2938-2941, 1993.

91. **Zhu F ET, and K. Schulten.** Pressure-induced water transport in membrane channels studied by molecular dynamics. *Biophysical Journal* 83: 154-160, 2002.